(1) Concrete-filled steel box specimens under constant axial force and cyclic lateral loading showed generally prominent earthquake-resistance characteristics in undergoing the inelastic action.

(2) The diaphragm over the filled-in concrete was found to be very effective in improving the strength, ductility and energy absorption capacity of the column. In the seismic design of partially concrete-filled steel bridge piers of box sections, it appears beneficial to provide a diaphragm over the filled-in concrete.

(3) In the specimens with small slenderness ratios, crack vertical to the weld occurred at approximately $H = H_{yo}$ with the exception of specimen SC45-25-5[3], which had a crack near the column base early at 88% of the maximum load. It might have resulted from low cycle fatigue. Accordingly, special attention is necessary to be paid on the welding surrounding the triangular ribs in practical constructions.

(4) When "collapse" is defined as occurring at the maximum load point and at a point where the load-carrying capacity is reduced to 95% of the maximum load, the ductility and energy absorption capacity are much different. That is, the parameters $\mu_{95}$ and $\hat{E}_{95}$ are considerably larger than the parameters $\mu_m$ and $\hat{E}_{max}$. This is contributed to the presences of the filled-in concrete and the diaphragm over the concrete.



# 6 MOMENT-CURVATURE RELATIONS FOR STEEL COLUMN SEGMENTS AND CONCRETE-FILLED STEEL COLUMN SEGMENTS

## 6.1 General Remarks

In the previous chapters, experimental investigations of concrete-filled steel box columns are presented. It is found that this type of steel-concrete composite columns generally exhibit flexural failure. This means that, the load-deflection relationships of concrete-filled steel box columns may rationally be determined from the point of view of flexural failure theory. One of the approximate methods is to integrate the moment-curvature relations along the member length. Thus, before we undertake the analysis of the load-deflection behavior of the column, the moment-curvature relations of hollow steel box section and concrete-filled steel box section will be presented in this chapter.

In the beginning, researches on the elasto-plastic response of column segments subjected to compression combined with a uniaxial bending moment in the past are to be briefly reviewed. In 1976, Chen and Atsuta proposed a series of approximate formulas for the relation between moment and curvature for short beam-column segments of various cross-sectional shapes, in which the stress-strain relationship of the material was assumed to be elastic-perfectly plastic. However, this kind of simple approach is less satisfactory for thin-walled plated steel structures because the effect of local buckling was not included. To overcome this shortcoming, Lee et al. (1987) calculated the moment-curvature relations using a numerical method originally proposed by Little (1979). However, it was found that the $M$-$P$-$\Phi$ relations calculated by Little's method are inaccurate in some cases (Usami and Fukumoto, 1989). In order to obtain a rigorous moment-curvature relation, an elasto-plastic, large displacement finite element analysis was carried out by Usami and Fukumoto (1989). However, for arbitrary curvature and arbitrary axial force in the analysis of beam-column members or frame structures, corresponding moment and tangent stiffness have to be calculated by interpolation from discreted data of the $M$-$P$-$\Phi$ relations. Moreover, Miwa et al. (1993) proposed a set of formulas to describe the moment-curvature relations for thin-walled steel box column segments based on a nonlinear finite element analysis. However, the

effect of strain-hardening was not taken into account in the analysis and the linear elastic behavior at the beginning of $M$-$P$-$\Phi$ curves was approximated by a parabolic curve.

For these reasons, the present research work is aimed at finding an accurate expression for the relation between moment and curvature for thin-walled steel box column segments and concrete-filled steel box column segments. For the purpose, the moment-curvature relation is first computed with the help of a newly developed analytical model in MARC research program (1988) for the loading condition of a pair of equal bending moments. Then, in order to take into account the effect of the moment gradient, the analytical model is modified to obtain the moment-curvature relation which is expected to be more appropriate for the strength and deformation analysis of the cantilever column treated in Chapters 4 and 5. In the case of concrete-filled steel section, the moment-curvature relation is computed by a simplified numerical computation method in which buckling is not included.

## 6.2 Moment-Curvature Relations for Steel Box Column Segments under Uniform Moment

To compute the $M$-$P$-$\Phi$ relation of locally buckled steel box stub-columns, the MARC research program was employed with introduction of appropriate analytical models.

### 6.2.1 Analytical Model

The basic assumptions are as follows: (1) Kirchhoff's assumption (Washizu, 1982) for a thin plate is valid; (2) Von Karman's strain versus displacement relations (Washizu, 1982) are used; (3) A linearly varying edge displacement increment is imposed along the loaded edge. (4) The von Mises yield criterion with normality flow rule is used to describe the material behavior of steel.

To obtain the $M$-$P$-$\Phi$ relation of a box stub-column shown in **Fig. 6.1**, an end moment, $M$, versus average curvature, $\Phi$, relation under a given constant axial force, $P$, must be established. For this purpose, a special analytical model was developed. The model will be explained using **Fig. 6.2**. Because of symmetry, only a quarter part of the box column was taken for analysis.



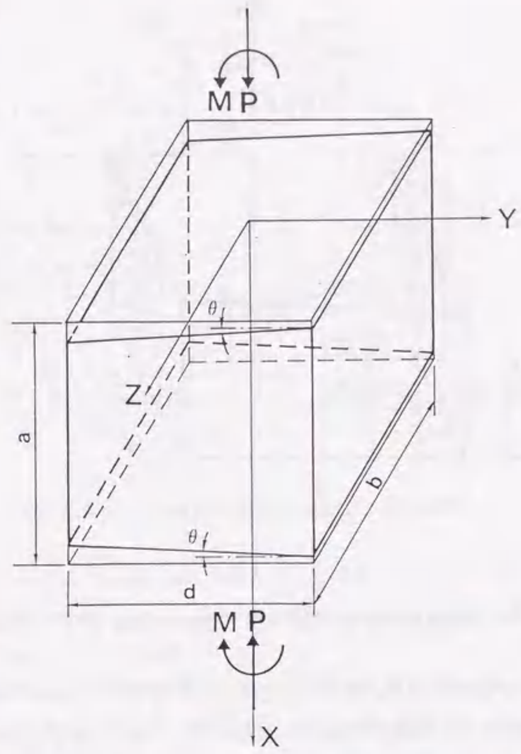


**Fig. 6.1 Box Segment to be Analyzed**

In the analytical model, an eight-node thin shell element was employed for the steel plate element. Moreover, to impose the rotation, $\theta_A$, and the axial displacement, $u_A$, at point 'A'(see **Fig. 6.2**), a beam element of an arbitrary length, which is located at an arbitrary point above the upper edge of the analyzed column, was used. The beam element was simply supported at the lower end (i.e., the point 'A') and free at the other end. To keep the same rotation between the beam element and upper edge, some rigid bars are necessary for connecting the point 'A' with the edge nodes of the column. For this purpose, a tying constraint involving linear dependence of nodal degrees-of-freedom was considered. This kind of tying constraint involves one tied node and one or more retained nodes, and a tying constraint condition. The degrees-of-freedom (for example,

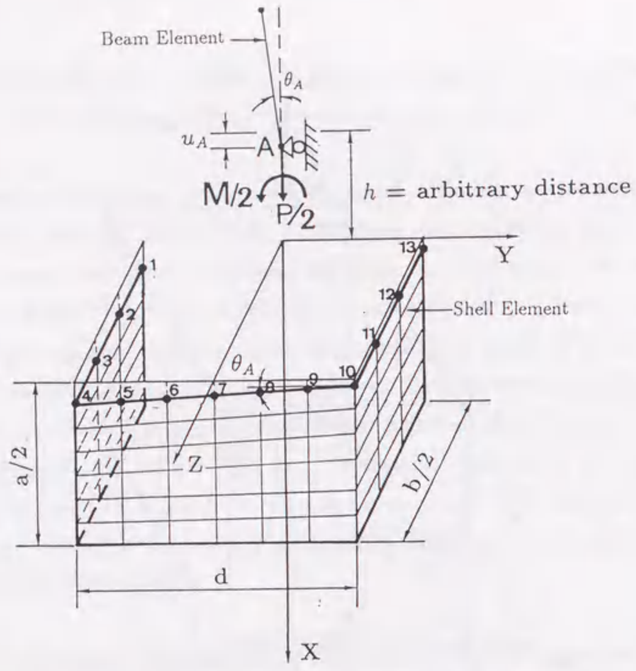


**Fig. 6.2 Analytical Model for Computing $M$-$P$-$\Phi$ Curves**

displacements and rotations) of the tied node are dependent on the degrees-of-freedom of the retained nodes through the tying condition. In the case of the problem under consideration, the constraint equations are:

$$u_i = u_A + \frac{d}{2}\theta_A, \qquad i = 1,2,3,4 \tag{6.1}$$

$$u_j = u_A - \frac{d}{6}(j-7)\theta_A, \qquad j = 5,6,...,9 \tag{6.2}$$

$$u_k = u_A - \frac{d}{2}\theta_A, \qquad k = 10,11,12,13 \tag{6.3}$$

These equations express all the '$u$' displacements of the upper edge nodes in terms of the displacement $u_A$ and rotation $\theta_A$ of the point A. This constraint condition can be defined by writing a user-subroutine in the MARC program.

The average curvature of the stub-column can be calculated from

$$\Phi = 2\theta_A / a \tag{6.4}$$



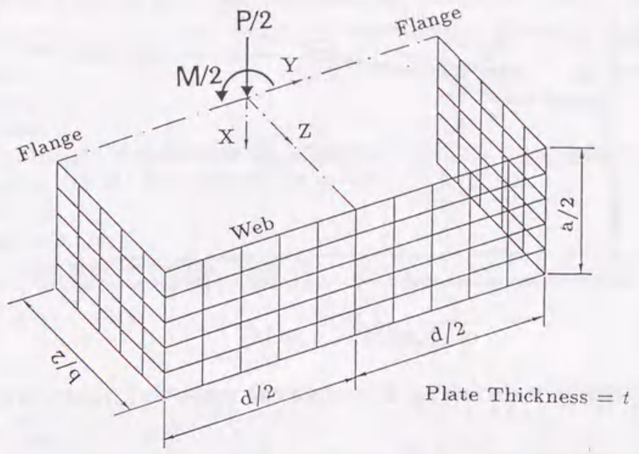


**Fig. 6.3 FEM Mesh used in the Analysis**

where $a$ is the stub-column length (see **Fig. 6.1**). The moment, $M$, is obtained as the reaction force at the beam end 'A'. The imposed rotation is successively increased until the desired curvature is attained.

The finite element mesh used in the analysis is as shown in **Fig. 6.3**. In this study, square and rectangular box-sections (the depth-to-breadth ratio, $d/b$, is 0.75) were considered. And the length of the column, $a$, was adopted to be $0.7b$ due to the fact that this value generally provides the lowest ultimate strength (Bradfield 1982). The web plate was discretized into 50 finite elements, while the number of elements in each half of the flange plate was 25. The residual stress pattern for each component plate is the well-known rectangular shape distribution, as was used in the analysis of the concrete-filled steel box column under pure compression (**Fig. 3.3**). The value of compressive residual stress, $\sigma_{rc}$, was adopted to be $0.25\sigma_y$ that is around the average value of measured residual stresses (*Guidelines* 1987). The initial out-of-flatness was assumed to be sinusoidal in both flange and web plates. The maximum initial flange and web deflections used were $b/500$ that is around the average value of measured initial deflections (*Guidelines* 1987). Here, $b$ is the flange plate width.

Based on the uniaxial tension test, a strain hardening model was proposed to rationally describe the strain hardening behavior of the structural steel of grade SS400.

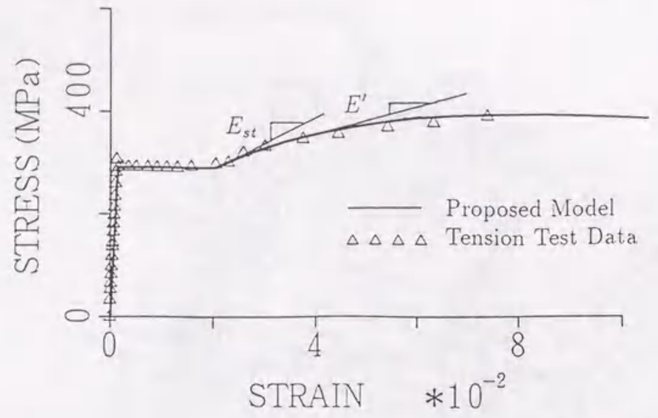


**Fig. 6.4 Stress-Strain Relationship Including the Effect of Strain-Hardening**

The proposed equation for the strain hardening coefficient $E'$ is as follows:

$$E' = (E_{st} - E_r)exp[-a(\varepsilon - \varepsilon_{st})] + E_r \tag{6.5}$$

where $E_{st}$ = initial strain hardening coefficient, $E_r$ = residual strain hardening constant, $a$ = strain hardening index, $\varepsilon$ = total strain, $\varepsilon_{st}$ = strain at the onset of strain hardening. By fitting the tension test data, these constants are determined as follows: $E_{st} = E/25.0$; $E_r = E_{st}/5.0$; $\varepsilon_{st} = 10.0\varepsilon_y$; and $a = 30.0$. Here, $E$ is the modulus of elasticity, and $\varepsilon_y$ is the yield strain. Equation (6.5) is applicable in the range of $0.0 \leq \varepsilon \leq 10.0$ %.

### 6.2.2 Moment-Curvature Relations

The moment, $M$, axial load, $P$, and curvature $\Phi$ were nondimensonalized with the quantities $M_y$, $P_y$, and $\Phi_y$ respectively. That is,

$$m = \frac{M}{M_y}, \quad p = \frac{P}{P_y}, \quad \varphi = \frac{\Phi}{\Phi_y} \tag{6.6}$$

where $M_y$ is yield bending moment ($=W\sigma_y$); $P_y$ is squash load ($=A_s\sigma_y$); and $\Phi_y$ is yield curvature ($=M_y/EI$).

To systematically study the moment-curvature relation of locally buckled steel box columns, elastic-plastic large-displacement analyses have been conducted on the columns with three different values of the width-thickness ratio parameter ($R$). The input data are summarized in **Table 6.1**.



**Table 6.1 Input Data for Analyses of Steel Box Stub-Columns**

| | |
|---|---|
| Modulus of Elasticity, $E$ | 206 GPa (21000 kgf/mm$^2$) |
| Yield stress, $\sigma_y$ | 235 MPa (24 kgf/mm$^2$) |
| Poisson Ratio, $\nu$ | 0.3 |
| Plate thickness, $t$ | 4.5 |
| Width-thickness ratio parameter of flange plate, $R$ | 0.200, 0.450, 0.616, 0.821, and 1.232 |
| Depth/breadth, $d/b$ | 0.75, 1.0 |
| Aspect ratio, $l/b$ | 0.7 |
| Residual stress, $\sigma_{rc}/\sigma_y$ | 0.25 |
| Maximum initial plate deflection, $\Delta_p/b$ | 1/500 |

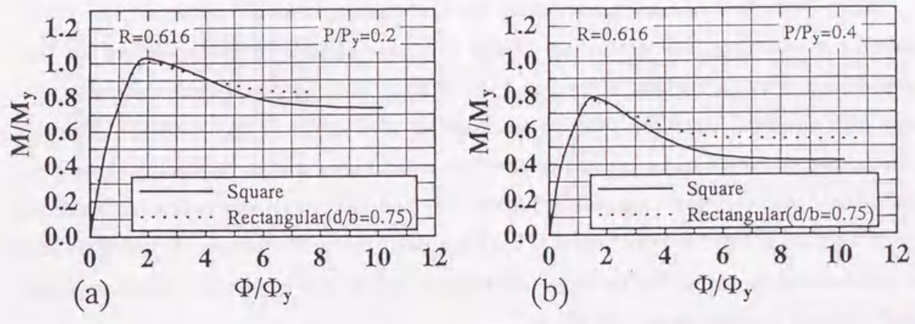


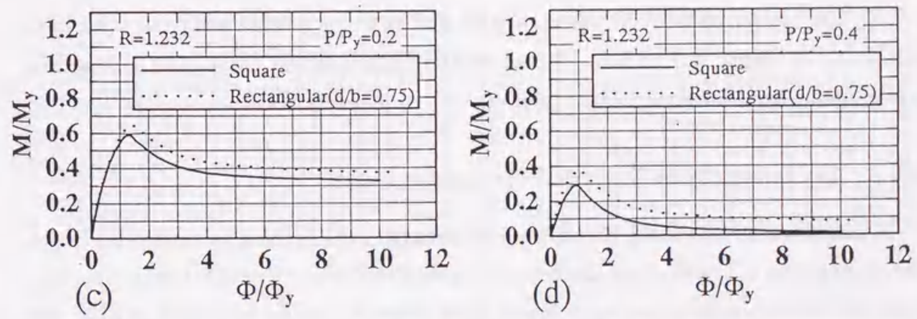


**Fig. 6.5 Computed Moment versus Curvature Curves — Effect of Cross-Sectional Shape**

The difference in the cross-sectional shape (i.e., square and rectangular) was first investigated. The ratios of depth ($d$) to breadth ($b$) considered were 0.75 and 1.0. **Fig. 6.5** is the computed $m$-$p$-$\varphi$ curves for the cases of $R = 0.616$ and $R = 1.232$ when

the axial force $P/P_y$ is 0.2 or 0.4. For the case of $R = 0.616$, the maximum strength is almost same for the rectangular and square shapes, but post-buckling strength is larger for the rectangular shape than that for the square shape. For the case of $R = 1.232$, both maximum and post-buckling strengths are smaller for the square shape than that for the rectangular shape. It was also found that the difference in the cross-sectional shape becomes noticeable as the width-thickness ratio and the axial thrust increase. These observations suggest that the proposed $m$-$p$-$\varphi$ approximate formula, which is given later, based on the analyses of the stub-columns of square box shapes is applicable for the practical designs, since the usual values of the parameter $R$ of existing bridge piers are less than 0.7.

Next, the effect of strain hardening on the elastic-plastic behavior of the stub-column is examined. The relatively large influence of the strain hardening on the post-buckling behavior can be seen in **Fig. 6.6**. It may be noted that this influence was also observed near the peak in the case of $R = 0.450$ [**Fig. 6.6(b)**]. Having this fact in mind it can be concluded that the effect of the strain hardening should be considered in the analysis, especially for the columns with small width-thickness ratios. As is seen from **Fig. 6.6(a)**, no local buckling occurred in the case of $R = 0.200$, and it will be used to obtain the moment-curvature relation for a steel box column segment *without local buckling* in section 6.2.6.

All the computed $M$-$P$-$\Phi$ curves of steel box columns plotted with the solid lines are shown in **Figs. 6.7** to **6.9**. As can be seen in the figure, there exist descending parts due to local buckling in all cases.

### 6.2.3 Evaluation of Pure Compression Strength of Plates

A set of formulas relating effective-width strength were derived as functions of both the magnitudes of initial out-of-flatness ($\Delta_p/b$) and compressive residual stress ($\sigma_{rc}/\sigma_y$) from an elastic-plastic large-displacement finite element analysis by Usami (1993). For simply supported plates in compression, the proposed ultimate strength formula is as follows:

$$\frac{P_u}{P_y} = \frac{1}{2R}[\beta - \sqrt{\beta^2 - 4R}] \tag{6.7}$$

in which



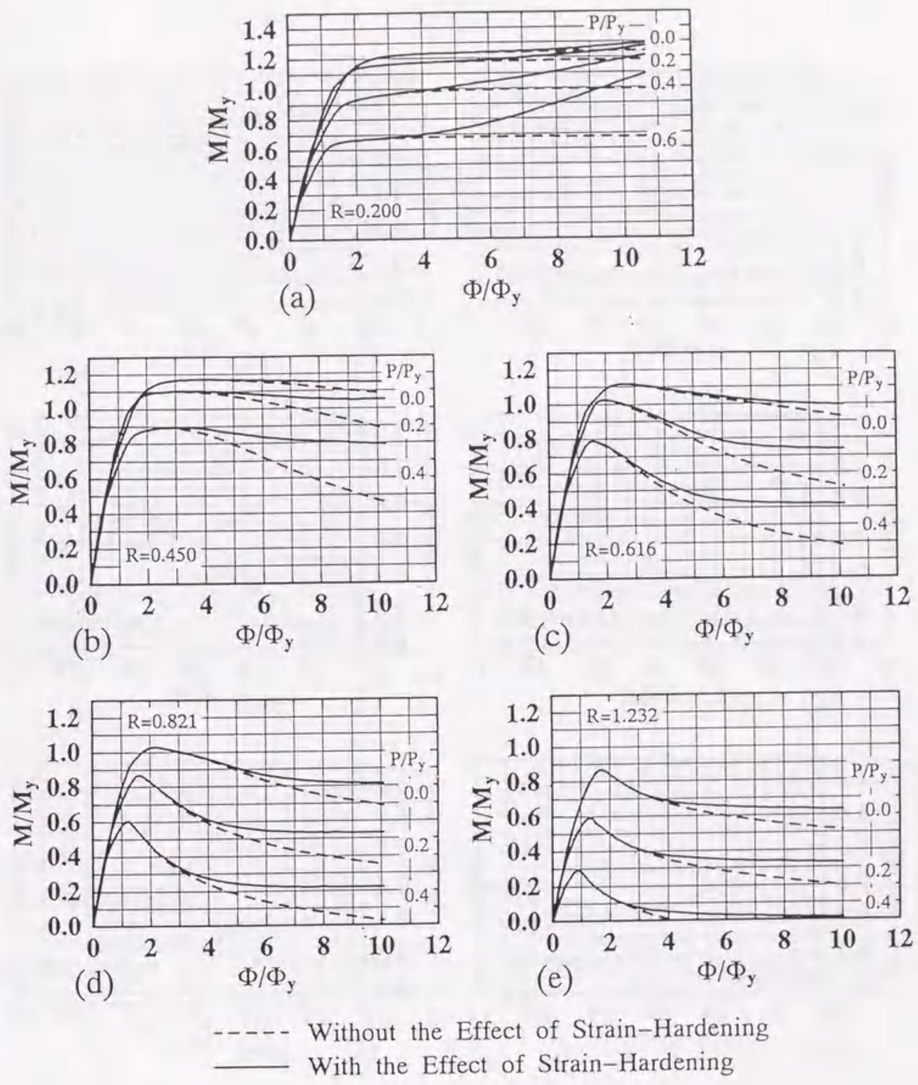


**Fig. 6.6 Computed Moment versus Curvature Curves — Effect of Strain-Hardening**

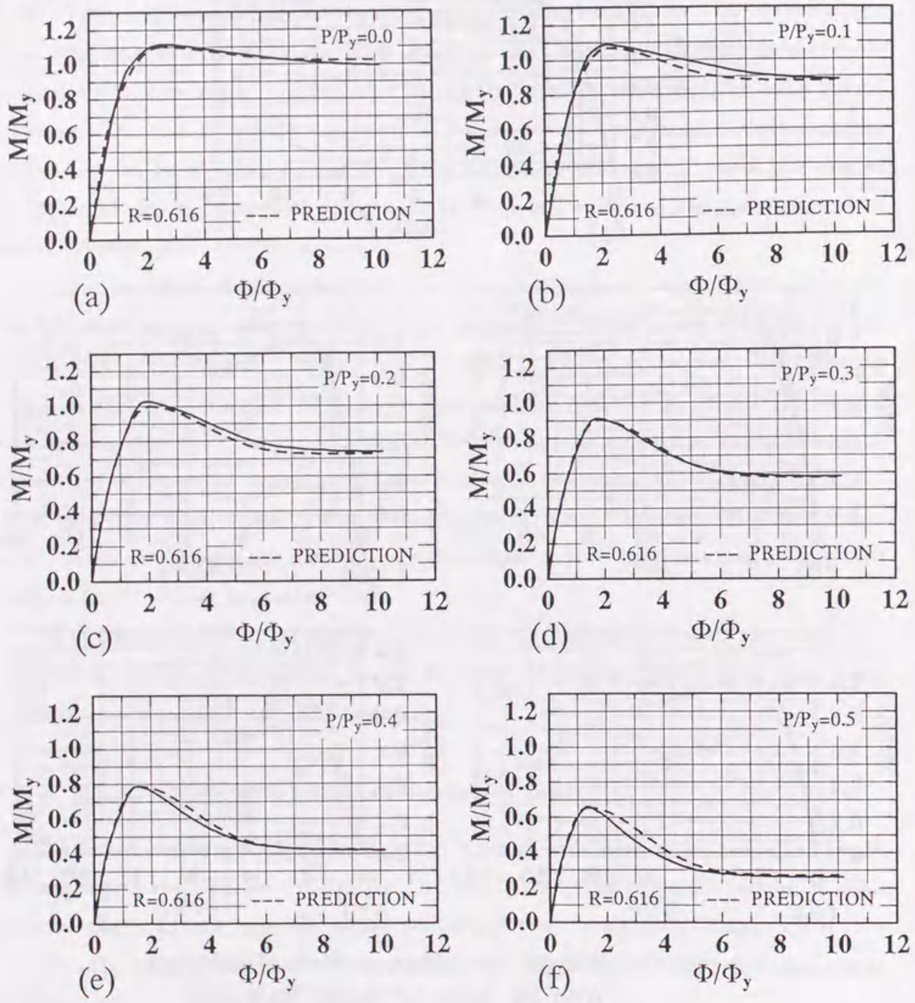


Fig. 6.7 Computed Moment versus Curvature Curves: $R$=0.616



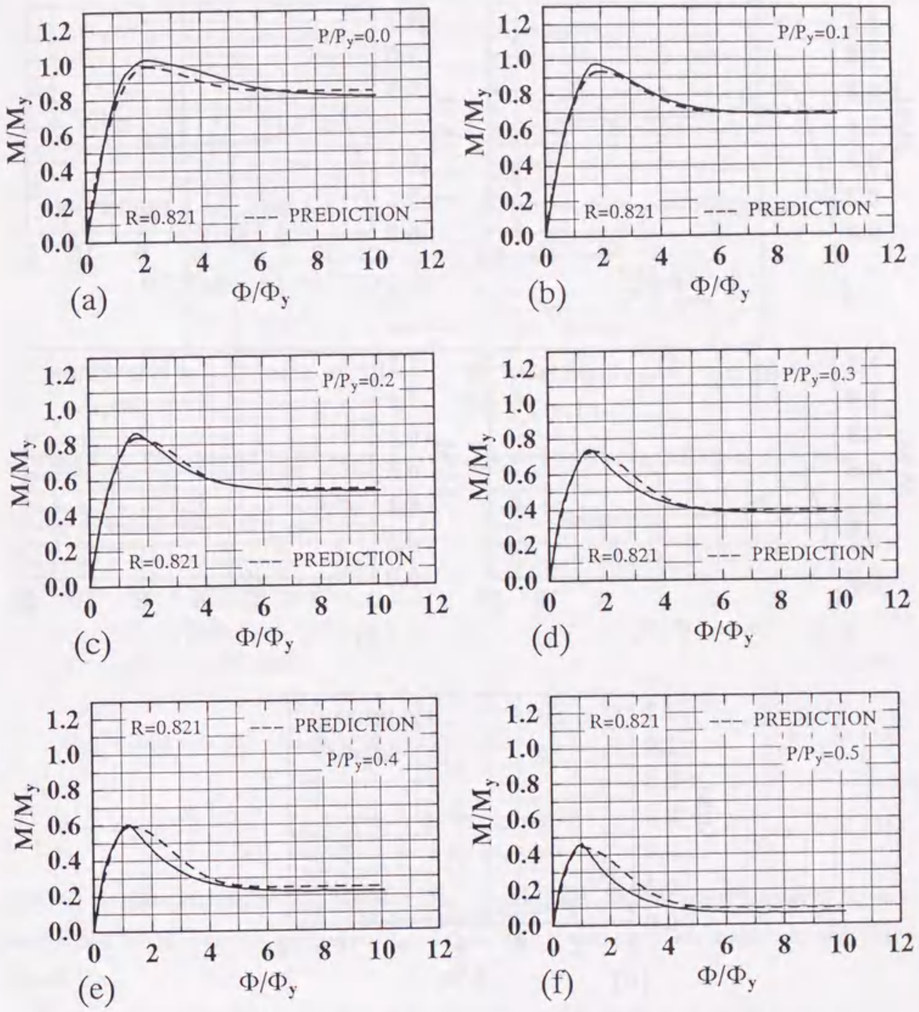


Fig. 6.8 Computed Moment versus Curvature Curves: $R$=0.821

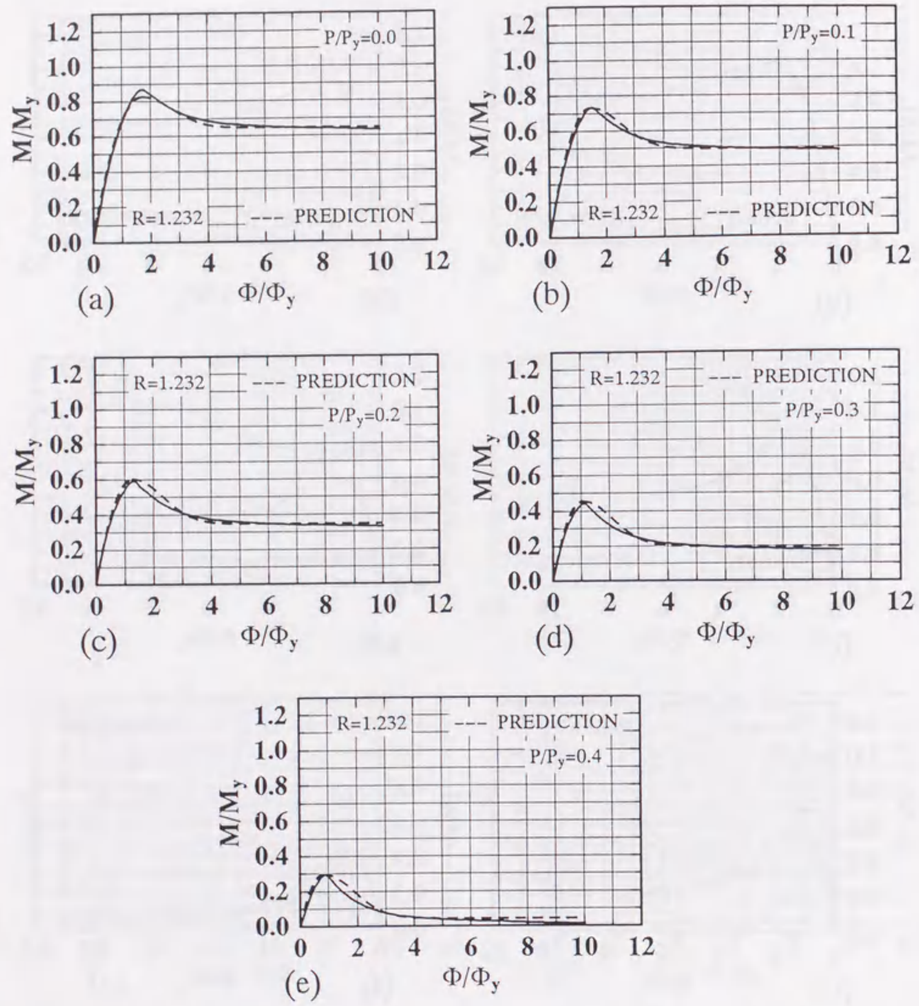


Fig. 6.9 Computed Moment versus Curvature Curves: $R$=1.232



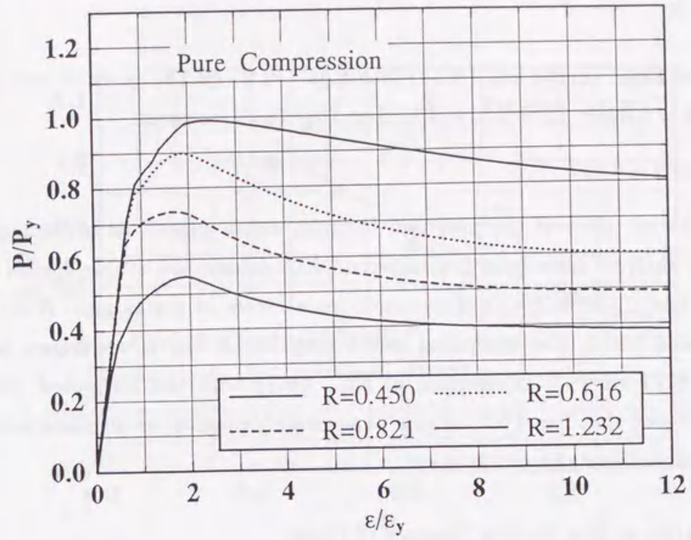


Fig. 6.10 Computed Load versus Average-Strain Curves of Stub-Columns

$$\beta = 1 + \overline{\alpha} \cdot (R - R_o) + R \tag{6.8}$$

$$R_o = A - B \cdot ln(\frac{\Delta_p}{b}) \leq 0.0 \tag{6.9}$$

$$A = -0.05 - 0.542 \cdot exp(-11.9\frac{\sigma_{rc}}{\sigma_y}) \tag{6.10}$$

$$B = +0.09 - 0.107 \cdot exp(-12.4\frac{\sigma_{rc}}{\sigma_y}) \tag{6.11}$$

$$\overline{\alpha} = -157(\frac{\Delta_p}{b})(\frac{\sigma_{rc}}{\sigma_y}) + 43(\frac{\Delta_p}{b}) + 1.2(\frac{\sigma_{rc}}{\sigma_y}) + 0.03 \tag{6.12}$$

Here, $R$ = plate slenderness parameter (i.e., width-thickness ratio parameter); $R_o$ = normalized plate slenderness parameter below which the plate strength reaches the squash load.

As described previously, the maximum initial out-of-flatness and compressive residual stress used in the analysis are

$$\frac{\Delta_p}{b} = \frac{1}{500} \tag{6.13}$$

$$\frac{\sigma_{rc}}{\sigma_y} = 0.25 \tag{6.14}$$

Substitution of **Eqs. (6.13)** and **(6.14)** into **Eqs. (6.9)-(6.12)** gives: $\overline{\alpha} = 0.338$; $A = -0.0777$; $B = 0.0948$; $R_o = 0.511$; and then **Eq. (6.8)** becomes:

$$\beta = 1.338R + 0.827 \tag{6.15}$$

To show the accuracy of the proposed formula, elastic-plastic large-displacement finite element analyses have been conducted on four square box stub-columns under pure compression. The width-thickness ratio parameters of plates are: $R = 0.450$, 0.616, 0.821, and 1.232. The computed load-average strain curves are shown in **Fig. 6.10**. **Fig. 6.11** shows a comparison of **Eq. (6.7)** with the computed ultimate strengths. It is seen that **Eq. (6.7)** is able to accurately predict the ultimate strengths of steel box stub-columns in compression.

### 6.2.4 Evaluation of Pure Bending Strength of Plates

For the plates under pure bending, ultimate strengths can be predicted using the following empirical formula proposed by Usami et al. (1985).

$$\frac{M_u}{M_p} = \frac{(2+3/\alpha)(b_e/b)+2+\alpha}{4+\alpha+3/\alpha} \leq 1.0 \tag{6.16}$$

where $M_u$ = ultimate bending strength; $M_p$ = full plastic bending moment. And $\alpha$ = (d/b)(w/t) = 1.0 for square box sections. Since $b_e/b$ in the above equation is the effective width of compression flange plate at the ultimate state, it should be replaced by **Eq. (6.7)**. Therefore, the proposed ultimate strength formula of a square box column becomes:

$$\frac{M_u}{M_p} = \frac{5}{8}\left(\frac{P_u}{P_y}\right) + \frac{3}{8} \tag{6.17}$$

This equation is plotted against the parameter $R$ in **Fig. 6.12**, and it agrees well with the computed results.

### 6.2.5 Interaction Curve of Locally Buckled Steel Box Columns

An interaction curve could be established in a nondimensional form

$$\left(\frac{P}{P_u}\right)^n + \left(\frac{M}{M_u}\right)^m = 1.0 \tag{6.18}$$



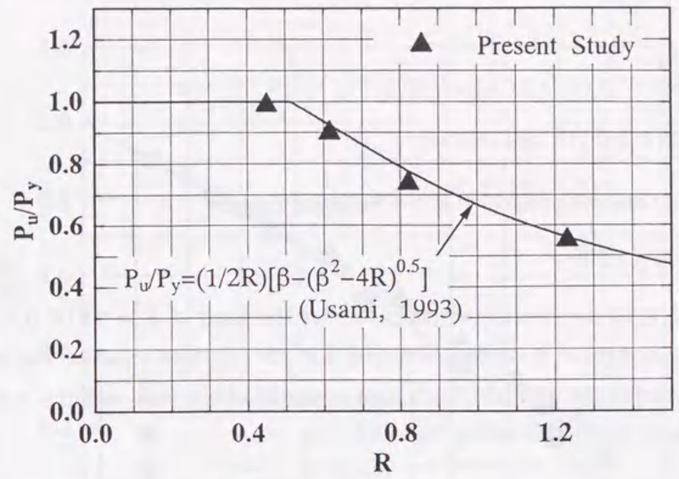


Fig. 6.11 Comparison of Computed Maximum Strength and Proposed Strength Formula—Pure Compression

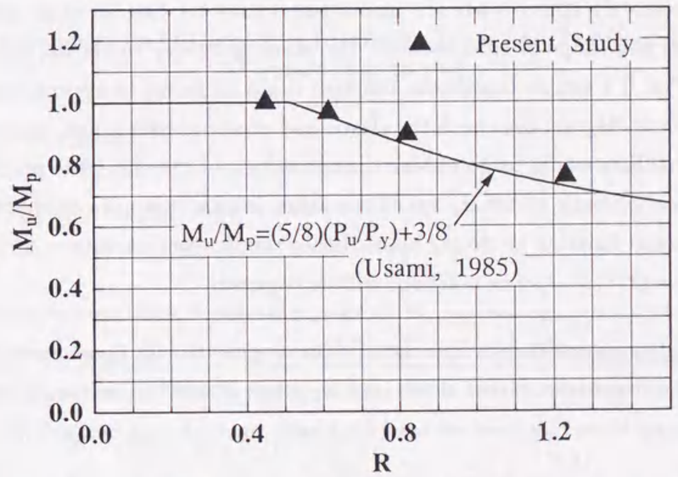


Fig. 6.12 Comparison of Computed Maximum Strength and Proposed Strength Formula—Pure Bending

in which two constants ($n$ and $m$) can be determined using the nonlinear least square method (Marquardt 1963). They are related to the width-thickness ratio parameter $R$ as follows:

$$n = \frac{1.333}{R^{0.401}} \tag{6.19}$$

$$m = 0.271R + 0.719 \tag{6.20}$$

These two equations are applicable in the following range:

$$0.511 \leq R \leq 1.500 \tag{6.21}$$

Shown in **Fig. 6.13** are the interaction curves for the cases of $R = 0.616$, 0.821, and 1.232. From these figures, it can be concluded that the proposed equation can be used to accurately predict the ultimate interaction strengths of box stub-columns subjected to combined axial load and bending moment.

### 6.2.6 Approximate Expressions of $m$-$p$-$\varphi$ Curves

An analytical stability theory requires that a reasonably simple analytical expression be found to accurately approximate the moment-curvature relation for each combination of material and shape of cross section. The stability theory would be, of course, greatly simplified if a simple continuous function could be found to approximate the moment-curvature diagram over both the elastic and elastic-plastic range, since under these conditions there would be no sudden discontinuity and therefore, the problem of locating the elastic-plastic boundary would not arise. In case it is not possible to find a single continuous function to closely approximate the moment-curvature curve over the complete range, two or more functions will be required.

Approximate $m$-$p$-$\varphi$ Expressions for Steel Box Column Segments *with Local Buckling*

According to the characteristics of the $m$-$p$-$\varphi$ curves obtained from numerical analyses, the following three functions are used for locally buckled steel box columns.

$$m = \varphi \tag{6.22}$$

for $0.0 \leq \varphi \leq \varphi_1$;

$$m = -a_o\varphi^2 + b_o\varphi + c_o \tag{6.23}$$



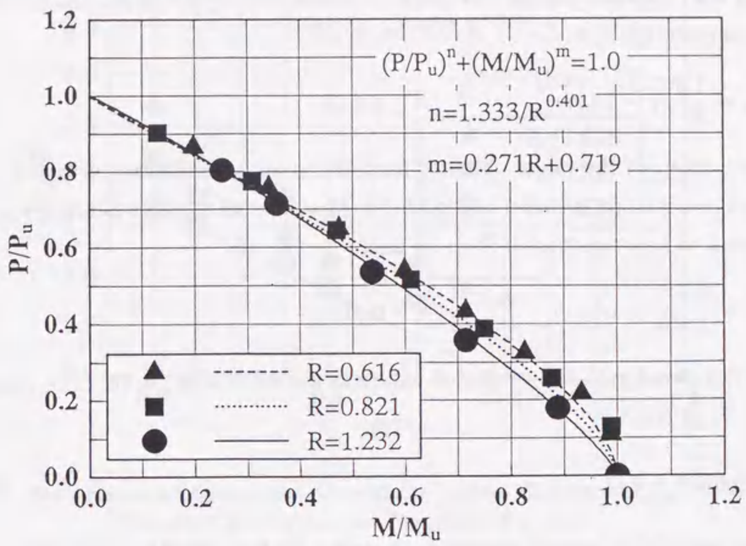


**Fig. 6.13 Comparison of Computed Maximum Loads and Proposed Interaction Formula [Eq. (6.18)]**

for $\varphi_1 \leq \varphi \leq \varphi_m$; and

$$m = (m_m - m_r)exp[-d_o(\varphi - \varphi_m)^2] + m_r \tag{6.24}$$

for $\varphi_m \leq \varphi$.

In the above equations, 9 quantities, namely $m_1$, $\varphi_1$, $m_m$, $\varphi_m$, $m_r$, $a_o$, $b_o$, $c_o$ and $d_o$, are to be determined apriori. It is found that the linear elastic range varies with the values of parameters $p(=P/P_y)$, $\sigma_{rc}/\sigma_y$ and $R$, and it can be expressed in the form

$$\varphi_1 = 1 - \frac{P}{P_y} - \frac{\sigma_{rc}}{\sigma_y} - \frac{R - 0.511}{R} \geq 0.0 \qquad (R \geq 0.511) \tag{6.25}$$

and

$$m_1 = \varphi_1 \tag{6.26}$$

On the other hand, the maximum bending strength, $m_m$, for an arbitrary axial force, $p$, can be obtained from the ultimate strength interaction formula proposed previously. By fitting the computed results, the curvature corresponding to the maximum bending moment is given by

$$\varphi_m = \frac{1.902}{R^{0.511}} - 2.167p \qquad (R \geq 0.511) \tag{6.27}$$

and a comparison of the values obtained from the computed moment-curvature curves and the above equation is shown in **Fig. 6.14**. Moreover, the remain bending moment, $m_r$, is found to be a function of $R$ and $p$ as

$$m_r = \frac{0.742}{R^{0.663}} - 1.500p \qquad (R \geq 0.511) \tag{6.28}$$

and it is compared with the computed values as shown in **Fig. 6.15**. The softening constant, $d_o$, is given by

$$d_o = 0.5R - 0.17 \tag{6.29}$$

The other material constants, namely $a_o$, $b_o$ and $c_o$ in **Eq. (6.23)** can be determined by solving the equation with the aid of three boundary conditions:

$$m|_{\varphi=\varphi_1} = m_1 \tag{6.30}$$

$$m|_{\varphi=\varphi_m} = m_m \tag{6.31}$$

$$\left.\frac{dm}{d\varphi}\right|_{\varphi=\varphi_m} = 0 \tag{6.32}$$

Thus, $a_o$, $b_o$ and $c_o$ are given by

$$a_o = \frac{m_m - m_1}{(\varphi_m - \varphi_1)^2} \tag{6.33}$$

$$b_o = \frac{2\varphi_m(m_m - m_1)}{(\varphi_m - \varphi_1)^2} \tag{6.34}$$

$$c_o = m_1 + \frac{\varphi_1^2(m_m - m_1)}{(\varphi_m - \varphi_1)^2} - \frac{2\varphi_m\varphi_1(m_m - m_1)}{(\varphi_m - \varphi_1)^2} \tag{6.35}$$



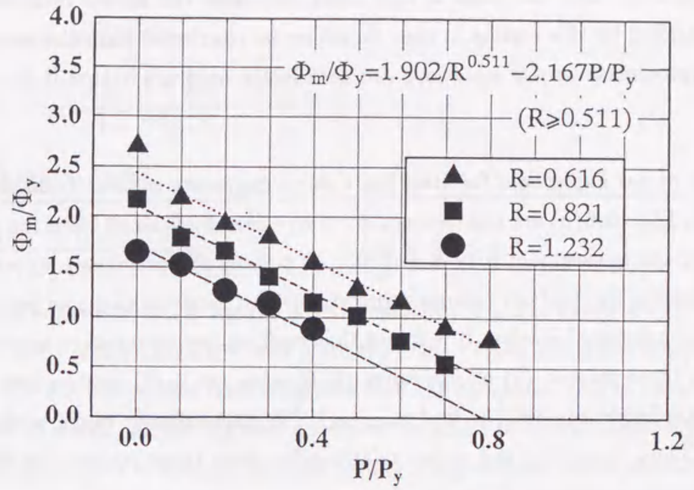


Fig. 6.14 Comparison of Computed Curvature Values Corresponding Maximum Bending Strengths and Proposed Formula

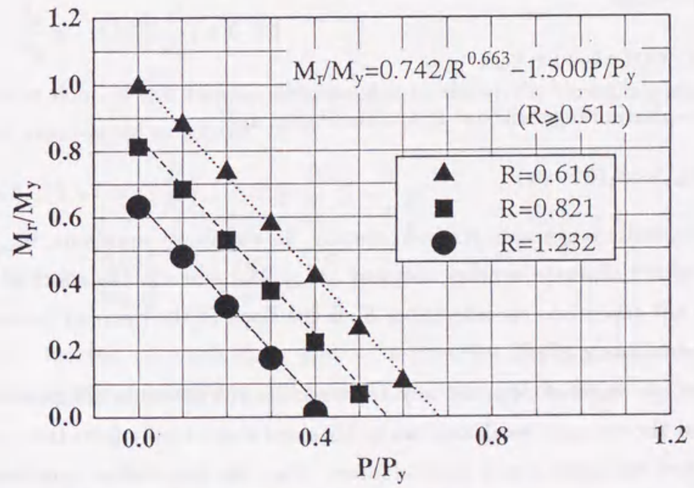


Fig. 6.15 Comparison of Computed Remain Bending Moments and Proposed Formula

The predicted $m$-$p$-$\varphi$ curves are also shown in **Figs. 6.7** to **6.9** by the dashed lines. Since the behavior near the peak is very important, and the failure of a column is usually controlled by this regime, it can, therefore, be concluded from the comparison that the approximate $m$-$p$-$\varphi$ equations are sufficiently accurate and will be of great use.

Approximate $m$-$p$-$\varphi$ Expressions for Steel Box Column Segments *without Local Buckling*

Shown in **Fig. 6.6(a)** are the moment-curvature curves obtained from the analysis of a steel box column segment with $R = 0.200$. As pointed out previously, approximate $m$-$p$-$\varphi$ expressions for steel box column segments without local buckling can be obtained by fitting the computed results. It is found that each moment-curvature curve can be divided into three ranges: (1) elastic range $(0, 0) \rightarrow (m_1, \varphi_1)$; (2) elasto-plastic range without strain-hardening $(m_1, \varphi_1) \rightarrow (m_{pcz}, \varphi_h)$; (3) elasto-plastic range with strain-hardening. Thus, to predict the $m$-$p$-$\varphi$ relations for these three ranges, the following three expressions are required:

$$m = \varphi \tag{6.36}$$

for the elastic range;

$$m = b_n \cdot exp(-a_n \varphi) + m_{pcz} \tag{6.37}$$

for the elasto-plastic range without strain-hardening; and

$$m = m_{pcz} + S_h(\varphi - \varphi_h) \tag{6.38}$$

for the elasto-plastic range with strain-hardening. In the above equations, $m_{pcz}$ is the nondimensionlized ultimate bending moment ($M_{pcz}/M_y$) wherein the effect of strain-hardening is not taken into consideration; $S_h$ is the slope of the moment increase due to the strain-hardening effect.

Generally, the value of $M_{pcz}$ for any cross section subjected to compression and bending about the strong or weak axis can be obtained theoretically from the equations of equilibrium of the internal and external forces. Since the box section considered here is square, the ultimate bending moments about strong and weak axes are the same. In the case of a box section under consideration, the value of $M_{pcz}$ is computed about $z$ axis (see **Fig. 6.3**). Hence, the ultimate bending moment, $M_{pcz}$, for arbitrary



axial force, $P/P_y$, can be easily calculated from the following equations (*Plastic* 1971; *Guidelines* 1987):

Neutral axis in web

$$\frac{M_{pcz}}{M_p} = 1 - \frac{[(\frac{P}{P_y})(1 + \frac{B}{D})]^2}{1 + \frac{2B(D+t)}{D^2}} \qquad 0 \leq \frac{P}{P_y} \leq \frac{1}{1 + \frac{B}{D}} \tag{6.39}$$

Neutral axis in flange

$$\frac{M_{pcz}}{M_p} = \frac{2(\frac{D+t}{D})(1 - \frac{P}{P_y})(1 + \frac{B}{D})}{1 + (1 + \frac{D+2t}{D})(\frac{B}{D})} \qquad \frac{1}{1 + \frac{B}{D}} \leq \frac{P}{P_y} \leq 1.0 \tag{6.40}$$

In the above equations, $M_p$ is the full plastic moment; $B$ is the flange width; $D$ is the web width and $t$ is the flange and web plate thickness. These equations are plotted in **Fig. 6.16** for the case of $R = 0.200$ together with the computed results obtained from the analysis of a box column segment in which the effect of strain-hardening was not taken into account. It is evident that the results computed by elasto-plastic analyses can be precisely predicted by theoretical equations (6.39) and (6.40).

By fitting the computed $m$-$p$-$\varphi$ curves, it was found that the values of $\varphi_h$ is a function of the axial force $p$ and given by

$$\varphi_h = \frac{\Phi_h}{\Phi_y} = -4.802(\frac{P}{P_y}) + 6.135 \tag{6.41}$$

Moreover, the slope of the moment increase due to the strain-hardening effect is approximately represented as follows.

$$S_h = 0.010 + 0.050(\frac{P}{P_y}) \qquad 0 \leq \frac{P}{P_y} \leq \frac{1}{1 + \frac{B}{D}} \tag{6.42}$$

$$S_h = 0.010 + \frac{0.050}{1 + \frac{B}{D}} \qquad \frac{1}{1 + \frac{B}{D}} \leq \frac{P}{P_y} \leq 1.0 \tag{6.43}$$

Furthermore, the two parameters, $a_n$ and $b_n$ in equation (6.37), can be determined easily by solving this equation with the help of the continuity condition at the yielding $(m_1, \varphi_1)$:

$$m|_{\varphi=\varphi_1} = m_1 \tag{6.44}$$

$$\left.\frac{dm}{d\varphi}\right|_{\varphi=\varphi_1} = 1 \tag{6.45}$$

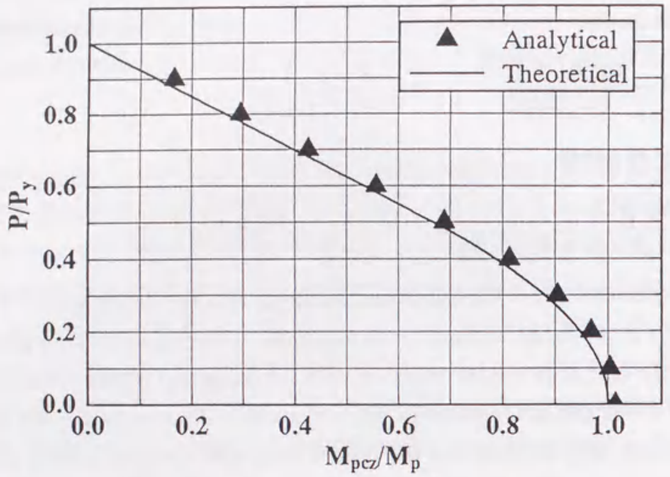


Fig. 6.16 Comparison of Computed Maximum Loads and Interaction Formula (Local Buckling is Ignored)

Thus, $a_n$ and $b_n$ are given by

$$a_n = \frac{1}{m_{pcz} - m_1} \tag{6.46}$$

$$b_n = -\frac{m_{pcz} - m_1}{e^{-m_1/(m_{pcz}-m_1)}} \tag{6.47}$$

The computed and predicted $m$-$p$-$\varphi$ curves are compared in **Fig. 6.17**. It can be seen that both curves are in good agreement for each case.



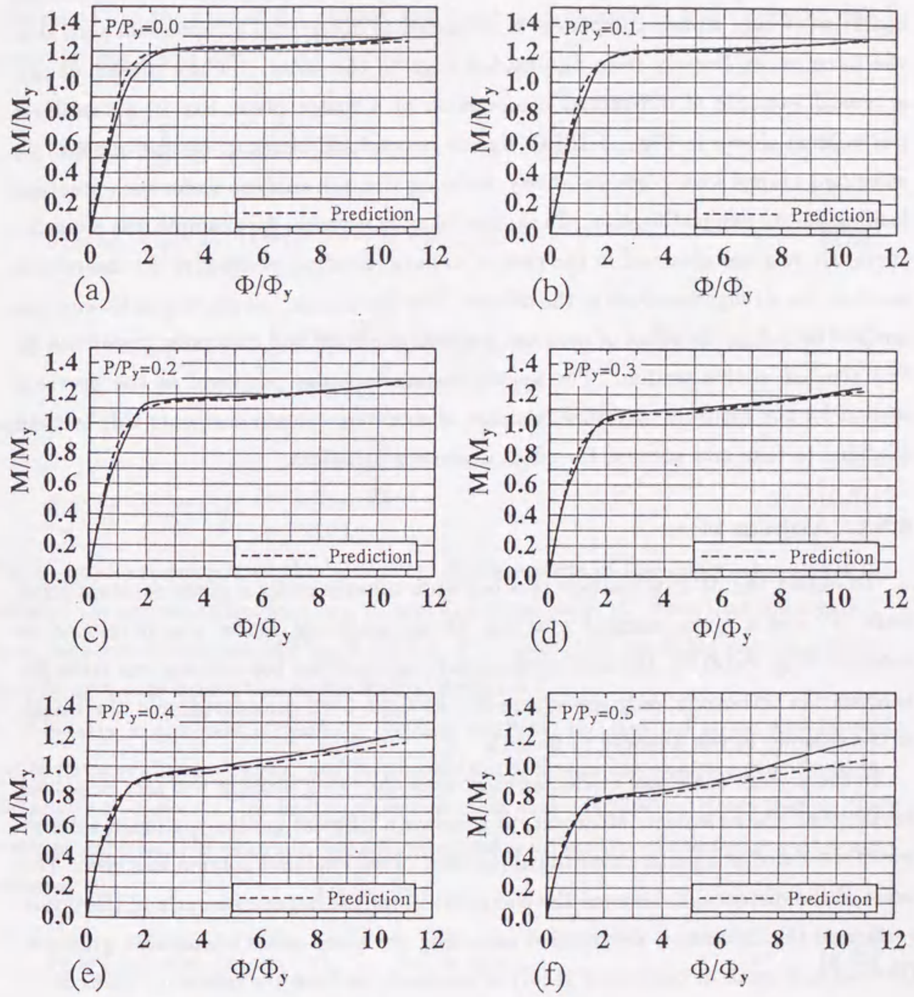


Fig. 6.17 Comparison of Computed and Predicted $m$-$p$-$\varphi$ curves (Local Buckling is Ignored)

## 6.3 Moment-Curvature Relations for Steel Box Column Segments under Moment Gradient

During the service life of plated structures, it is not difficult to conceive of loading conditions where a plate component is subjected to differential compression such that the force varies linearly from one loaded edge to the other. In the present study, a typical example of differential compression of a flange plate, say in a cantilever box column shown in **Fig. 6.18(a)**, due to nonuniform bending, can be quoted. To safeguard against local plate instability, buckling strength analysis under such practical loading has its own justification. To the best of an knowledge, for example, the moment-curvature relation obtained in the case of uniform bending would give a conservative result in the strength analysis of the column. For this reason, the elasto-plastic analysis method including the effect of moment gradient of a steel box column segment will be first treated in this section. The approximation formulas proposed in the previous section for the moment-curvature relations of steel box column segments will be then modified to take into account the effect of moment gradient.

### 6.3.1 Analytical Model

To obtain the $M$-$P$-$\Phi$ relation of a box stub-column under a given constant axial force, $P$, and a given moment gradient, $G$, an analytical model was developed as shown in **Fig. 6.18(b)**. Because of symmetry, only half the box column was taken for analysis. In this study, only the square box-sections were considered, and the length of the column, $a$, was adopted to be $0.7b$.

In the present analytical model, an eight-node thin shell element was also employed for the steel plate element. Moreover, to generate a moment gradient, a beam element which is located at a point above the upper edge of the analyzed column was used. The value of the distance, $\ell$, between the end point 'A' of the beam element and the upper surface of the column, is determined according the given value of moment gradient. Obviously, if small displacement theory is assumed, we have the following relation:

$$G = \frac{M_1}{M_2} = \frac{H \cdot \ell}{H \cdot (\ell + a)} \tag{6.48}$$

where $M_1$ and $M_2$ are the moments applied to the upper surface and lower surface, respectively [see **Fig. 6.18(a)**]. Note that the constant axial force is applied to the



upper surface of the column, and the lower edge of the column was fixed. On the other hand, the beam element was free at the top end, and connected at the point 'A' with the edge nodes of the column through some invisible rigid bars, namely some tying constraints. In the case of the present analytical model shown in **Fig. 6.18(b)**, the constraint equations are:

$$u_i = u_A - \frac{d}{2}\theta_A, \qquad i = 1, 2, ..., 6 \tag{6.49}$$

$$u_j = u_A + \frac{d}{10}(j - 11)\theta_A, \qquad j = 7, 8, ..., 15 \tag{6.50}$$

$$u_k = u_A + \frac{d}{2}\theta_A, \qquad k = 16, 17, ..., 21 \tag{6.51}$$

and

$$v_l = v_A + \ell\theta_A, \qquad l = 1, 2, ..., 21 \tag{6.52}$$

These equations express all the '$u$' and '$v$' displacements of the upper edge nodes in terms of the degrees of freedom ($u_A$, $v_A$ and $\theta_A$) of the point 'A'. Note that the rotation $\theta_A$ is negative in the case of **Fig. 6.18(b)**. This constraint condition can be defined by writing a user-subroutine in the MARC program.

Similarly in the case of uniform bending moment, the residual stress and initial out-of-flatness of plate panels, and strain-hardening of steel material are considered in the analysis. However, the initial plate deflection shape is different from that in the previous analysis. For example, the following initial deflections of the flange plates are assumed:

$$\delta_f = \delta_{f,max} sin(\frac{x}{a}\pi) cos(\frac{z}{b}\pi), \qquad for \;\; x \leq \frac{a}{2} \tag{6.53}$$

$$\delta_f = \delta_{f,max} \frac{1}{2}[1 - cos(\frac{2x}{a}\pi)] cos(\frac{z}{b}\pi), \qquad for \;\; \frac{a}{2} \leq x \leq a \tag{6.54}$$

where $\delta_{f,max} = b/500$ ($b$ is flange width). Similar equations are used for the web plate.

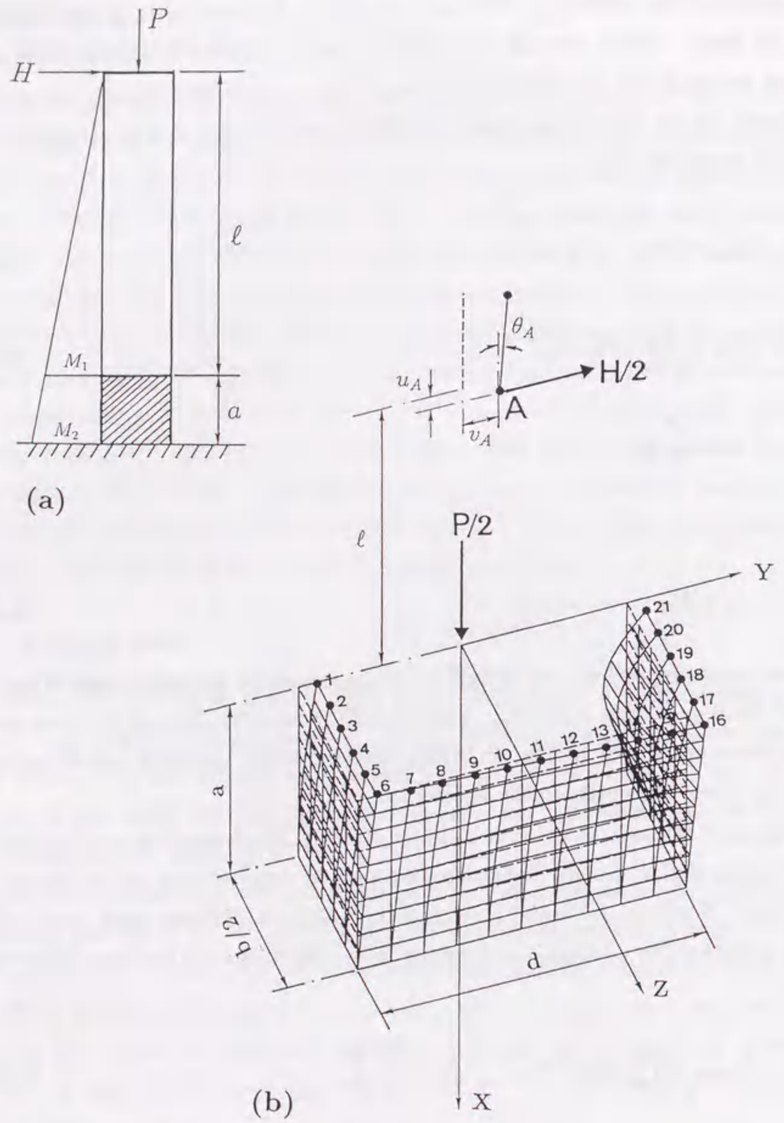


**Fig. 6.18 Analytical Model for Computing $M-P-\Phi$ Curves Including the Effect of Moment Gradient**



### 6.3.2 Numerical Results

In the discussion of numerical results, the moment, $M_2$, at the lower edge of the column segment will be used.

In order to check the accuracy of the present analytical model, the result of a box column segment is compared with the result of an entire column. The dimensions of the box column segment are: $b = 154.0$ mm, $d = 115.5$ mm, $t = 4.51$ mm ($R = 0.664$), and $a = 0.7b = 107.8$ mm. The distance between the lower end of the beam element and the upper edge of the segment is: $\ell = 654.2$ mm. On the other hand, the section dimensions of the entire column are completely the same as those of the column segment, and the height $h$ is taken to be 762 mm which is equal to the summation of $a$ and $\ell$.

**Fig. 6.19** shows the computed moment-curvature curve ($M/M_y$ - $\Phi/\Phi_y$) of the box column segment by the solid line, while the computed moment-curvature curve of the whole column by the dotted line. The moment was calculated by $M = H(\ell+a)$ in the former case, and by $M = Hh + P\Delta$ in the latter case. Here, $\Delta$ is the horizontal displacement at the column top. In the case of the whole column, the average curvature was obtained by $\Phi = (u_U+u_L)/(d \cdot a)$. As can be seen from **Fig. 6.19**, the numerical result of a box column segment using the present analytical model is shown to be in good agreement with the result by analyzing an entire column.

The $M$-$P$-$\Phi$ relations have been computed for the column segments having the same parameter values and material properties as in the uniform moment case of the previous section when the moment gradient $G$ is 0.6, 0.7, 0.8, and 0.9. It is found that the maximum bending moment is increased as the moment gradient is decreased, while the average curvature corresponding the maximum bending moment remains *unchanged*. In order to obtain the interaction formula including the effect of the moment gradient, the influence of the moment gradient on the maximum bending strength is investigated for different values of the width-thickness ratio parameter ($R$). As a result, it is found that the ultimate strength formula [**Eq. (6.17)**] under pure bending should be modified as follows:

$$\frac{M_u}{M_p} = \left[\frac{5}{8}\left(\frac{P_u}{P_y}\right) + \frac{3}{8}\right] f(G,R) \leq 1.0 \tag{6.55}$$

where $f(G,R)$ is a function of the moment gradient $G$ and width-thickness ratio pa-

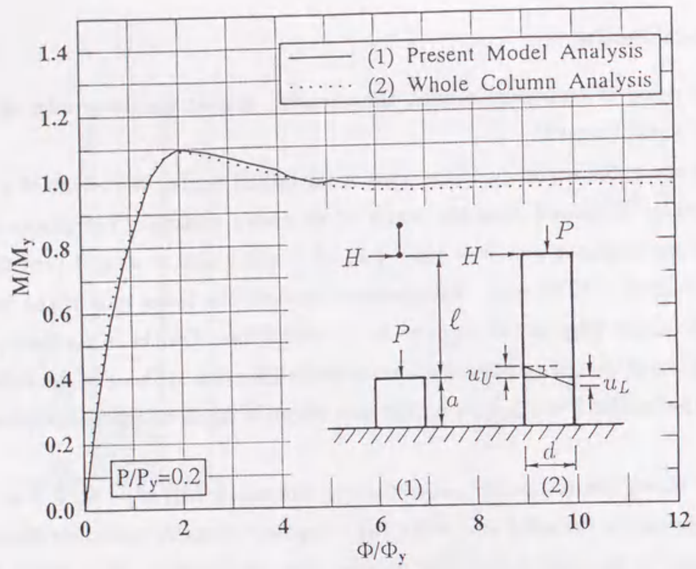


Fig. 6.19 Comparison of Present Model Analysis and Column Analysis

rameter $R$ in the form:

$$f(G,R) = 1.0 + 0.325R\sqrt{G - G^2} \tag{6.56}$$

This equation is obtained by fitting the computed maximum strengths as shown in **Fig. 6.20**. In this figure, the computed strengths are the relative values with respect to the uniform bending case ($G = 1.0$). **Fig. 6.21** shows a comparison of the modified ultimate bending strength formula [**Eq. (6.55)**] and the computed results. Based on this modification, an interaction curve [**Eq. (6.18)**] proposed in the previous section is shown in **Fig. 6.22** by comparison to the computed results in the cases of $R = 0.616$ and $R = 0.821$. It is seen that the proposed interaction formula is still applicable as long as the pure bending ultimate strength, $M_u$, is evaluated using the modified equation [**Eq. (6.55)**]. Furthermore, the $M$-$P$-$\Phi$ relations under moment gradient can be obtained using the approximation expressions proposed in the previous section.



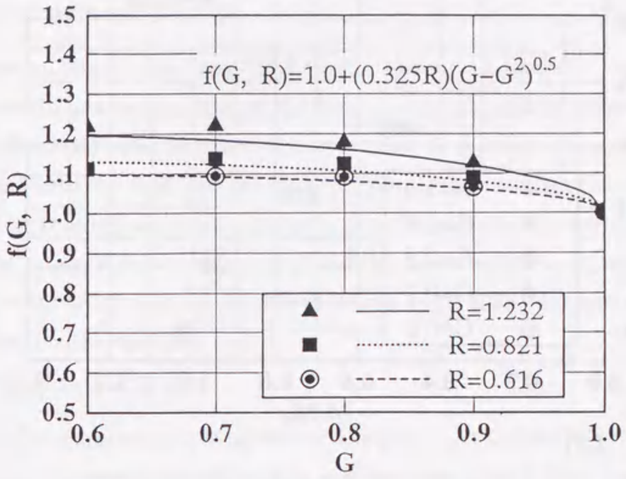


Fig. 6.20 Modification Factor f(G, R)

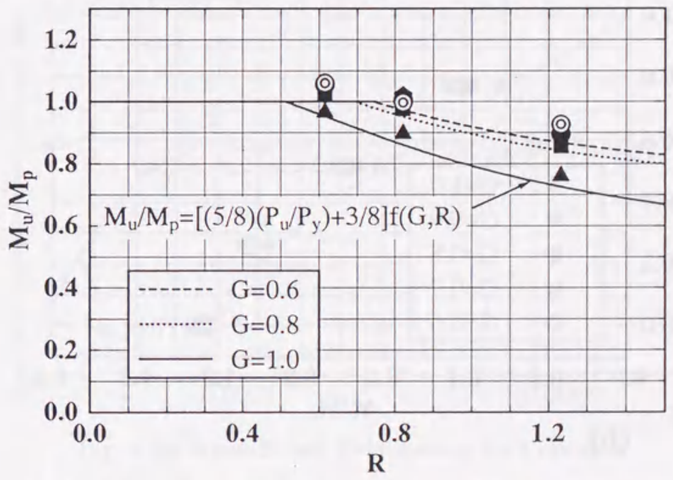


Fig. 6.21 Comparison of Modified Pure Bending Ultimate Strength Formula and Computed Results

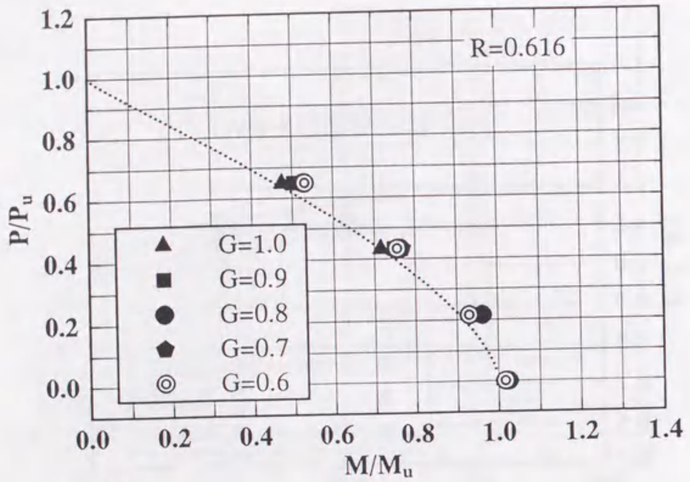


(a)

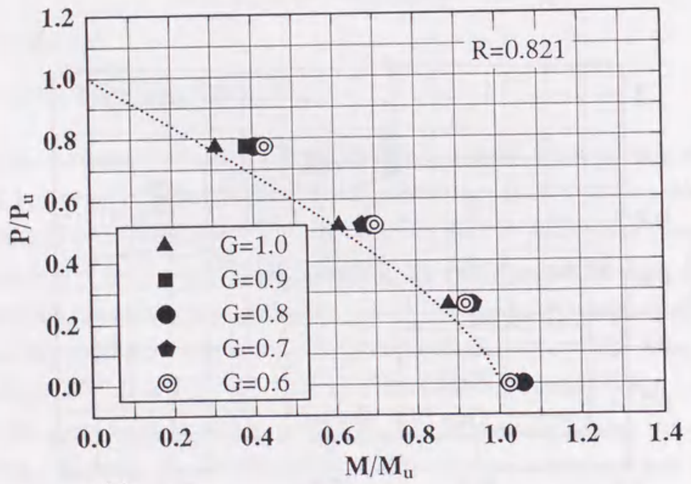


(b)

**Fig. 6.22 Comparison of Interaction Formula and Computed Results**



## 6.4 Moment-Curvature Relations for Concrete-Filled Steel Box Column Segments

### 6.4.1 Numerical Analysis Method

Since the concrete in a concrete-filled steel box column is laterally confined to some extent, the elastic-plastic behavior of the filled-in concrete will be different from that of the unconfined concrete. In this study, an increase in ductility is assumed due to the interaction between the steel and the concrete. On the basis of Burdtte and Hilsdrof's tests (1971) on confined concrete specimens, the ultimate concrete compressive strain, at which the concrete would be crushed, will be taken herein as $\varepsilon_u = 0.0060$. The stress-strain relation of concrete used is shown in **Fig. 6.23**. For the path 0-1, it is assumed to follow the equation

$$f_c = f_{ck}[2(\frac{\varepsilon_c}{\varepsilon_o}) - (\frac{\varepsilon_c}{\varepsilon_o})^2] \tag{6.57}$$

where $f_{ck}$ is the characteristic compressive strength. $\varepsilon_o$ is the strain corresponding to the maximum compressive strength ($f_{ck}$), and assumed to be 0.0023 regardless of the compressive strength (In fact, it varies slightly as the compressive strength changes, but the variation is ignored in this model).

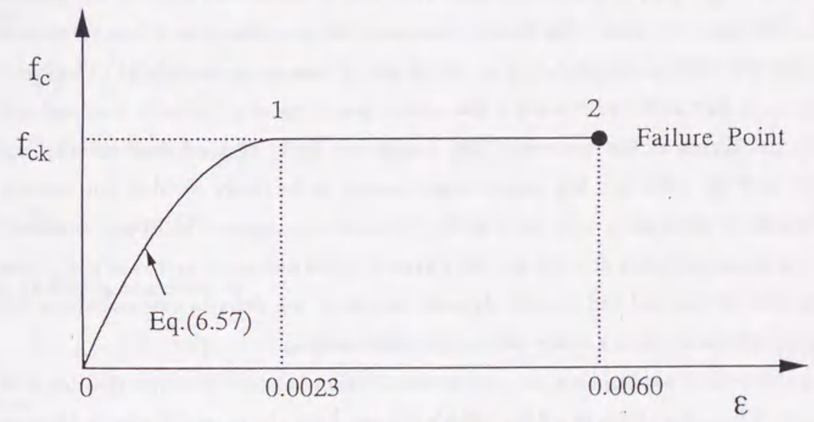


**Fig. 6.23 Stress-Strain Relationship for Concrete**

The $M$-$P$-$\Phi$ relation of the concrete-filled steel box column segments is computed without considering local buckling by a simplified numerical computation method instead of the one available in the MARC program. Since a detailed description of the

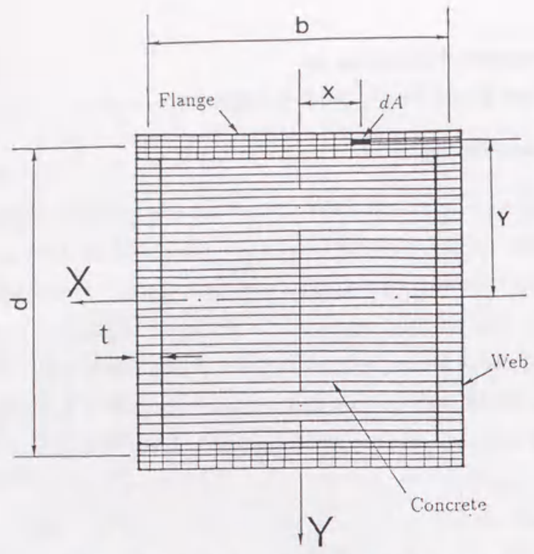


**Fig. 6.24 Fine Mesh for Concrete-Filled Steel Cross-Section**

computational procedure for constructing $M$-$P$-$\Phi$ curves is given elsewhere (Kakiuchi, 1988), only its outline is presented here.

Shown in **Fig. 6.24** is a concrete-filled steel box cross section used in the present analysis. The same residual stress distribution as in the analysis of steel box columns is assumed for the steel component, but no initial out-of-flatness is considered. The bending moment is assumed to be applied about the x-axis passing through the centroid, and the axial thrust at the centroid. The flanges are finely divided, horizontally and vertically, and the webs and the concrete are needed to be finely divided horizontally only. Because of symmetry, only one eighth of the column segment has been analyzed.

The basic assumptions are: (1) all the physical quantities such as stress and strain are computed at the centroid of each element, and they are definite everywhere in the element; (2) plane sections remain plane after deformation.

From the second assumption, the strain distribution is linear through the depth of the section. Thus, the strain in a fiber, which is away from the center line by a distance $y$, is given by

$$\varepsilon = \varepsilon_c + \Phi \cdot y + \varepsilon_r \tag{6.58}$$

where $\varepsilon_c$ = axial strain at the centroid; $\Phi$ = curvature; and $\varepsilon_r$ = residual strain.



The increment of strain is

$$\Delta\varepsilon = \Delta\varepsilon_c + \Delta\Phi \cdot y \tag{6.59}$$

Here, $\Delta$ denotes the increment of the corresponding quantity.

The stress increment is then expressed, with the tangent modulus $E_t$ of the material, as

$$\Delta\sigma = E_t \cdot \Delta\varepsilon \tag{6.60}$$

The axial thrust and the bending moment are then computed by

$$-\Delta P = \int_A \Delta\sigma dA \tag{6.61}$$

$$\Delta M = \int_A \Delta\sigma y dA \tag{6.62}$$

Note that the increment of the axial thrust is positive when it is compressive.

Substituting **Eqs. (6.59)** and **(6.60)** into **Eqs. (6.61)** and **(6.62)** gives

$$\begin{Bmatrix} -\Delta P \\ \Delta M \end{Bmatrix} = \begin{bmatrix} Q_{11} & Q_{12} \\ Q_{21} & Q_{22} \end{bmatrix} \begin{Bmatrix} \Delta\varepsilon_c \\ \Delta\Phi \end{Bmatrix} \tag{6.63}$$

where

$$Q_{11} = \int_A E_t dA \tag{6.64}$$

$$Q_{12} = \int_A E_t y dA \tag{6.65}$$

$$Q_{22} = \int_A E_t y^2 dA \tag{6.66}$$

**Eq. (6.63)** is rewritten as

$$\{\Delta f\} = [Q]\{\Delta x\} \tag{6.67}$$

where

$$\{\Delta f\} = \begin{Bmatrix} -\Delta P \\ \Delta M \end{Bmatrix} \quad \text{(general force)} \tag{6.68}$$

$$\{\Delta x\} = \begin{Bmatrix} \Delta\varepsilon_c \\ \Delta\Phi \end{Bmatrix} \quad \text{(general deformation)} \tag{6.69}$$

$$[Q] = \begin{bmatrix} Q_{11} & Q_{12} \\ Q_{21} & Q_{22} \end{bmatrix} \qquad \text{(tangent stiffness equation)} \tag{6.70}$$

**Eqs. (6.67)** are the incremental tangent stiffness equations used in the present numerical analysis.

Based on the equations formulated above, a computer program was written to carry out the analysis of concrete-filled steel box columns subjected to a constant axial load and bending moment. The solution was evaluated using Newton-Raphson iterative method. Details of the numerical convergence scheme are to be found in Kakiuchi (1988). The iteration was conducted at each increment until the axial compressive force is equal to its given value within the specified tolerance. That is,

$$|p_o - p_1| < \epsilon \cdot \max(1, p_o) \tag{6.71}$$

Here, $p_o$ is the given axial force; $p_1$ is the current axial force; and $\epsilon = 10^{-4}$.

For concrete-filled steel box segments, the nondimensional variables are now defined by

$$m = \frac{M}{M_{pc,o}}, \quad \varphi = \frac{\Phi}{\Phi_y}, \quad p = \frac{P}{P_{yc}} \tag{6.72}$$

in which, $M_{pc,o}$ is the computed ultimate bending moment of concrete-filled steel columns when the axial load is zero, $\Phi_y$ is the yielding curvature of steel columns. $P_{yc}$ is the full plastic axial force (squash load) of the concrete-filled steel column, defined as

$$P_{yc} = A_s \sigma_y + A_c f_{ck} \tag{6.73}$$

in which $f_{ck}$ = characteristic compressive strength, $A_c$ = net concrete area.

The input data of the steel component in the analysis is the same as in the analysis of steel box stub-columns shown in **Table 6.1**. The characteristic compressive strength of the concrete is 240, 400, and 500 kgf/cm$^2$ respectively.

**Figs. 6.25** to **6.27** show the moment-curvature relationships for various values of $R$ , $f_{ck}$ and $p$. The axial force was maintained constant in each analysis. Note that the strain-hardening effect of steel material is not considered at present.



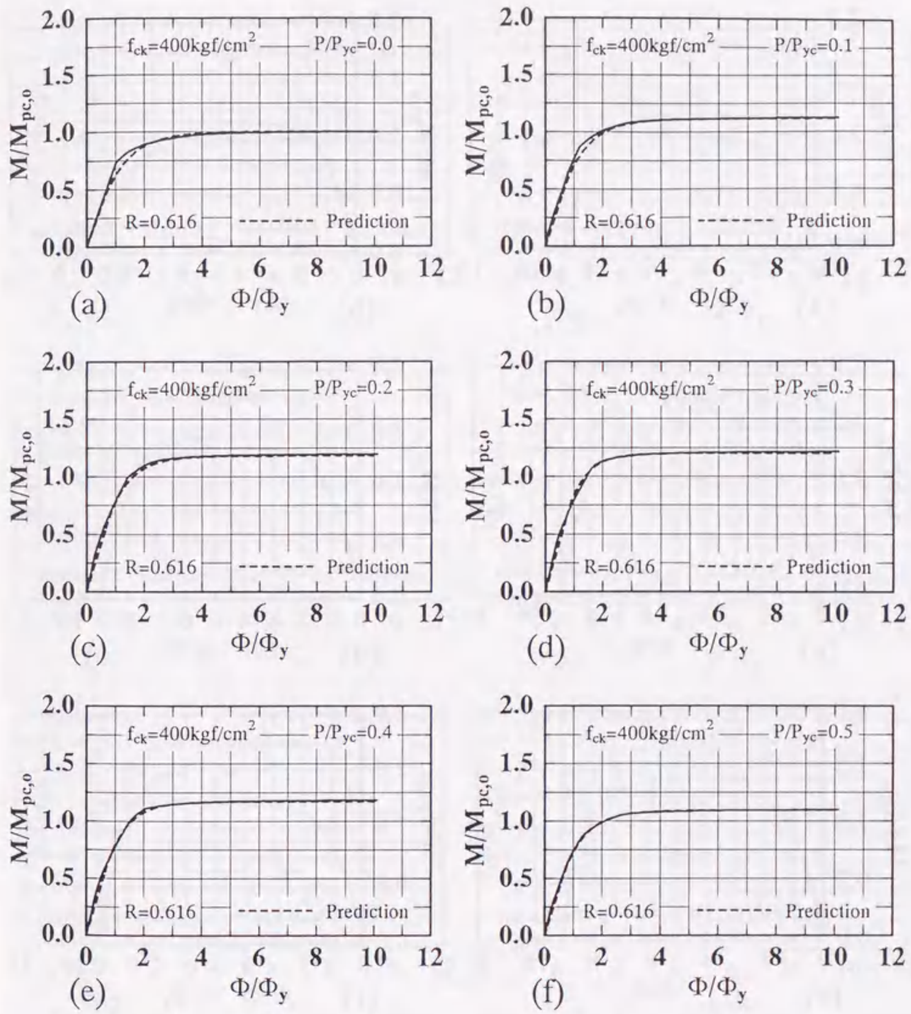


**Fig. 6.25 Computed Moment versus Curvature Curves: $R$=0.616**

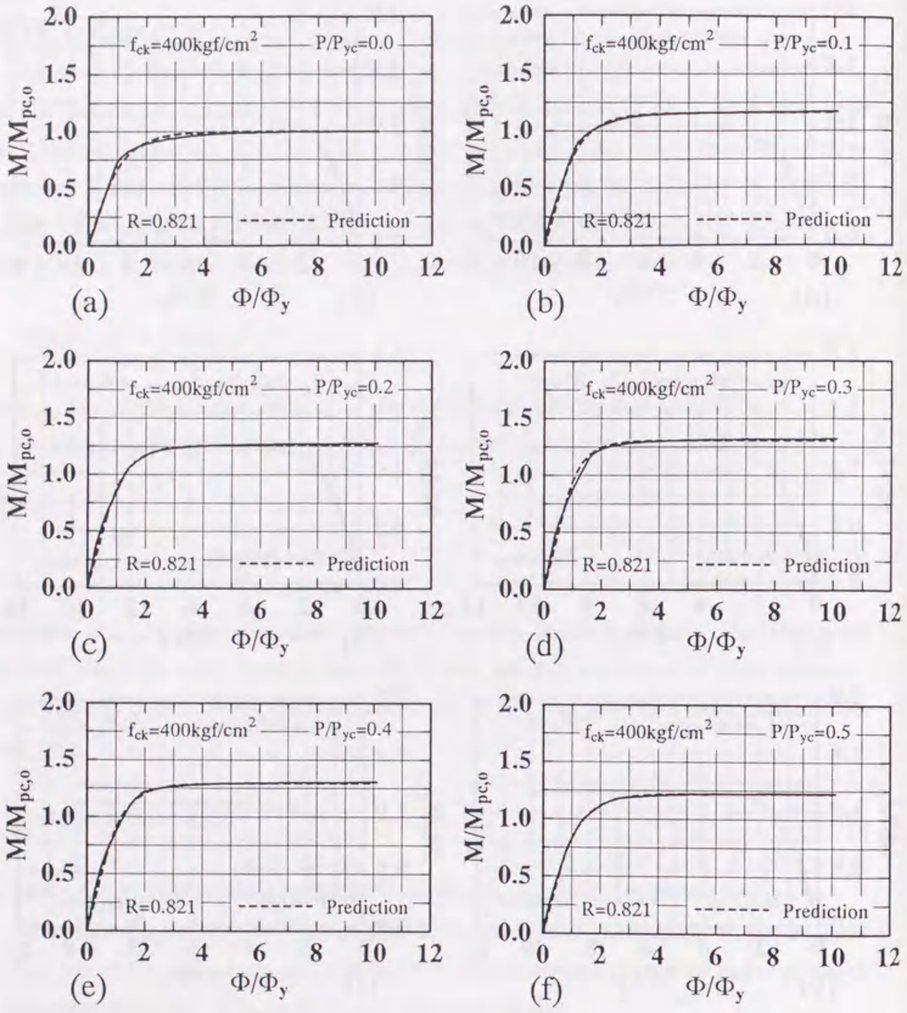


Fig. 6.26 Computed Moment versus Curvature Curves: $R$=0.821



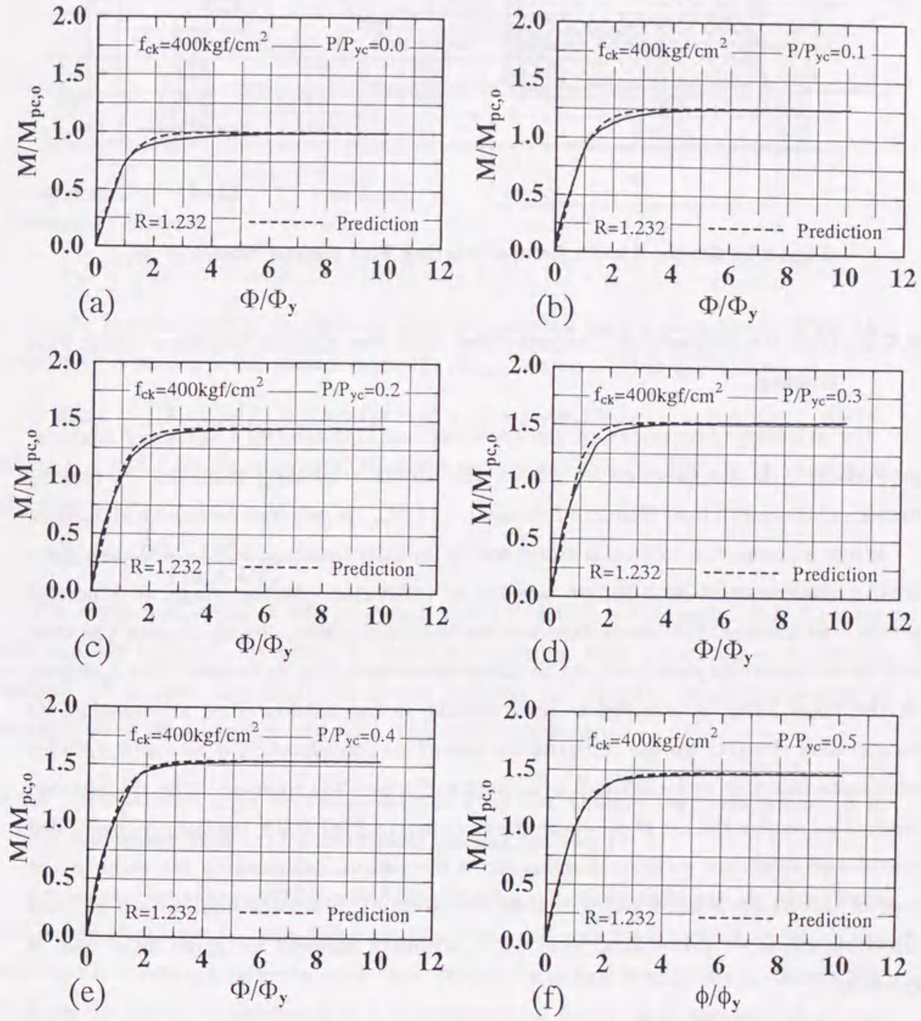


Fig. 6.27 Computed Moment versus Curvature Curves: $R$=1.232

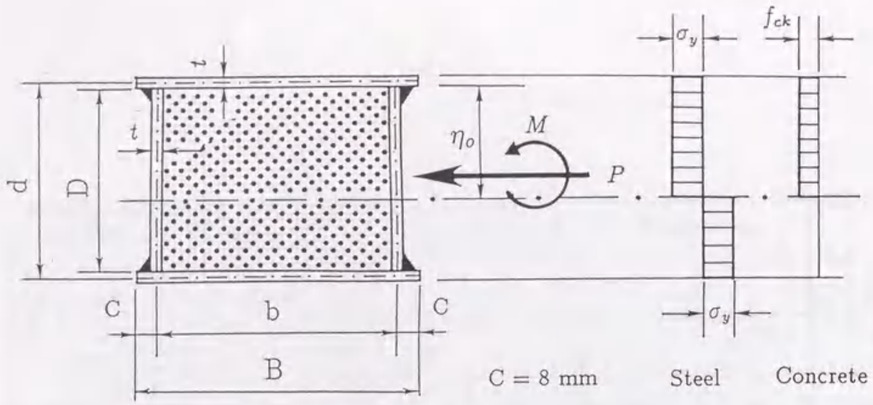


**Fig. 6.28 Stress Blocks for Calculating Full Plastic Moment $M_{pc}$**

### 6.4.2 Ultimate Moments of Concrete-Filled Steel Box Column Segments under Pure Bending

For arbitrary dimensions of the cross section and arbitrary values of material properties, it is not practical to obtain the ultimate bending moments by making numerical computations. Hence, a formulation of $M_{pc,o}$ is required for practical designs.

When a composite column is subjected to uniaxial bending, failure will take place on the attainment of its ultimate moment of resistance. At this stage, it is normal practice to assume that the section has become fully plastic, in which case the steel will have reached its yield level, $\sigma_y$, in compression as well as in tension. The concrete, on the other hand, is assumed to have cracked in the tension zone, and reached its compressive strength on the compression side. This consideration is also adequate for composite columns under a small axial load and a bending moment. The calculations are carried out by the use of stress blocks as shown in **Fig. 6.28**, for the concrete-filled unstiffened steel box section. Similar stress blocks and calculations are valid in the case of the concrete-filled stiffened steel box section. From the equilibrium of axial direction, depth of the neutral axis, $\eta_o$, at ultimate moment for given axial load is given by

$$\eta_o = \frac{2Dt\sigma_y + P}{(B - t - 2C)f_{ck} + 4t\sigma_y} \tag{6.74}$$

where $P$ = applied axial load; and $C$ = 8 mm = width of projecting plate element (see **Fig. 6.28**). Full plastic moment, $M_{pc}$, of concrete-filled steel box sections is then



**Table 6.2 Comparison of Predictions of $M_{pc,o}/M_y$ by Eq. (6.76) with Numerical Computations**

| $R$ | $f_{ck}$ (kgf/cm$^2$) | | | | | |
|---|---|---|---|---|---|---|
| | 240 | | 400 | | 500 | |
| | Computed | Predicted | Computed | Predicted | Computed | Predicted |
| 0.616 | 1.327 | 1.323 | 1.368 | 1.369 | 1.387 | 1.388 |
| 0.821 | 1.342 | 1.343 | 1.387 | 1.388 | 1.404 | 1.406 |
| 1.232 | 1.373 | 1.374 | 1.411 | 1.414 | 1.426 | 1.429 |

obtained as follows:

$$M_{pc} = \frac{1}{2}(B - t - 2C)\eta_o^2 f_{ck} + [B(D + t) + \eta_o^2 + (D - \eta_o)^2]t\sigma_y - (\eta_o - \frac{D}{2})P \tag{6.75}$$

In the above equation, the effect of axial compression load is considered. When the axial force is zero, the full-plastic moment, $M_{pc,o}$, can be written as follows:

$$M_{pc,o} = \frac{1}{2}(b - t)\eta_o^2 f_{ck} + [(b + t)d + \eta_o^2 + (d - t - \eta_o)^2]t\sigma_y \tag{6.76}$$

where $b$, $d$ and $t$ are dimensions of the cross section as shown in **Fig. 6.24**. And $\eta_o$ is given by

$$\eta_o = \frac{2(d - t)t\sigma_y}{(b - t)f_{ck} + 4t\sigma_y} \tag{6.77}$$

The computed values of $M_{pc,o}$ for each case ($R$=0.616, 0.921, and 1.232; $f_{ck}$=240, 400, and 500 kgf/cm$^2$) are given in **Table 6.2** together with the results of numerical analysis. It is seen that Eq.(6.76) closely predicts the ultimate bending moment of concrete-filled steel box columns when the axial load is zero.

### 6.4.3 Interaction Curves for Concrete-Filled Steel Box Column Segments Subjected to Combined Axial Load and Ultimate Bending Moment

An interaction curve could be established giving the combinations of the axial force and bending moment to cause full plasticity of the concrete-filled section, in which the steel and concrete components reach their respective design strengths simultaneously. Such results could be presented in a nondimensional form, as in the case of a steel section.

The following interaction formula is proposed to predict the ultimate bending strengths of concrete-filled steel box columns:

$$(1+c)p^2 - cp + m_{pc} = 1.0 \tag{6.78}$$

where $c$ is the shape parameter. It is found that $c$ is a function of the parameters $R$ and $f_{ck}$. By using least square fitting, the relation between $c$ and the two variables ($R$, $f_{ck}/\sigma_y$) is given by

$$c = 2.50R + 14.0\frac{f_{ck}}{\sigma_y} - 2.50 \tag{6.79}$$

Shown in **Fig. 6.29** are the interaction curves together with the results of numerical Computations.

### 6.4.4 Approximate Expressions of $m$-$p$-$\varphi$ Curves

In the case of concrete-filled steel box columns, the following two functions are used to approximate the $m$-$p$-$\varphi$ diagram:

$$m = a_{oo}\varphi \tag{6.80}$$

for the elastic range, and

$$m = c_{oo} \cdot exp(-b_{oo}\varphi) + m_{pc} \tag{6.81}$$

for the plastic range.

In the above expressions, the yield moment $m_1$, the corresponding yield curvature $\varphi_1$, and the flow moment $m_{pc}$ can be known from the numerical computations, the rest of the parameters in the two equations, namely $a_{oo}$, $b_{oo}$ and $c_{oo}$ can be determined easily by solving the simultaneous equations with the help of the continuity condition at the yielding ($m_1$, $\varphi_1$).

$$m_1 = a_{oo}\varphi_1 \tag{6.82}$$

$$m_1 = c_{oo} \cdot e^{-b_{oo}\varphi_1} + m_{pc} \tag{6.83}$$

The results are given by

$$a_{oo} = \frac{m_1}{\varphi_1} \tag{6.84}$$

$$b_{oo} = \frac{m_1}{\varphi_1(m_{pc} - m_1)} \tag{6.85}$$



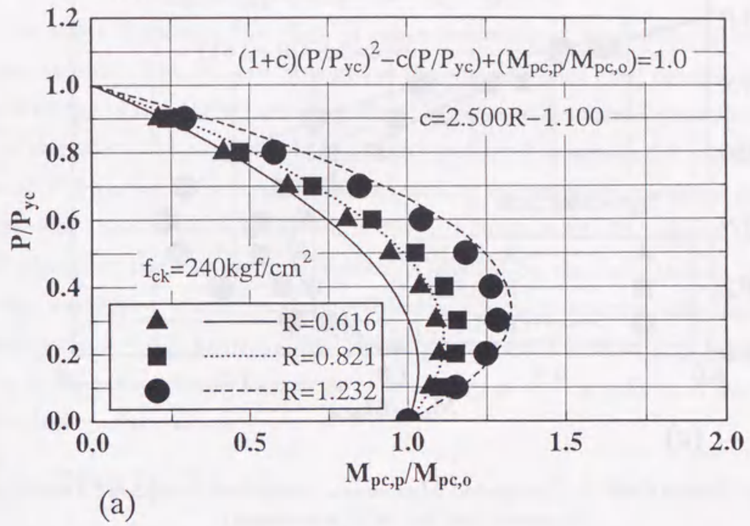


(a)

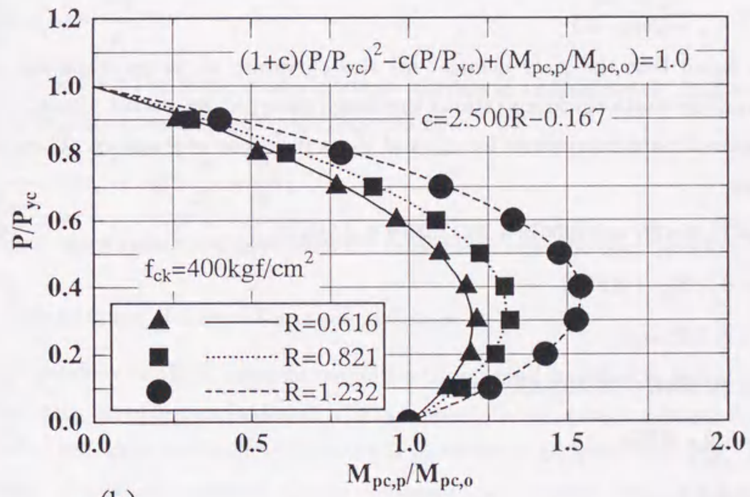


(b)

**Fig. 6.29 Comparison of Computed Maximum Loads and Proposed Interaction Formula [Eq. (6.78)] (to be continued)**

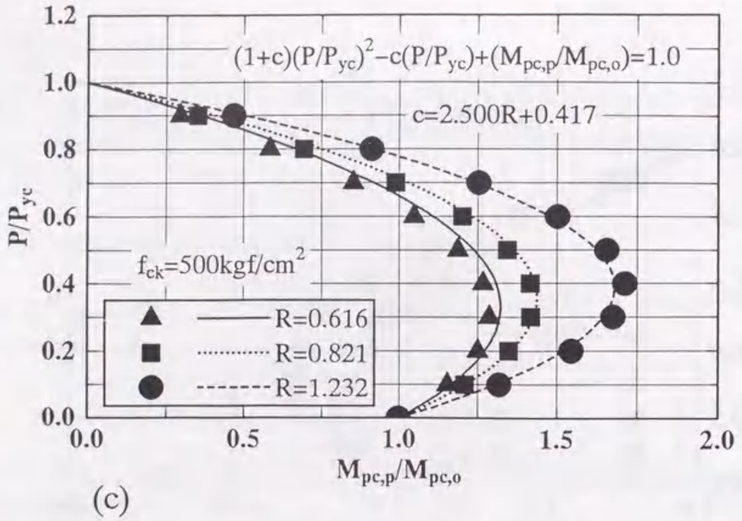


(c)

**Fig. 6.29 Comparison of Computed Maximum Loads and Proposed Interaction Formula [Eq. (6.78)] (continued)**

$$c_{oo} = -\frac{m_{pc} - m_1}{e^{-m_1/(m_{pc}-m_1)}} \tag{6.86}$$

It was found that the yield moment $m_1$ and curvature $\varphi_1$ varies when the axial force ($p$) and the width-thickness ratio of the flange plate ($R$) are varied. Thus, we can give the approximate expressions for $m_1$ and $\varphi_1$ as functions of $p$ and $R$. These were obtained as

$$m_1 = (1.0347R + 0.2905)p + (0.13339R + 0.28615) \tag{6.87}$$

$$\varphi_1 = 0.7070p + 0.5329 \tag{6.88}$$

for $0.0 \leq p \leq 0.3$; and

$$m_1 = (0.634R + 0.539)(1.0 - p) \tag{6.89}$$

$$\varphi_1 = 1.0 - 0.85p \tag{6.90}$$

for $0.3 \leq p \leq 0.9$.

Examples of approximate $m$-$p$-$\varphi$ relationship obtained using the above parameter functions are also shown in **Figs. 6.25** to **6.27**, in which the solid lines show the actual $m$-$p$-$\varphi$ relationship whereas the dashed lines show the approximate one. It can be seen that both curves are almost identical.



### 6.4.5 Strain-Hardening Effect on $m$-$p$-$\varphi$ Curves

In the above discussion the effect of strain-hardening of steel material was not taken into account. The ultimate strength of the concrete-filled steel column segment will increase due to the strain-hardening effect. In order to determine quantitively the nature of this effect, the strain-hardening model presented in section 6.2 will be used.

The $M$-$P$-$\Phi$ curves of concrete-filled steel column segments are computed again in each case, and some of them are shown in **Figs. 6.30** to **6.32**. It is found that the onset of change in the moment is significantly affected by the axial thrust. Said in detail, the starting at which the strain-hardening occurs is deferred with increasing axial force when $p \leq 0.3$, and advanced with increasing axial force when $p \geq 0.3$. The following equations are found to provide close fittings of the curvatures at which the strain-hardening effect occurs:

$$\frac{\Phi_h}{\Phi_y} = 10.0p + 7.0 \tag{6.91}$$

for $0.0 \leq p \leq 0.3$; and

$$\frac{\Phi_h}{\Phi_y} = 10.0(\frac{0.3}{p})^{0.6} \tag{6.92}$$

for $0.3 \leq p \leq 0.9$. The slope of the moment increase is approximately 0.02 and the moment after the curvature $\Phi_h/\Phi_y$ is computed by

$$\frac{M}{M_{pc,0}} = m_{pc} + 0.02(\frac{\Phi}{\Phi_y} - \frac{\Phi_h}{\Phi_y}). \tag{6.93}$$

where $m_{pc}$ is the moment obtained from the interaction equation **Eq. (6.88)**.

### 6.4.6 Determination of Critical Curvature at Failure

In the previous sections, moment-curvature curves tend to infinity. But it is suggested that each curve be terminated at a certain point. In the stress-strain relationship for concrete, the ultimate strain of concrete is assumed to be 0.006 [see **Fig. 6.23**]. Accordingly, the column segment can be considered to be failed when strain in the concrete at the top compression fiber reaches this value. The curvature of the segment at this state is referred to as the critical curvature, and is denoted by $\Phi_f$. Values of $\Phi_f$ obtained from the analysis are shown in **Fig. 6.33**. The following expression is found to give close approximations as shown in the figure.

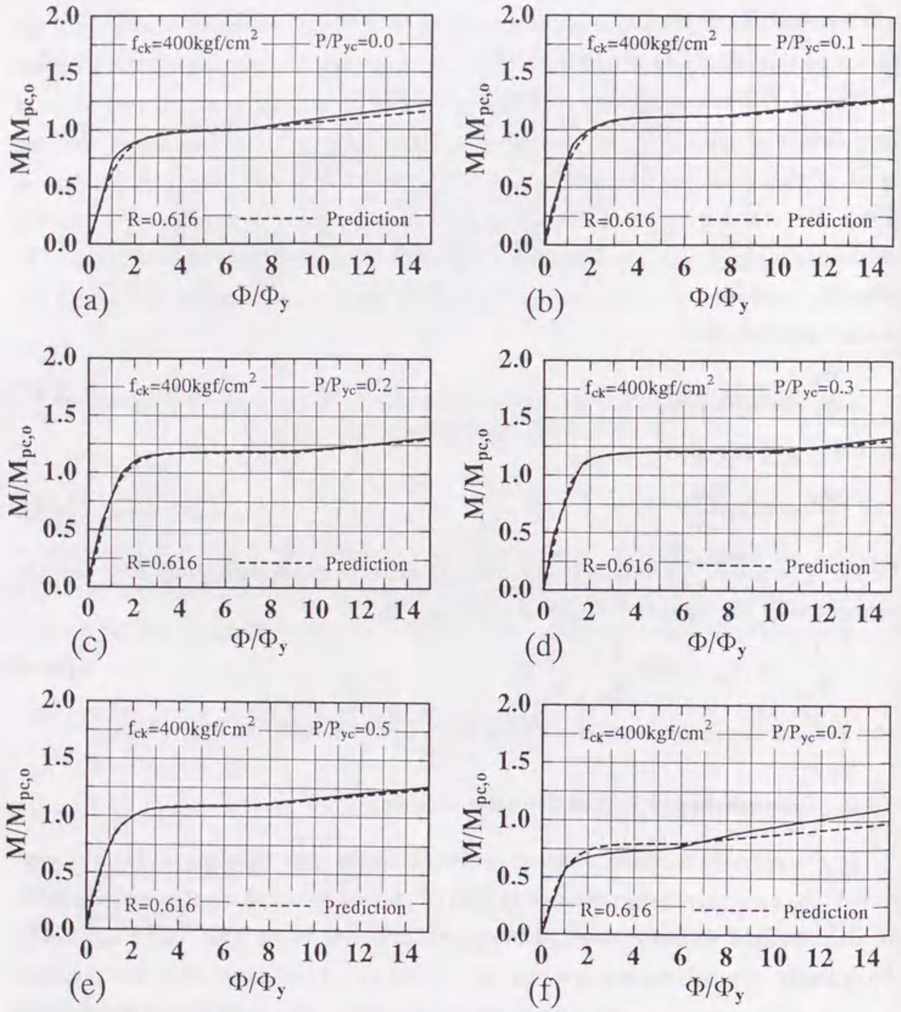


Fig. 6.30 Computed Moment versus Curvature Curves: $R$=0.616
Strain-hardening effect is included



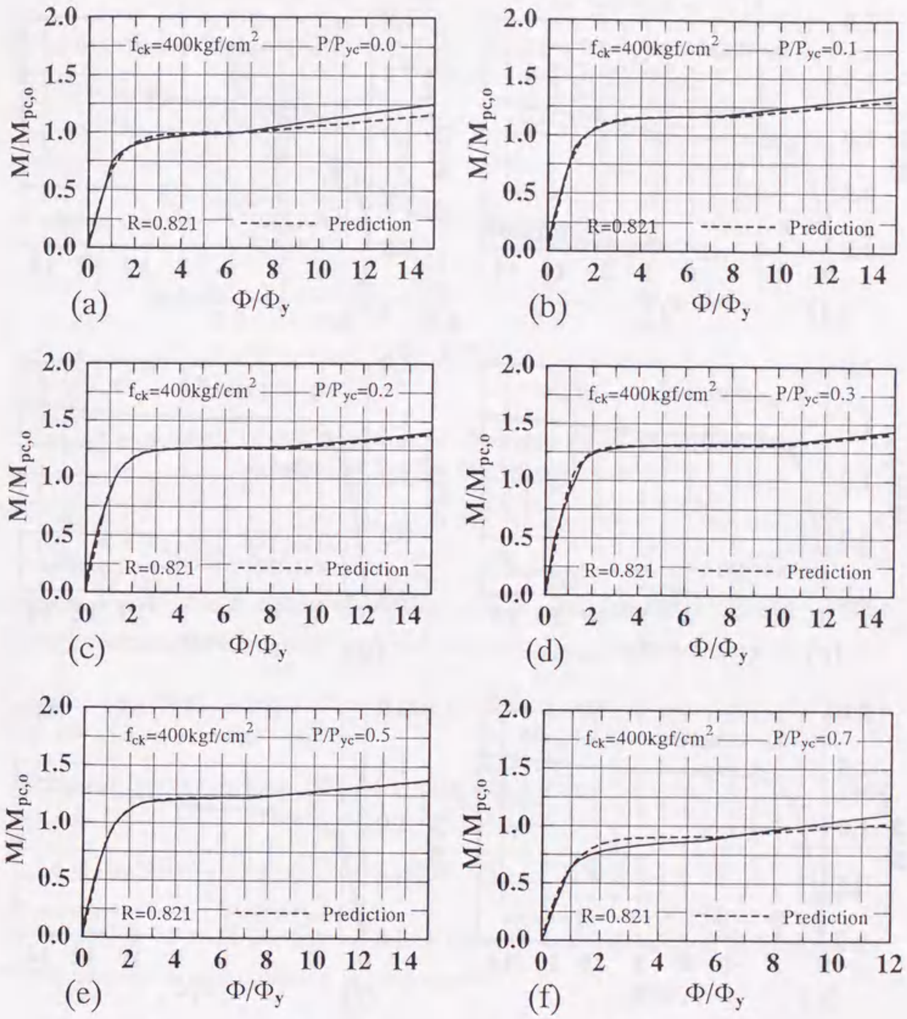


Fig. 6.31 Computed Moment versus Curvature Curves: $R$=0.821
Strain-hardening effect is included

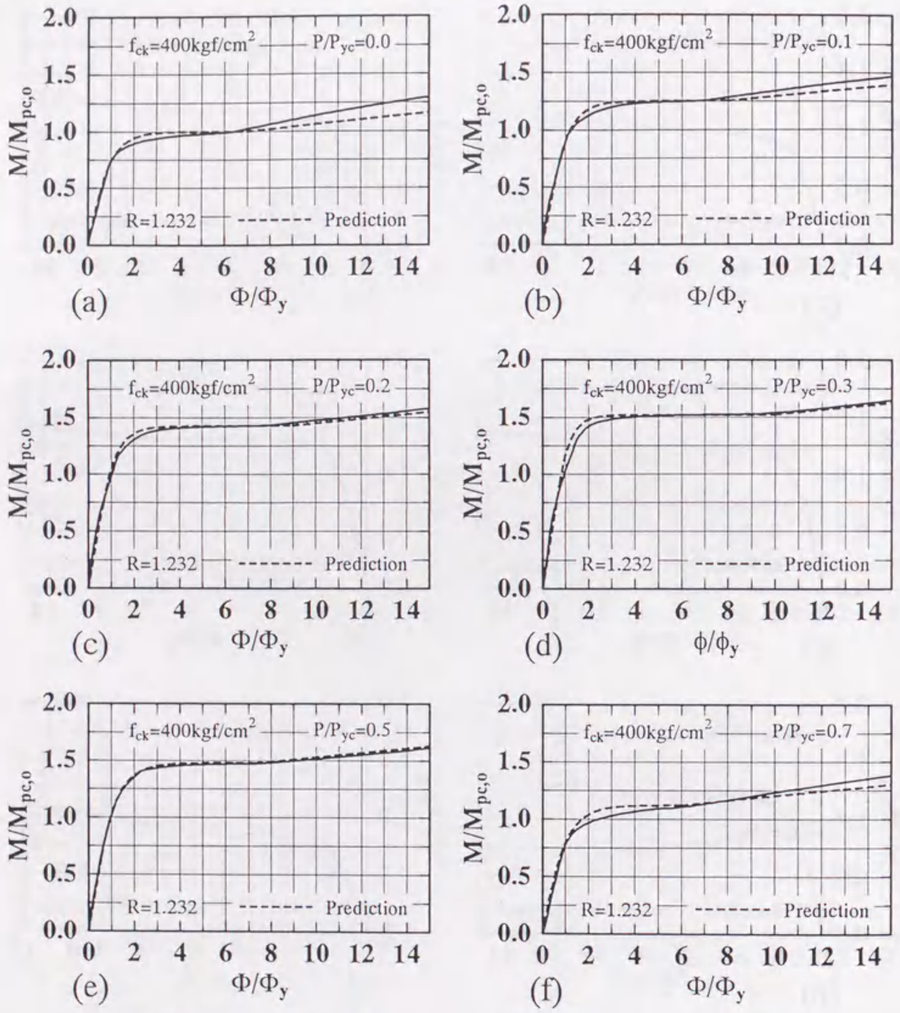


Fig. 6.32 Computed Moment versus Curvature Curves: $R$=1.232
Strain-hardening effect is included



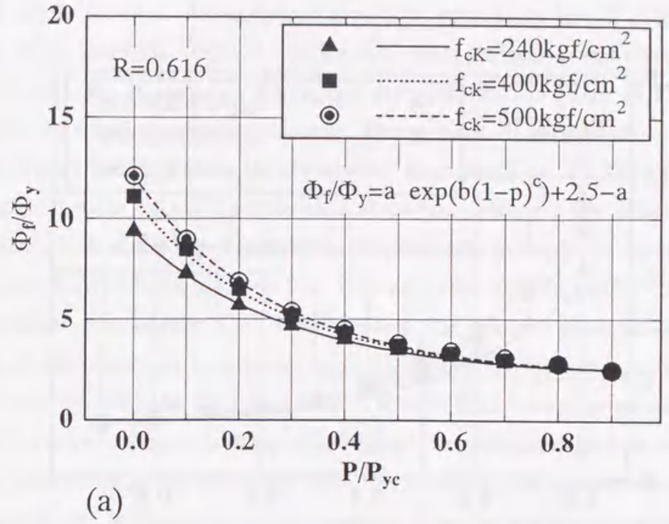


Fig. 6.33 Critical Curvatures of Concrete-Filled Steel Column Segments at Failure (to be continued)

$$\frac{\Phi_f}{\Phi_y} = a \cdot exp[b(1-p)^c] + 2.5 - a \tag{6.94}$$

where $a$, $b$ and $c$ are functions of width-thickness ratio parameter, $R$, and ratio of concrete compressive strength to steel yield stress, $f_{ck}/\sigma_y$, which are given by

$$a = -0.0403R - 0.0410(\frac{f_{ck}}{\sigma_y}) + 0.3446R(\frac{f_{ck}}{\sigma_y}) + 2.5480 \tag{6.95}$$

$$b = +0.2825R + 1.8760(\frac{f_{ck}}{\sigma_y}) + 0.7012R(\frac{f_{ck}}{\sigma_y}) + 0.9075 \tag{6.96}$$

$$c = -0.2984R - 1.9400(\frac{f_{ck}}{\sigma_y}) + 2.1530R(\frac{f_{ck}}{\sigma_y}) + 2.3430 \tag{6.97}$$

Eq. (6.94) is of great importance in the strength and deformation analysis of the column member as will be shown in next chapter.

## 6.5 Summary

The moment-curvature relationships for both steel box section and concrete-filled steel box section subjected to compression combined with uniaxial bending moment are

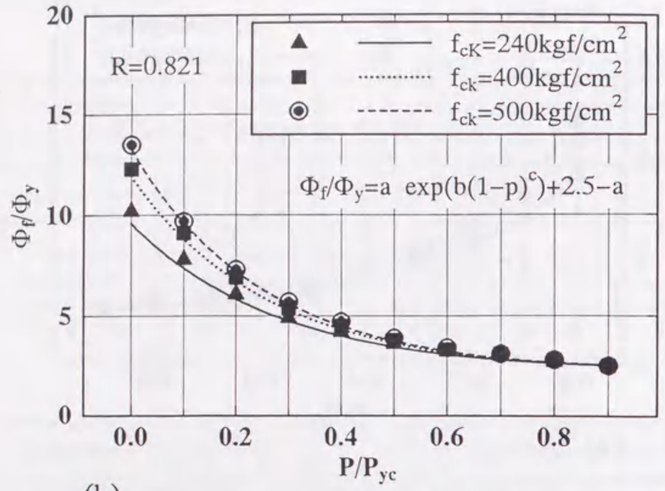


(b)

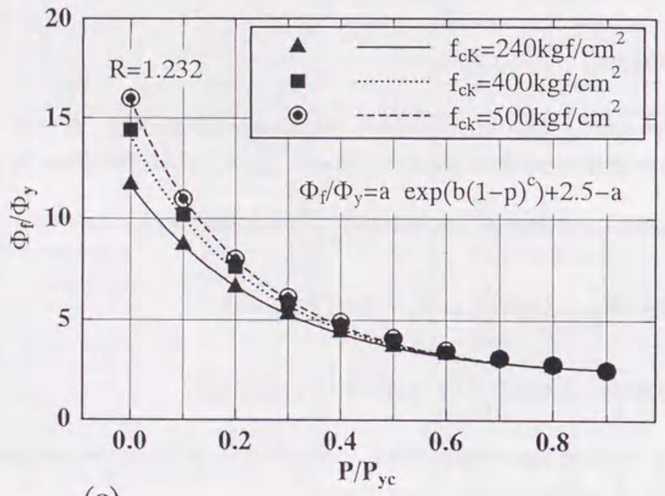


(c)

Fig. 6.33 Critical Curvatures of Concrete-Filled Steel Column Segments at Failure (continued)



presented in this chapter. An analytical model for computing the $M$-$P$-$\Phi$ curves was proposed. In the analysis, residual stress, initial plate deflection and strain hardening were considered. As a result, an interaction strength formula [**Eq. (6.18)**] was proposed for locally buckled steel box columns. The moment-thrust-curvature relationship can be accurately predicted by a set of proposed formulas [**Eqs. (6.22)-(6.24)**]. Since the numerical results obtained in the case of uniform moment are usually conservative, the analytical model was then modified to take into account the effect of moment gradient, and a modification factor f(G, R) was introduced to predict the moment-thrust-curvature relationship. On the other hand, the moment gradient did not affect the value of the curvature corresponding to the maximum bending moment. Moreover, a set of approximate formulas [**Eqs. (6.36)-(6.38)**] were proposed to predict the moment-thrust-curvature relationship of steel box column segments without local buckling. In the case of concrete-filled steel box sections, the moment-curvature relations are computed without considering local buckling by a simple numerical method in which local buckling is not taken into account. When the strain-hardening effect is not considered, the ultimate bending strength can be predicted using a proposed interaction formula [**Eq. (6.78)**]. The $M$-$P$-$\Phi$ curves can be closely approximated by two continuous functions [**Eqs. (6.80)** and **(6.81)**]. Finally, in order to take into account the effect of strain-hardening, a modification was made in the approximation expressions of the $M$-$P$-$\Phi$ relationships.

# 7 STRENGTH AND DEFORMATION ANALYSIS OF PARTIALLY CONCRETE-FILLED STEEL BOX COLUMNS

## 7.1 General Remarks

In Chapter 3, a three-dimensional analytical finite element method is used for finding the load-deformation response of concrete-filled steel box columns in pure compression. It has been shown that the elasto-plastic analysis of the composite members like concrete-filled steel box columns is destined to be complex, since the following aspects are still not ripe: (1) the constitutive relationship of the confined concrete; (2) the contact model for considering the bonding, friction and slip actions between two different materials. Moreover, the analysis of such nonlinear problems is time consuming even for simple cases. However, in many instances, the determination of the maximum loads and displacements is of greater practical importance. The development of efficient methods for computing the load-carrying and deformation capacities in a more simple way, therefore, is of great practical interest to engineers.

This chapter is concerned with the development of such a method. To obtain the complete load-deformation behavior of the columns, the $M - P - \Phi$ relations given in the last chapter are integrated along the member axis with the use of the finite element technique. This procedure is first described in detail, and is followed by a comparison of the numerical results with the experiments. Next, design charts for determining the ultimate strengths and corresponding deformations of the concrete-filled steel box columns under constant axial force and lateral load are presented. Finally, a design recommendation for determining the optimum length of the filled-in concrete is proposed.

## 7.2 Numerical Analysis Method

For the sake of simplicity, the discussion is restricted to the cantilever-types of concrete-filled steel box columns subjected to a constant axial force $P$ and an increasing lateral load $H$ at the top, as shown in **Fig. 7.1**. In the present analysis, a beam-column element shown in **Fig. 7.2** that includes only the flexural deformation is employed.



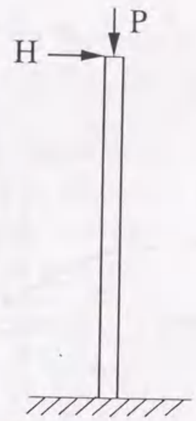


**Fig. 7.1 Cantilever Column to be Analyzed**

### 7.2.1 Derivation of the Stiffness Equation

To formulate the stiffness equation of the column member, the following assumptions are made in the analysis:

1. Changes in the geometrical configuration of the member due to axial force remain negligible. In other words, the shortening resulting from the axial force is always very small and can be neglected;
2. Axial force does not vary in magnitude during the deformation;
3. Initial out-of-straightness of the member is not considered;
4. $M - P - \Phi$ relations of both the hollow steel section and the concrete-filled steel section are known.

In the deformed configuration of the column in the absence of transverse load, the equilibrium equation is obtained as

$$M'' - Pv'' = 0 \tag{7.1}$$

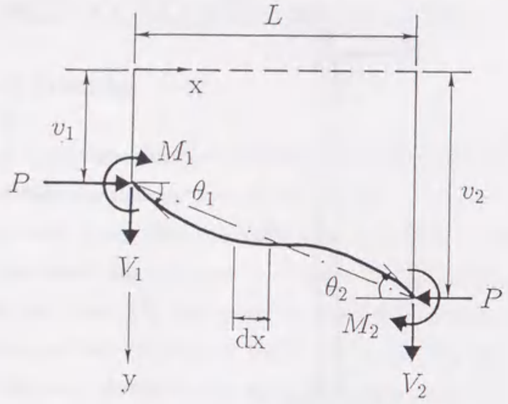


**Fig. 7.2 Beam-Column Element**

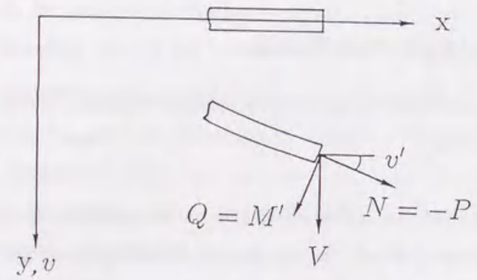


**Fig. 7.3 Member's Transverse Load**

where $M$ is the bending moment; $P$ is the axial compressive force; $v$ is the deflection; and primes denote the derivatives with respect to the column axis $x$.

Multiplying both sides of **Eq. (7.1)** by the virtual displacement $\delta v$, and Integrating it by parts along the length of the column yields:

$$-\int_0^L M\delta v''dx - P\int_0^L v'\delta v'dx = [(M' - Pv')\delta v]_0^L - [M\delta v']_0^L \tag{7.2}$$

Here it should be noted that a lateral force ($V$) normal to the member axis before the deformation, as shown in **Fig. 7.3**, can be related to $M$ and $P$ by



$$V = Qcosv' + Nsinv' \doteq Q + Nv' = M' - Pv' \tag{7.3}$$

Hence, **Eq. (7.2)** can be rewritten as

$$-\int_0^L M\delta v''dx - P\int_0^L v'\delta v'dx = [V\delta v]_0^L - [M\delta v']_0^L \tag{7.4}$$

In order to establish the incremental form of the above equation, it is necessary to substitute $M+\Delta M$, $v+\Delta v$ and $V+\Delta V$ for $M$, $v$ and $V$ respectively in **Eq. (7.4)**. $M$, $v$ and $V$ are the bending moment, deflection and lateral force at a certain equilibrium state, while $\Delta M$, $\Delta v$ and $\Delta V$ are their increments. Thus,

$$-\int_0^L (M+\Delta M)\delta v''dx - P\int_0^L (v'+\Delta v')\delta v'dx = [(V+\Delta V)\delta v]_0^L - [(M+\Delta M)\delta v']_0^L \tag{7.5}$$

Note that the constitutive relation is

$$\Delta M = -B\Delta v'' \tag{7.6}$$

where $B$ is the tangent stiffness of the $M - P - \Phi$ curves for given values of the axial force $P$ and curvature $\Phi = -v''$. Substituting **Eq. (7.6)** in the first term of **Eq. (7.5)**, and rearranging it gives

$$\int_0^L B\Delta v''\delta\Delta v''dx - P\int_0^L \Delta v'\delta\Delta v'dx = [\Delta V\delta\Delta v]_0^L - [\Delta M\delta\Delta v']_0^L + [V\delta\Delta v]_0^L - [M\delta\Delta v']_0^L + \int_0^L M\delta v''dx + P\int_0^L v'\delta v'dx \tag{7.7}$$

**Eq. (7.7)** will now be written in matrix form as follows. The deflection increment, $\Delta v(x)$, can be expressed in terms of the shape function $\mathbf{N}(x)$ as

$$\Delta v(x) = \mathbf{N}(x)\Delta\mathbf{d} \tag{7.8}$$

where $\Delta\mathbf{d}$ is the nodal displacement increment vector, and given by

$$\Delta\mathbf{d}^T = [\Delta v_1, \Delta v_1', \Delta v_2, \Delta v_2'] \tag{7.9}$$

where $\Delta v_i$ and $\Delta v_i'$ ($i = 1, 2$) are the deflection increment and rotation increment at node $i$. Shape function $\mathbf{N}(x)$ is

$$\mathbf{N}(x) = [N_1, N_2, N_3, N_4] \tag{7.10}$$

where $N_i$ $(i = 1, 2, 3, 4)$ are the interpolation function given by

$$\begin{aligned} N_1 &= 3(1-\frac{x}{L})^2 - 2(1-\frac{x}{L})^3 \\ N_2 &= x(1-\frac{x}{L})^2 \\ N_3 &= 3(\frac{x}{L})^2 - 2(\frac{x}{L})^3 \\ N_4 &= -(L-x)(\frac{x}{L})^2 \end{aligned} \tag{7.11}$$

Substitution of **Eq. (7.8)** into **Eq. (7.7)** gives

$$\delta\Delta\mathbf{d}^T(\int_0^L B\mathbf{N}''^T \cdot \mathbf{N}''dx)\Delta\mathbf{d} - \delta\Delta\mathbf{d}^T(P\int_0^L \mathbf{N}'^T \cdot \mathbf{N}'dx)\Delta\mathbf{d} =$$
$$\delta\Delta\mathbf{d}^T\Delta\mathbf{r} + \delta\Delta\mathbf{d}^T\mathbf{r} + \delta\Delta\mathbf{d}^T[\int_0^L M\mathbf{N}''^T dx) + (P\int_0^L \mathbf{N}'^T\mathbf{N}'dx)\mathbf{d}] \tag{7.12}$$

where

$$\Delta\mathbf{r} = \begin{Bmatrix} \Delta V_1 \\ \Delta M_1 \\ \Delta V_2 \\ \Delta M_2 \end{Bmatrix} = \begin{Bmatrix} -\Delta V(0) \\ \Delta M(0) \\ \Delta V(L) \\ -\Delta M(L) \end{Bmatrix} \tag{7.13}$$

$$\mathbf{r} = \begin{Bmatrix} V_1 \\ M_1 \\ V_2 \\ M_2 \end{Bmatrix} = \begin{Bmatrix} -V(0) \\ M(0) \\ V(L) \\ -M(L) \end{Bmatrix} \tag{7.14}$$

Since $\delta\Delta\mathbf{d}^T$ is arbitrary, we obtain from **Eq. (7.12)** the incremental stiffness equation of the element.

$$(\mathbf{k} - P\mathbf{k}_G)\cdot\Delta\mathbf{d} = \Delta\mathbf{r} + \mathbf{r} - \mathbf{f} \tag{7.15}$$

where $\Delta\mathbf{r}$ and $\mathbf{r}$ are the incremental and total nodal force vectors, respectively. And

$$\mathbf{k} = \int_0^L B\mathbf{N}''^T \cdot \mathbf{N}''dx \tag{7.16}$$

$$\begin{aligned} \mathbf{k}_G &= \int_0^L \mathbf{N}'^T \cdot \mathbf{N}'dx \\ &= \frac{1}{30L}\begin{bmatrix} 36 & 3L & -36 & 3L \\ & 4L^2 & -3L & -L^2 \\ & Sym. & 36 & -3L \\ & & & 4L^2 \end{bmatrix} \end{aligned} \tag{7.17}$$



$$\mathbf{f} = -\int_0^L M\mathbf{N}''^T dx - P\mathbf{k}_G \cdot \mathbf{d} \tag{7.18}$$

where $\mathbf{k}$ = tangent stiffness matrix of the element; $\mathbf{k}_G$ = geometrical stiffness matrix of the element; $\mathbf{f}$ = nodal force vector obtained from the internal forces, and so is termed the equivalent nodal force vector of the element. The bending moment, $M$, may be obtained from the $M - P - \Phi$ curves for given values of $P$ and $\Phi(x)$. Note that the curvature $\Phi(x)$ at each integration point of a element is evaluated as

$$\Phi(x) = -v''(x) = -\mathbf{N}''(x)\mathbf{d} \tag{7.19}$$

where

$$N''(x) = [-\frac{6}{L^2} + \frac{12}{L^3}x, -\frac{4}{L} + \frac{6}{L^2}x, \frac{6}{L^2} - \frac{12}{L^3}x, -\frac{2}{L} + \frac{6}{L^2}x] \tag{7.20}$$

Once the stiffness matrix of each element has been determined, the total stiffness matrix of the structure or member is generated by a simple summation of the individual stiffness and loads at the nodes using the compatibility of displacements and slopes. Accordingly, the total stiffness equation for the structure may be written as

$$(\mathbf{K} - P\mathbf{K}_G)\cdot\Delta\mathbf{D} = \Delta\mathbf{R} + \mathbf{R} - \mathbf{F} \tag{7.21}$$

where $\mathbf{K}$ = stiffness matrix of the entire structure; $\mathbf{K}_G$ = geometrical stiffness matrix of the entire structure; $\Delta\mathbf{D}$ = generalized displacement increment vector; $\Delta\mathbf{R}$ = generalized load increment vector; $\mathbf{R}$ = generalized load vector; and $\mathbf{F}$ = equivalent load vector of the entire structure. **Eqs. (7.21)** are the incremental stiffness equations used in the present numerical analysis.

### 7.2.2 Numerical Integration and Solution Procedure

In order to integrate the $M - P - \Phi$ relations along the length of the member, the column is divided into a number of segments.

The evaluation of integrals of $\int_a^b F(x)dx$ by classical (i.e., exact integration) methods is either difficult or impossible due to the complicated form of the integrand $F$. For this reason, numerical integration is required. In this study, the Gauss-Lobatto numerical integration formula is utilized, because the two end points of each element are necessarily two sample points. For the polynomials of degree less than 5, this method

gives accurate solution in the case of four sample points (O. C. Zienkiewicz and K. Morgan, 1984). Thus, the number of sample points adopted is four.

**Eq. (7.21)** provides a set of non-linear equations. Since the solutions near and just after the peak of the load-displacement curve are usually difficult to obtain, the displacement-control method will be used. The solution procedure is as follows. For simplicity, by setting

$$\tilde{\mathbf{K}} = \mathbf{K} - P\mathbf{K}_G \tag{7.22}$$

**Eq. (7.21)** can be rewritten as

$$\tilde{\mathbf{K}} \cdot \Delta\mathbf{D} = \Delta\mathbf{R} + \mathbf{R} - \mathbf{F} \tag{7.23}$$

or

$$\begin{bmatrix} \tilde{K}_{11} & \tilde{K}_{12} & \cdots & \tilde{K}_{1i} & \cdots & \tilde{K}_{1n} \\ & \tilde{K}_{22} & \cdots & \tilde{K}_{2i} & \cdots & \tilde{K}_{2n} \\ & & & \cdot & \cdot & \cdot \\ & & & \cdot & \cdot & \cdot \\ & & & \cdot & \cdot & \cdot \\ Sym. & & & \tilde{K}_{ii} & \cdots & \tilde{K}_{in} \\ & & & & \cdot & \\ & & & & \cdot & \\ & & & & \cdot & \\ & & & & & \tilde{K}_{nn} \end{bmatrix} \begin{Bmatrix} \Delta d_1 \\ \Delta d_2 \\ \cdot \\ \cdot \\ \cdot \\ \Delta d_i \\ \cdot \\ \cdot \\ \cdot \\ \Delta d_n \end{Bmatrix} = \tag{7.24}$$

$$\begin{Bmatrix} \Delta R_1 \\ \Delta R_2 \\ \cdot \\ \cdot \\ \cdot \\ \Delta R_i \\ \cdot \\ \cdot \\ \cdot \\ \Delta R_n \end{Bmatrix} + \begin{Bmatrix} R_1 \\ R_2 \\ \cdot \\ \cdot \\ \cdot \\ R_i \\ \cdot \\ \cdot \\ \cdot \\ R_n \end{Bmatrix} - \begin{Bmatrix} F_1 \\ F_2 \\ \cdot \\ \cdot \\ \cdot \\ F_i \\ \cdot \\ \cdot \\ \cdot \\ F_n \end{Bmatrix} \tag{7.25}$$

where $\Delta d_i$ is supposed to be a prescribed displacement increment. Then,

$$R_k = \Delta R_k = 0, \qquad k = 1, 2, ..., n \tag{7.26}$$

except for $R_i$ (reaction force) and $\Delta R_i$ ( reaction force increment). In summary, to compute $\{\Delta\mathbf{D}\}$ the following steps are required:



1. Give an increment of displacement $\Delta d_i$;
2. Put $\tilde{K}_{ii} = 1$, and $\tilde{K}_{1i} = \tilde{K}_{2i} = ... = \tilde{K}_{ni} = \tilde{K}_{i1} = \tilde{K}_{i2} = ... = \tilde{K}_{in} = 0$;
3. Put $R_i = \Delta d_i$, and $R_1 = R_2 = ... = R_n = \Delta R_1 = ... = \Delta R_n = F_i = 0$;
4. Move

$$\Delta d_i \begin{Bmatrix} \tilde{K}_{1i} \\ \tilde{K}_{2i} \\ \cdot \\ \cdot \\ \cdot \\ 0 \\ \cdot \\ \cdot \\ \cdot \\ \tilde{K}_{ni} \end{Bmatrix}$$

to the right hand side. Thus, we have

$$\begin{bmatrix} \tilde{K}_{11} & \tilde{K}_{12} & \cdots & 0 & \cdots & \tilde{K}_{1n} \\ & \tilde{K}_{22} & \cdots & 0 & \cdots & \tilde{K}_{2n} \\ & & & \cdot & \cdot & \cdot \\ & & & \cdot & \cdot & \cdot \\ & & & \cdot & \cdot & \cdot \\ 0 & 0 & \cdots & 1 & \cdots & 0 \\ & & & \cdot & & \cdot \\ & & & \cdot & & \cdot \\ & & & \cdot & & \cdot \\ & & & 0 & & \tilde{K}_{nn} \end{bmatrix} \begin{Bmatrix} \Delta d_1 \\ \Delta d_2 \\ \cdot \\ \cdot \\ \cdot \\ \Delta d_i \\ \cdot \\ \cdot \\ \cdot \\ \Delta d_n \end{Bmatrix} = \tag{7.27}$$

$$-\Delta d_i \begin{Bmatrix} \tilde{K}_{1i} \\ \tilde{K}_{2i} \\ \cdot \\ \cdot \\ \cdot \\ -1 \\ \cdot \\ \cdot \\ \cdot \\ \tilde{K}_{ni} \end{Bmatrix} - \begin{Bmatrix} F_1 \\ F_2 \\ \cdot \\ \cdot \\ \cdot \\ 0 \\ \cdot \\ \cdot \\ \cdot \\ F_n \end{Bmatrix} \tag{7.28}$$

5. Solve the above equation for $\{\Delta \mathbf{D}\}$;

6. Add $\{\Delta \mathbf{D}\}$ to $\{\mathbf{D}\}$;

7. Calculate reaction force increments

$$\Delta R_k = [\tilde{K}_{1k}, \tilde{K}_{2k}, ..., \tilde{K}_{nk}]\{\Delta \mathbf{D}\}, \qquad k = 1, 2, ..., n \tag{7.29}$$

and add $\{\Delta \mathbf{R}\}$ to $\{\mathbf{R}\}$;

8. Update total stiffness matrix $[\tilde{\mathbf{K}}]$ using updated displacements $\{\mathbf{D}\}$;

9. Calculate unblanced forces $\{\mathbf{F}\}$ from **Eq. (7.18)**;

10. Repeat procedures (2) to (9) until

$$\frac{\|\Delta \mathbf{D}\|}{\|\mathbf{D}\|} \leq 10^{-9} \tag{7.30}$$

is satisfied, where $\| \ \|$ is the Euclidian norm.

According to the solution algorithm discussed previously, a finite-element program for the solution of one-dimensional nonlinear problems was made. It includes: generation of the element matrices using numerical integration, assembly of element equations, imposition of the boundary conditions, and solution of the equations for the nodal point values of the primary variables.

In a subsequent section, the analysis of cantilever types of concrete-filled steel box columns using the developed program will be conducted, and comparisons of predicted ultimate strength and deformation capacity with the experimental results will be presented.



## 7.3 Failure Criterion

In the previous chapter, the concept of critical curvature of the concrete-filled steel column segment was introduced. In order to define a failure criterion for the column analysis, this concept can be utilized. However, it is too conservative if the column is considered to be failed when the maximum curvature reaches the critical curvature [$\Phi_f$, **Eq. (6.94)**]. For this reason, it seems rational to define the failure of the concrete-filled part to occur when the average curvature within a certain length reaches the critical curvature. The determination of this effective failure length can be made with reference to the failure mode observed in the test specimens. It has been shown in the previous chapters that the length of the failed part is in a range of $0.5b$ to $1.0b$ ($b$ is the flange width). Accordingly, the effective failure length is taken to be $0.7b$ in the present analysis. In case the length of the filled-in concrete, $l_c$, is less than $0.7b$, the effective failure length is taken to be $l_c$.

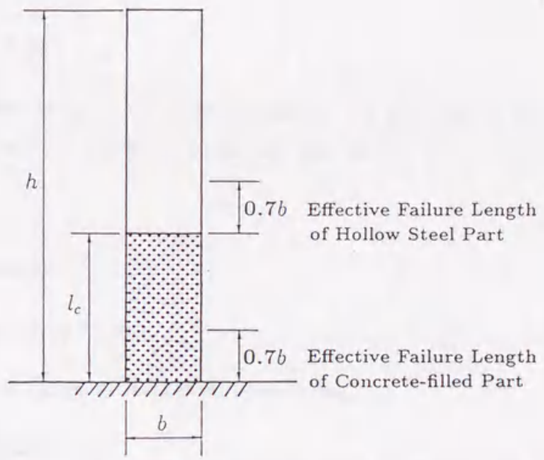


**Fig. 7.4 Effective Failure Length Concept**

Similarly, the failure of the hollow steel section part is defined to occur when the average curvature of all the integration points within a $0.7b$ length reaches the value of the curvature $\Phi_m$. Here, $\Phi_m$ is the curvature corresponding to the maximum bending

moments and it has been given in **Eq. (6.27)**.

In summary, the column is considered to be failed when either of the following two conditions is satisfied (see **Fig. 7.4**):

$$\Phi_{ave,c} = \Phi_f \tag{7.31}$$

$$\Phi_{ave,s} = \Phi_m \tag{7.32}$$

where $\Phi_{ave,c}$ and $\Phi_{ave,s}$ are the average curvatures of the concrete-filled part and hollow steel part, respectively.



## 7.4 Comparison of Ultimate Strength and Deformation Capacity with Experimental Results

In the following analysis, the moment-curvature relations ignoring local buckling, which were given in Chapter 6, will be used in order to show that the present analytical method is of great importance and simple for practical use. This is because the moment-curvature relation for any cross section and any material can be easily calculated without considering local buckling by a simplified numerical computation method as in section 6.4 using a personal computer. Thus, in the case of the hollow steel section, the moment-curvature expressions used are:

$$m = \varphi \tag{7.33}$$

for the elastic range;

$$m = b_n \cdot exp(-a_n\varphi) + m_{pcz} \tag{7.34}$$

for the elasto-plastic range without strain-hardening; and

$$m = m_{pcz} + S_h(\varphi - \varphi_h) \tag{7.35}$$

for the elasto-plastic range with strain-hardening. In the case of the concrete-filled steel section, the moment-curvature equations used are:

$$m = a_{oo}\varphi \tag{7.36}$$

for the elastic range, and

$$m = c_{oo} \cdot exp(-b_{oo}\varphi) + m_{pc} \tag{7.37}$$

for the elasto-plastic range without strain-hardening.

$$m = m_{pc} + 0.02(\varphi - \varphi_h) \tag{7.38}$$

for the elasto-plastic range without strain-hardening. Explanations of all the parameters and coefficients in above equations were given previously.

To ensure the capability of the present analytical method for finding the maximum load and corresponding deformation of the concrete-filled thin-walled steel column, the computed results using this method are compared with the results of several available

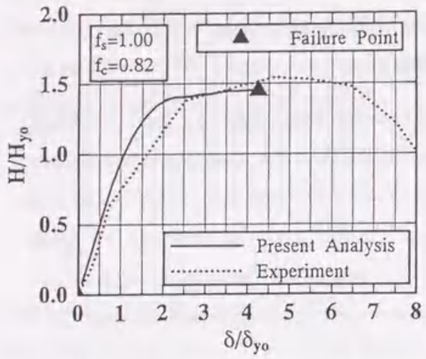


(a) UU2
($R_f$=0.664, λ=0.362, $l_c$/h=0.3)

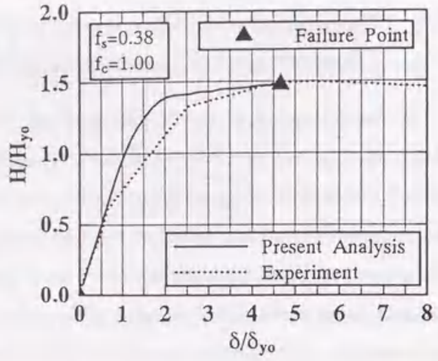


(b) UU3
($R_f$=0.664, λ=0.362, $l_c$/h=0.5)

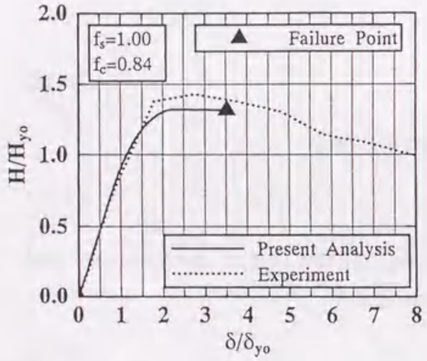


(c) UU5
($R_f$=0.664, λ=0.577, $l_c$/h=0.3)

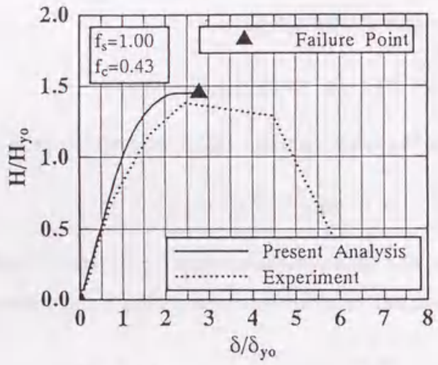


(d) UU7
($R_f$=0.854, λ=0.381, $l_c$/h=0.3)

**Fig. 7.5 Comparisons of Computed Results by Present Analysis and Experimental Data Given in Chapter 4**

experimental data with different values of the parameters $R_f$, $\overline{\lambda}$ and $l_c/h$. In the analysis of each test specimen, the dimensions and material properties given in chapters 4 and 5 are used.

**Figs. 7.5** and **7.6** show the comparison between the computed results and the experimental data of eight test specimens. The computation was terminated when the failure condition was satisfied. In each figure, the point, denoted by a mark ▲, is the



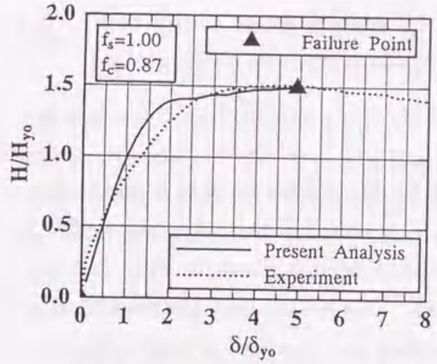


(a) UC70–25–3[0]
($R_f$=0.750, λ=0.276, $l_c$/h=0.3)

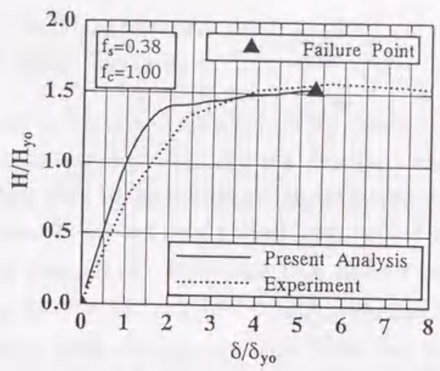


(b) UC70–25–5[3]
($R_f$=0.750, λ=0.276, $l_c$/h=0.5)

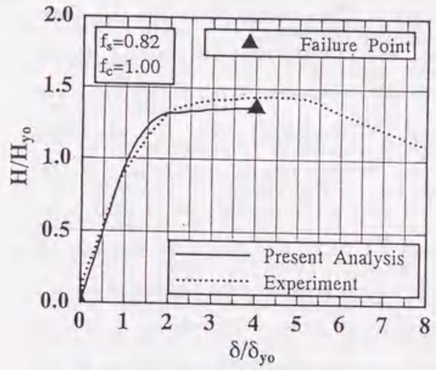


(c) UC70–40–3[0]
($R_f$=0.750, λ=0.429, $l_c$/h=0.3)

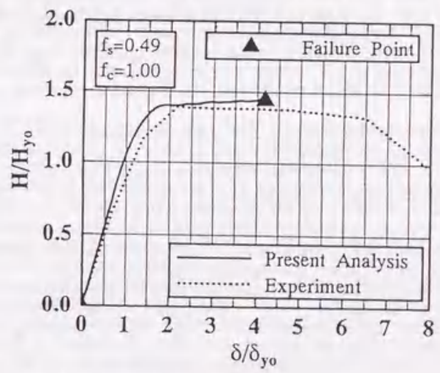


(d) UC90–40–5[3]
($R_f$=0.961, λ=0.434, $l_c$/h=0.5)

**Fig. 7.6 Comparisons of Computed Results by Present Analysis and Experimental Data Given in Chapter 5**

point at which the column is considered to be failed. These points were determined based on the previous failure criterion. As describe in the previous section, at the failure point, failure occurred at either the hollow steel section part or concrete-filled steel section part. The degrees of damage of the sections are represented by two indices, $f_s$ and $f_c$, which are defined as

$$f_s = \frac{\Phi_{ave,s}}{\Phi_m} \tag{7.39}$$

$$f_c = \frac{\Phi_{ave,c}}{\Phi_f} \tag{7.40}$$

It is clear that at the failure point, $f_s$ or $f_c$ will be unity. That is, $f_s$=1.0 means that the hollow steel section part has failed, and $f_c$=1.0 indicates that the concrete-filled steel section part has failed. In the case of specimen UU2 shown in **Fig. 7.5(a)**, for example, $f_s$=1.0 and $f_c$=0.82 were obtained. This means that the steel section part has failed while the concrete-filled steel section part was still in good condition. The magnitude of $f_c$ manifests the damage degree of the concrete-filled steel section part. On the other hand, in the case of specimen UU3 [**Fig. 7.5(b)**], the values of the two indices are obtained as: $f_s$=0.38 and $f_c$=1.0. This means that the concrete-filled steel section part of the column has failed. It is noted that the failure modes of the columns observed in the analysis are generally consistent with those observed in the tests except for two specimens (UU5 and UC70-40-3[0]). For the specimen UU5, the numerical analysis gives the values of two damage degree indices as $f_s$=1.00 and $f_c$=0.84. This implies that both the hollow part and concrete-filled part were substantially damaged. The case of the specimen UC70-40-3[0] was also similar. It is also evident that the predicted maximum loads and corresponding deformation are in very good agreement with experimental results in all cases. Therefore, it can be concluded that the present simple analytical model gives satisfactory predictions of the maximum loads and corresponding deformations and it will be of great importance in practical seismic design.



## 7.5 Parametric Study on the Ultimate Strength and Deformation of Concrete-Filled Steel Columns

It is of great practical use to have an empirical formula or design chart for determining the ultimate strength and corresponding deformation capacity of a member. For this purpose, a parametric study will be conducted by applying the proposed simple analytical method.

### 7.5.1 Input Data

In designing steel bridge piers of thin-walled box sections, main design parameters are width-thickness ratio parameter ($R_f$) and slenderness ratio parameter ($\overline{\lambda}$). Moreover, it has been shown in the experimental study that the axial force ($P$) significantly affect the column behavior. Therefore, the effect of the axial force must be investigated. For the concrete-filled steel bridge piers, the length of the filled-in concrete, $l_c$, is needed to be determined.

In the present study, the values of the parameters $R_f$ and $\overline{\lambda}$ were determined based on the practical investigations on the constructed bridge piers. It should be pointed out that the use of columns with large width-thickness ratio and slenderness ratio, e.g., $R$=0.9 and $\overline{\lambda}$=0.6, is of great importance in designing steel bridge piers with filled-in concrete, although such columns were not common in the past. The values of the parameters used are summarized in **Table 7.1** together with the material properties of steel and concrete.

**Table 7.1 Input Data for Parametric Analysis**

| Property or Parameter | | Value |
|---|---|---|
| Young's Modulus | $E(kgf/mm^2)$ | 21000.0 |
| Yield Stress | $\sigma_y(kgf/mm^2)$ | 24.0 |
| Poisson's Ratio | $\nu$ | 0.3 |
| Plate thickness | $t(mm)$ | 20 |
| Width-thickness ratio parameter | $R$ | 0.6, 0.7, 0.8, 0.9 |
| Slenderness ratio parameter | $\overline{\lambda}$ | 0.2. 0.4, 0.6 |
| Axial force ratio | $P/P_y$ | 0.0, 0.2, 0.4, 0.6 |
| Length of filled-in concrete | $l_c/h$ | 0.1, 0.3, 0.5, 0.7 |
| Compressive Strength | $f_{ck}(kgf/mm^2)$ | 2.40 |

### 7.5.2 Ultimate Strength and Deformation

Using the previous simple analytical method, calculations were carried out for each combination of the width-thickness ratio parameters ($R_f$), slenderness ratio parameter ($\overline{\lambda}$), length of the filled-in concrete ($l_c/h$), and axial force ($P/P_y$). As a result, the load-deformation curves were obtained for all the cases. Based on the failure criterion, the ultimate strengths and corresponding deformations were found. In order to be of use in practical engineering, the obtained ultimate strengths and deformations were arranged in the form of design charts as shown in **Figs. 7.7** and **7.8**, respectively. In the figures, loads and deformations are non-dimensionalized with $H_{yo}$ and $\delta_{yo}$, which can be easily calculated using **Eqs. (4.3)** and **(4.4)**. Accordingly, the ultimate strengths and corresponding deformations can be determined approximately by interpolation from the given design charts if the values of the parameters (i.e., $R_f$, $\overline{\lambda}$, $l_c/h$ and $P/P_y$) are known.



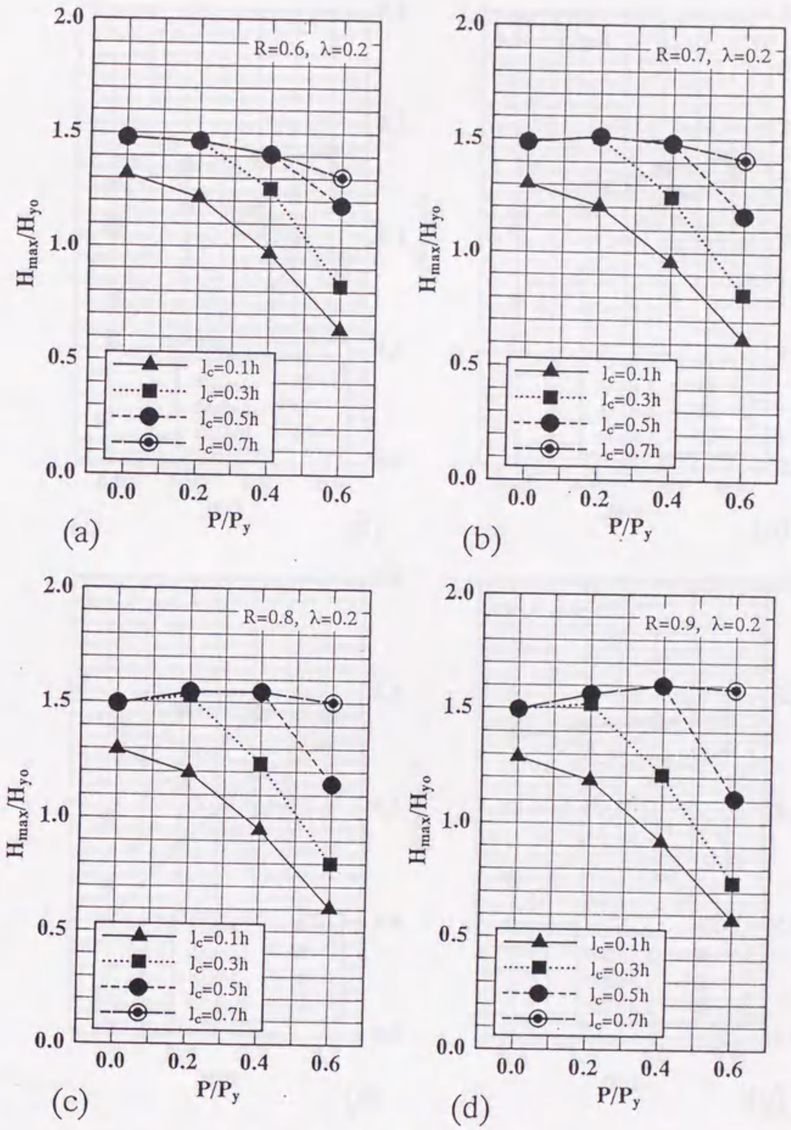


Fig. 7.7 Design Charts for Determining Ultimate Strengths of Concrete-Filled Steel Box Columns (to be continued)

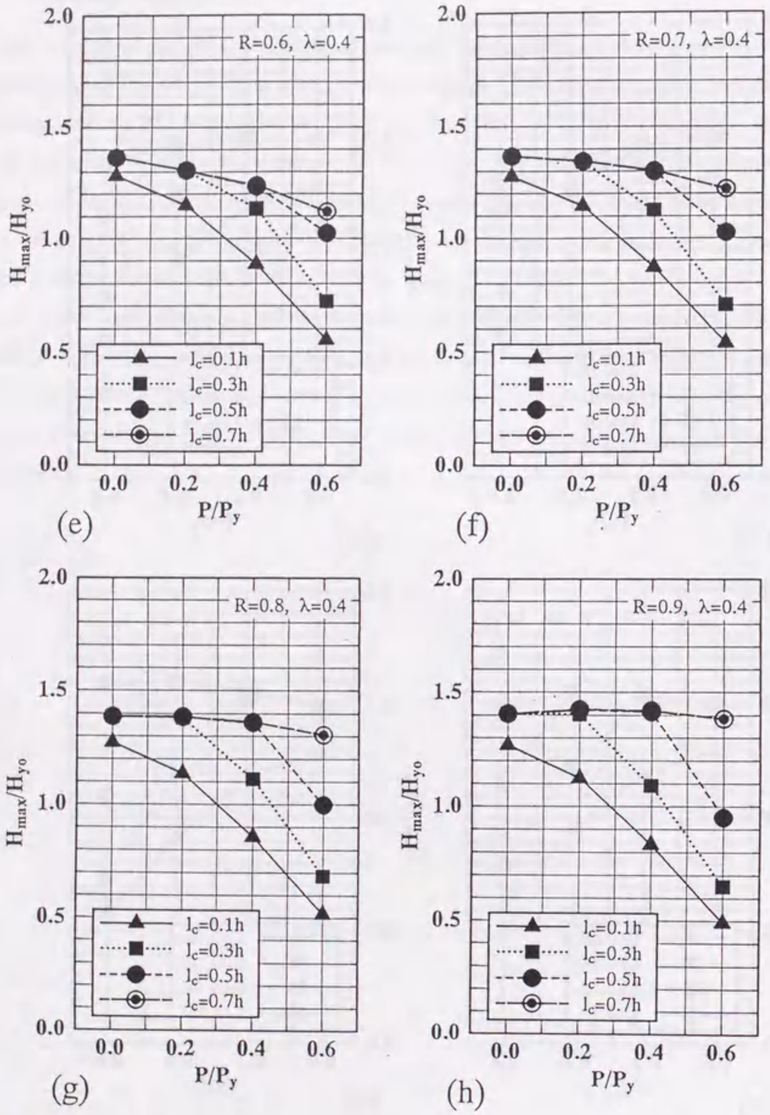


Fig. 7.7 Design Charts for Determining Ultimate Strengths of Concrete-Filled Steel Box Columns (continued)



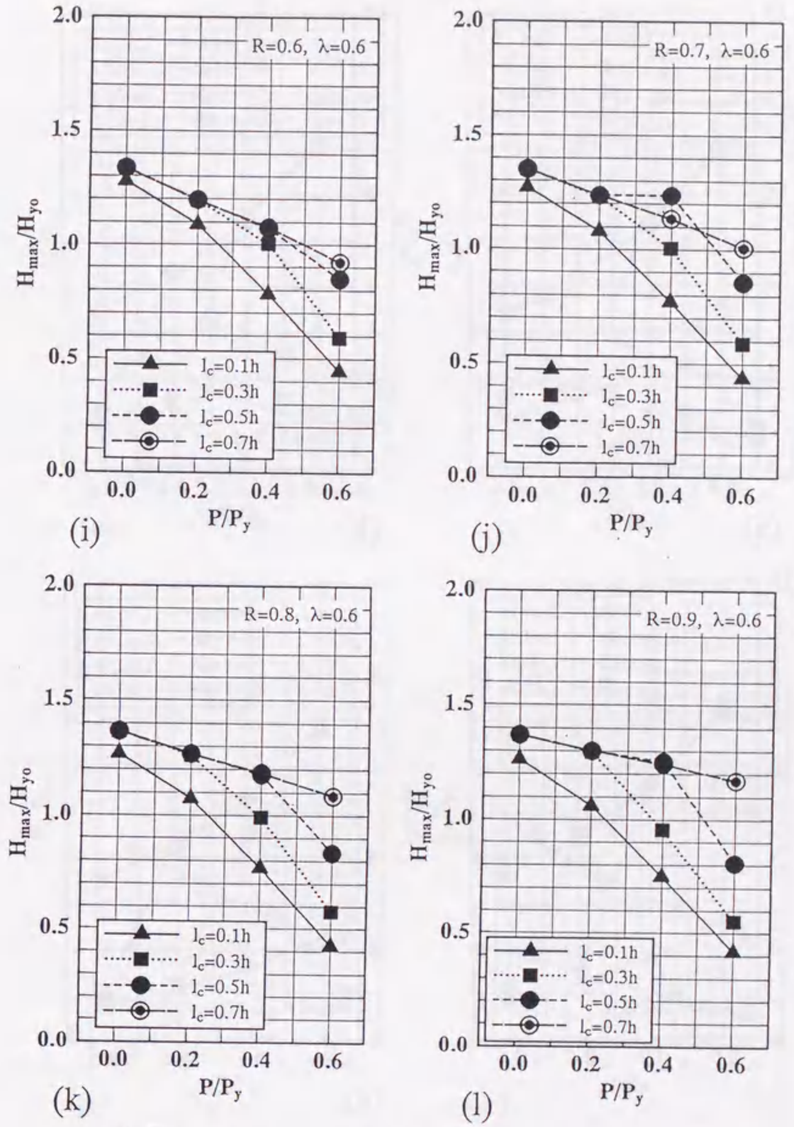


Fig. 7.7 Design Charts for Determining Ultimate Strengths of Concrete-Filled Steel Box Columns (continued)

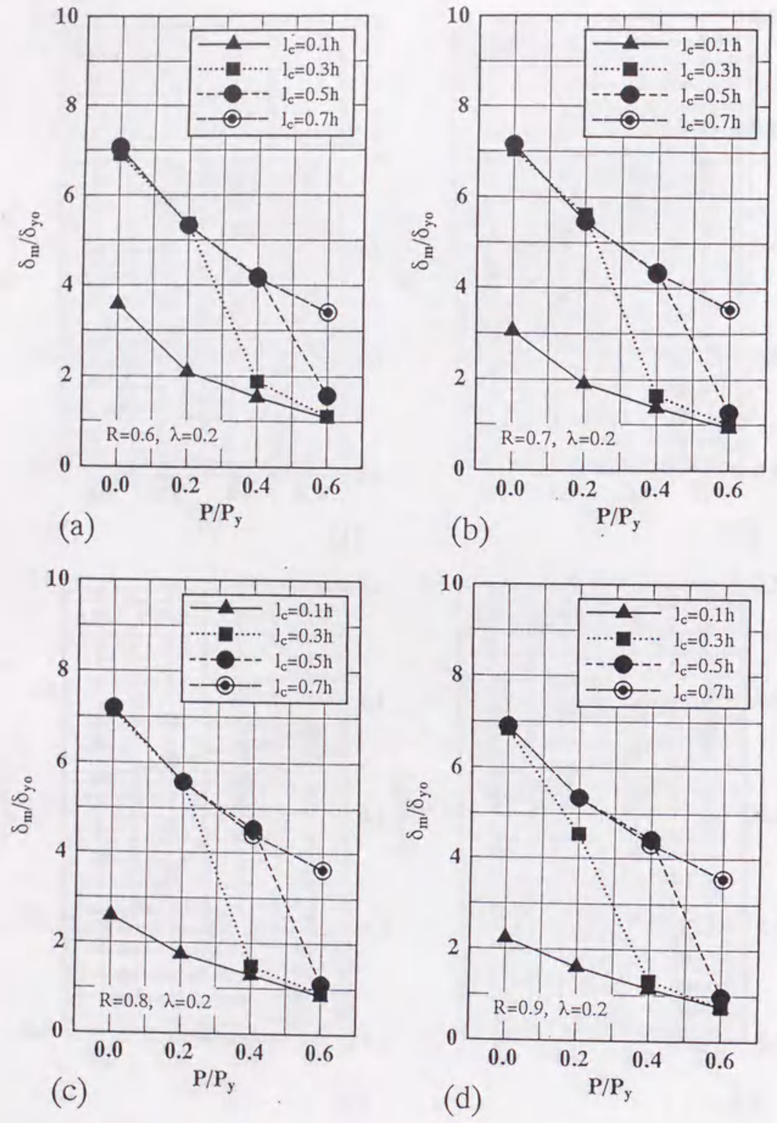


Fig. 7.8 Design Charts for Determining Ultimate Deformations of Concrete-Filled Steel Box Columns (to be continued)



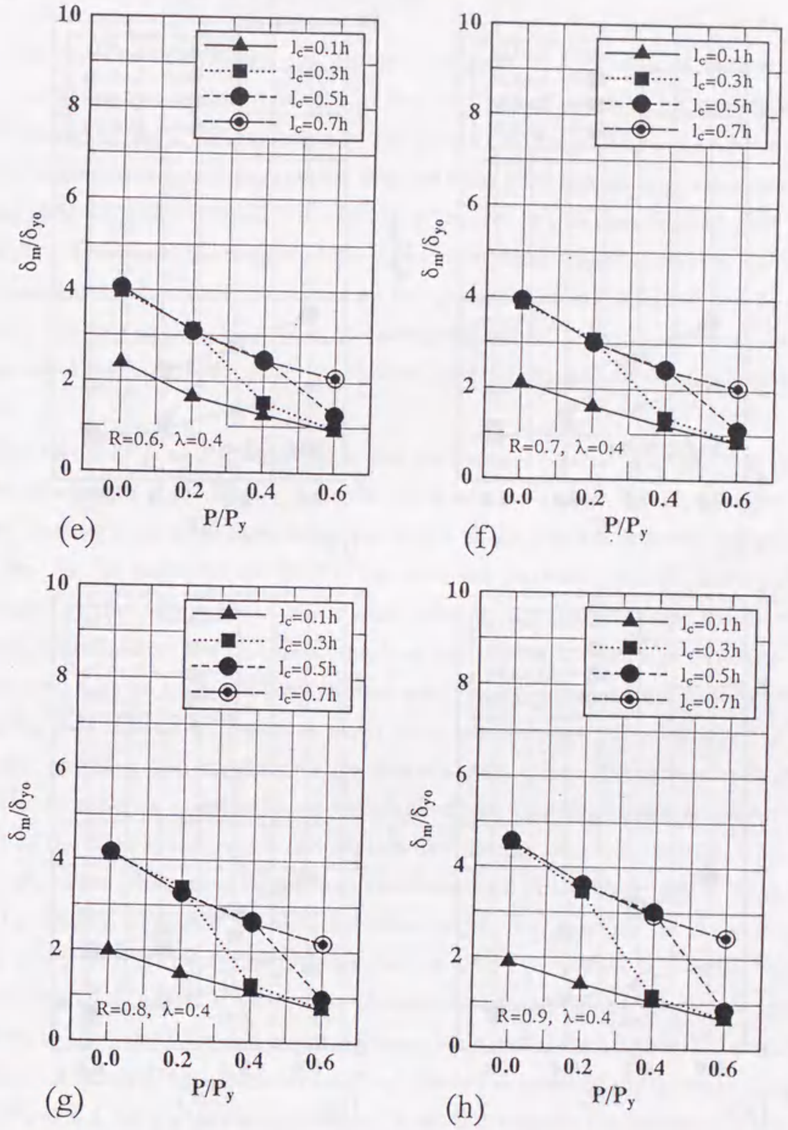


Fig. 7.8 Design Charts for Determining Ultimate Deformations of Concrete-Filled Steel Box Columns (continued)

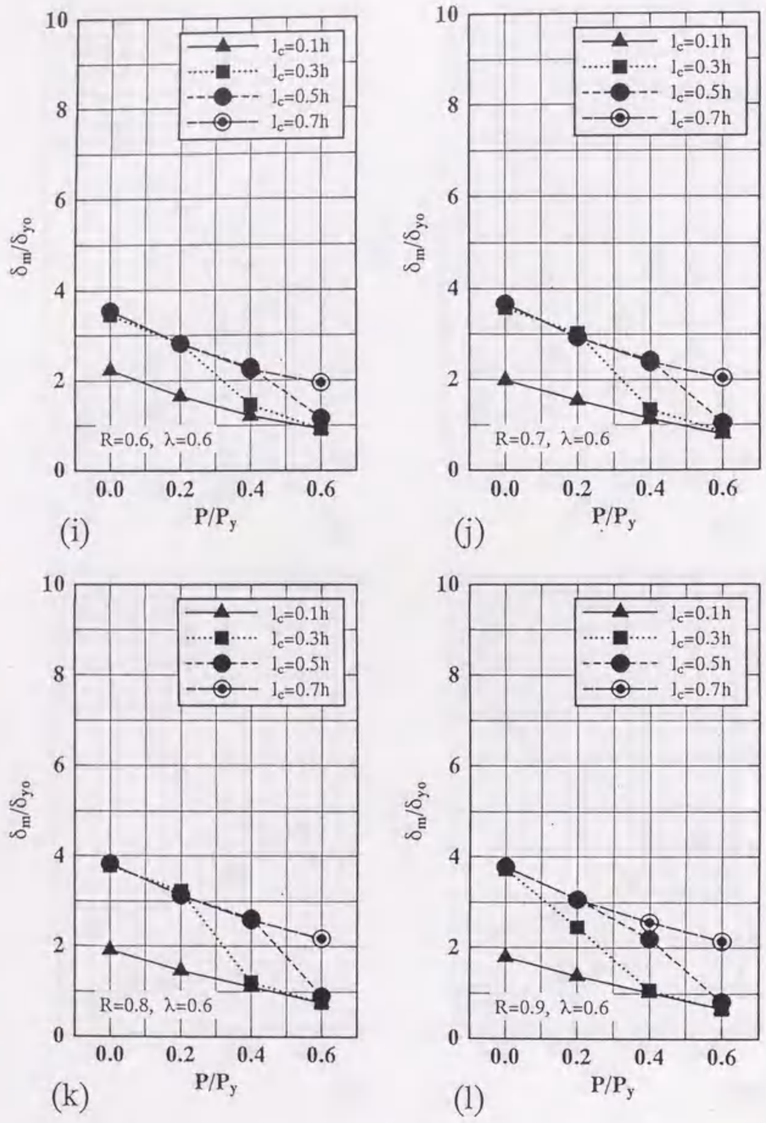


**Fig. 7.8 Design Charts for Determining Ultimate Deformations of Concrete-Filled Steel Box Columns (continued)**



### 7.5.3 Optimum Length of Filled-in Concrete

As discussed previously, the degree of damage of a column at failure can be represented by two indices $f_s$ and $f_c$. The two indices seem to be good measures for determining the optimum length of the filled-in concrete. From the view point of ultimate-seismic design, it is expected that both the steel section and concrete section attain their ultimate states simultaneously at failure. In this case, both $f_s$ and $f_c$ will be unity. Therefore, the length of the filled-in concrete which generates the above-mentioned critical state is considered to be optimum. If the designed length of the filled-in concrete exceeds this value, the additional weight of the concrete would make designing of the foundation more complicated, and thereby leading to an uneconomical design.

The values of $f_s$ and $f_c$ obtained in the analysis are plotted in **Figs. 7.9** to **7.11** against the length of the filled-in concrete. As is seen from these figures, columns failed at the steel sections in all cases when the length of the filled-in concrete was taken to be $0.1h$. As the length of the filled-in concrete was increased to $0.3h$, some columns still failed at the steel sections, while some failed at the concrete-filled steel sections. As mentioned above, the optimum length of the filled-in concrete is obtained when the column fails at both the steel section and concrete-filled section simultaneously. Actually, it is difficult to obtain an exact value which makes the column fail at both sections, and it is also meaningless for practical use. Thus, the optimum length of the filled-in concrete is defined from the point of view of practical use as follows. The length of the filled-in concrete is divided into five discrete values: $0.1h$, $0.3h$, $0.5h$, $0.7h$ and $1.0h$. Then, first value larger than the theoretical optimum length in **Figs. 7.9** to **7.11** is taken to be the practical optimum length. For example, in the case of $R_f = 0.6$ and $\overline{\lambda} = 0.2$, the optimum length of the filled-in concrete is $0.3h$ for $P/P_y = 0.0$ [see **Fig. 7.9(a)**]. It is found that the optimum length of the filled-in concrete is sensitive to the axial force and width-thickness ratio parameter. **Table 7.2** contains a summary of values of the optimum length of filled-in concrete of the columns analyzed for $P/P_y \leq 0.4$. Of particular significance is the fact that all the values of $l_c$ are $0.3h$ and $0.5h$ with one exception (i.e., the case of $R = 0.9$, $\overline{\lambda} = 0.6$ and $P/P_y = 0.4$). Thus, it may be concluded that in most cases the length of filled-in concrete can be taken as 0.3 or 0.5 times of the column height. Based on the above discussions, the following

design recommendation is proposed for determining the optimum length of the filled-in concrete:

(1) $R_f \leq 0.7$

$$for \;\; 0.0 \leq \frac{P}{P_y} \leq 0.2, \quad l_c = 0.3h \tag{7.41}$$

$$for \;\; 0.2 < \frac{P}{P_y} \leq 0.4, \quad l_c = 0.5h \tag{7.42}$$

$$for \;\; 0.4 < \frac{P}{P_y} \leq 0.6, \quad l_c = 0.7h \tag{7.43}$$

(2) $0.7 < R_f \leq 0.9$

$$for \;\; \frac{P}{P_y} = 0.0, \qquad l_c = 0.3h \tag{7.44}$$

$$for \;\; 0.0 < \frac{P}{P_y} \leq 0.4, \quad l_c = 0.5h \tag{7.45}$$

$$for \;\; 0.4 < \frac{P}{P_y} \leq 0.6, \quad l_c = 0.7h \tag{7.46}$$

According to the above recommendation, the proposed lengths of filled-in concrete for the columns are also given in **Table 7.2**. There are three columns for which the proposed length is different from the calculated one. In two of these, the length of filled-in concrete is proposed to be $0.5h$ instead of the calculated value $0.3h$. Obviously, this change does not affect the safety of the column. For the third column of $R = 0.9$, $\overline{\lambda} = 0.6$ and $P/P_y = 0.4$, the proposed length of filled-in concrete is decreased from $0.7h$ to $0.5h$. As will be given in **Table 8.2**, however, the value of the reduction factor $RF_m$ for the equivalent seismic coefficient of this column is 0.167 and it is still safe although the proposed length of filled-in concrete is smaller than the calculated length.



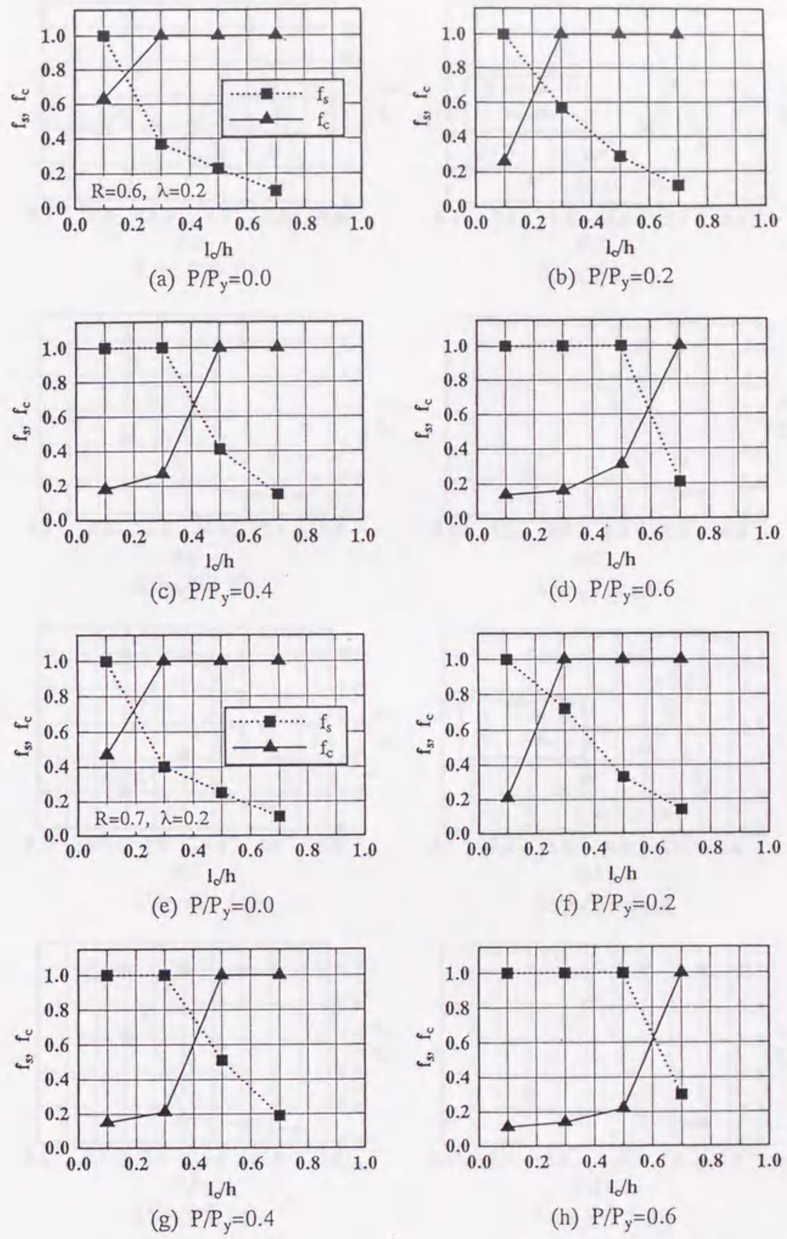


(a) P/P$_y$=0.0 (b) P/P$_y$=0.2

(c) P/P$_y$=0.4 (d) P/P$_y$=0.6

(e) P/P$_y$=0.0 (f) P/P$_y$=0.2

(g) P/P$_y$=0.4 (h) P/P$_y$=0.6

**Fig. 7.9 $f_s$ and $f_c$ Values of Analyzed Columns: $\overline{\lambda} = 0.2$ (to be continued)**

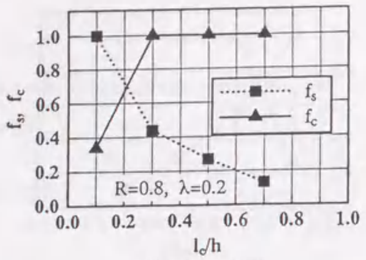

(i) $P/P_y$=0.0

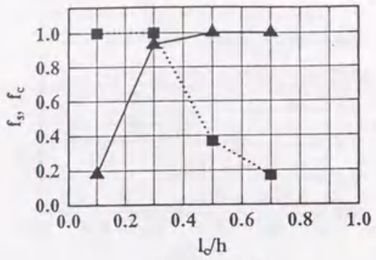

(j) $P/P_y$=0.2

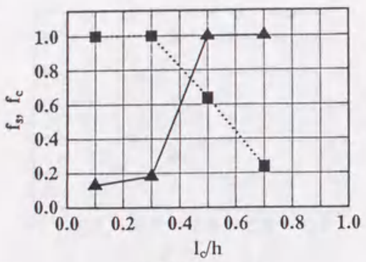

(k) $P/P_y$=0.4

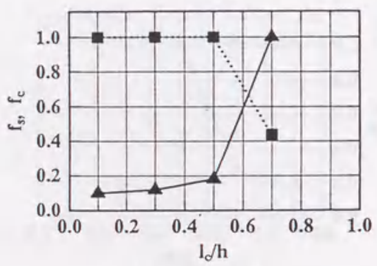

(l) $P/P_y$=0.6

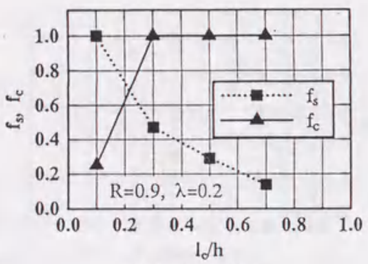

(m) $P/P_y$=0.0

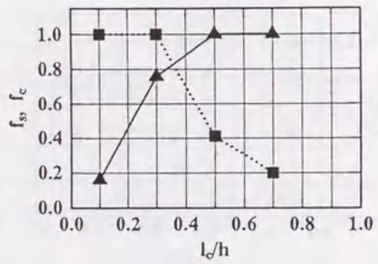

(n) $P/P_y$=0.2

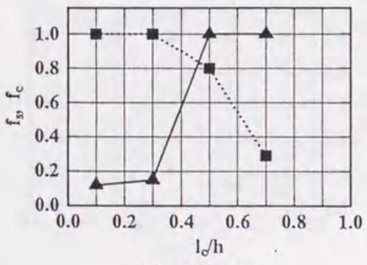

(o) $P/P_y$=0.4

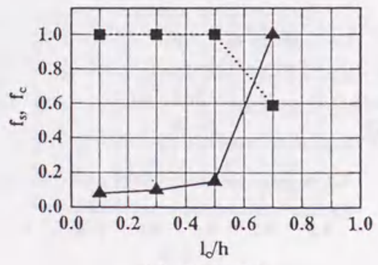

(p) $P/P_y$=0.6

Fig. 7.9 $f_s$ and $f_c$ Values of Analyzed Columns: $\overline{\lambda} = 0.2$ (continued)



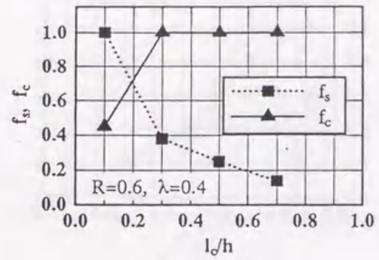

(a) $P/P_y$=0.0

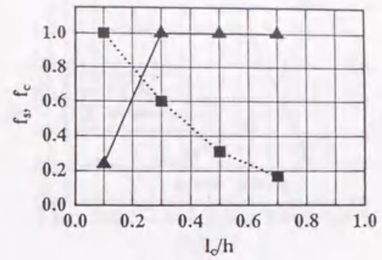

(b) $P/P_y$=0.2

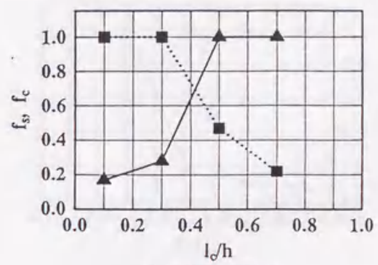

(c) $P/P_y$=0.4

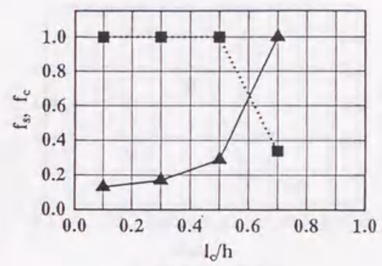

(d) $P/P_y$=0.6

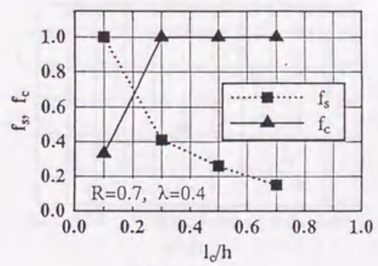

(e) $P/P_y$=0.0

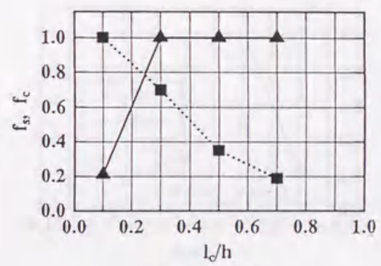

(f) $P/P_y$=0.2

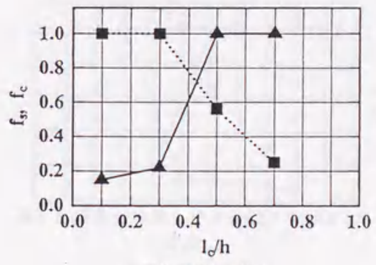

(g) $P/P_y$=0.4

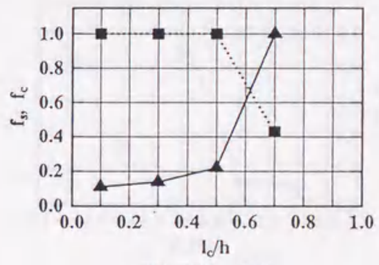

(h) $P/P_y$=0.6

Fig. 7.10 $f_s$ and $f_c$ Values of Analyzed Columns: $\overline{\lambda} = 0.4$ (to be continued)

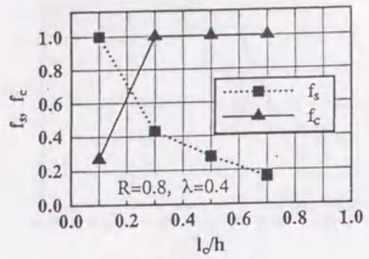

(i) $P/P_y$=0.0

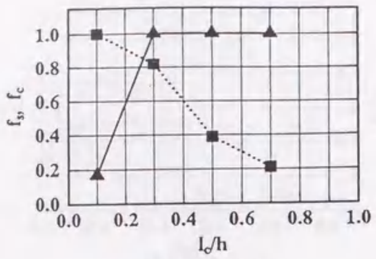

(j) $P/P_y$=0.2

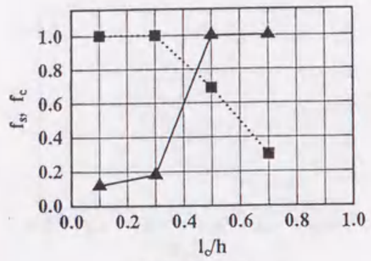

(k) $P/P_y$=0.4

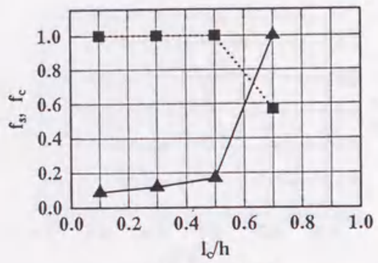

(l) $P/P_y$=0.6

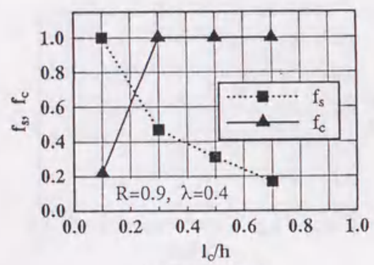

(m) $P/P_y$=0.0

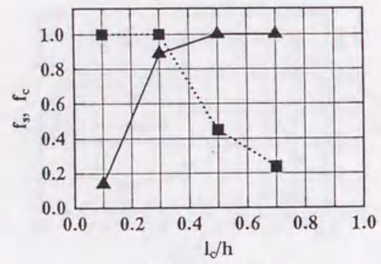

(n) $P/P_y$=0.2

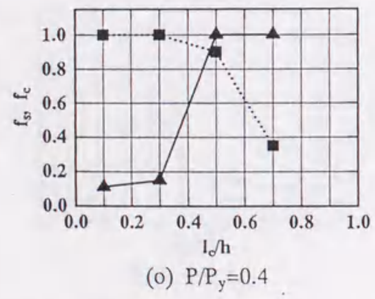

(o) $P/P_y$=0.4

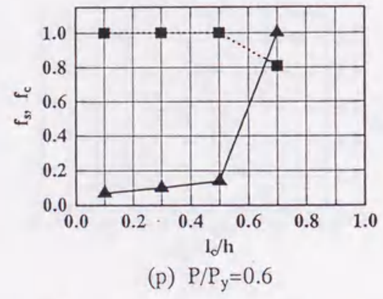

(p) $P/P_y$=0.6

Fig. 7.10 $f_s$ and $f_c$ Values of Analyzed Columns: $\overline{\lambda} = 0.4$ (continued)



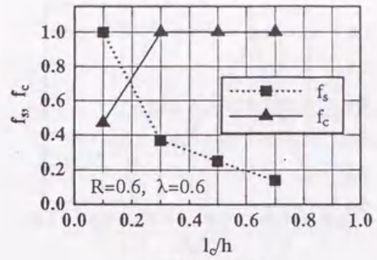

(a) $P/P_y$=0.0

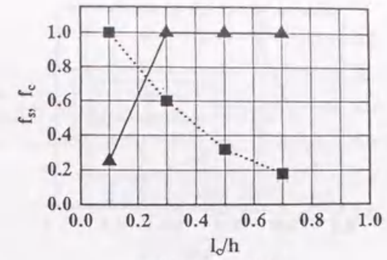

(b) $P/P_y$=0.2

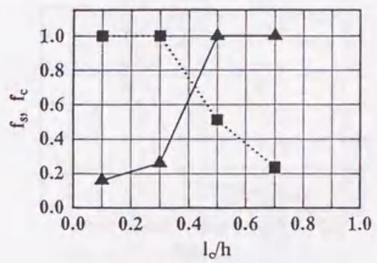

(c) $P/P_y$=0.4

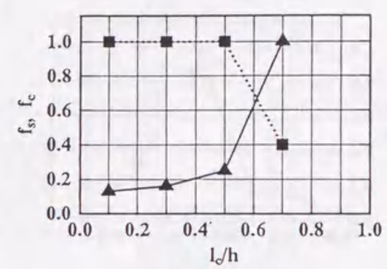

(d) $P/P_y$=0.6

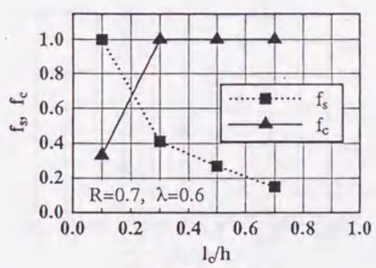

(e) $P/P_y$=0.0

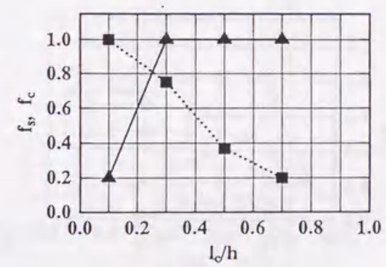

(f) $P/P_y$=0.2

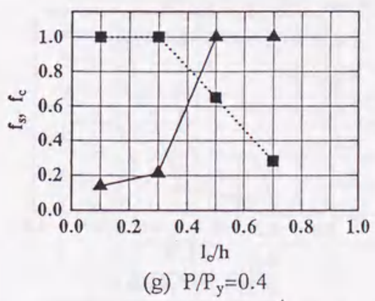

(g) $P/P_y$=0.4

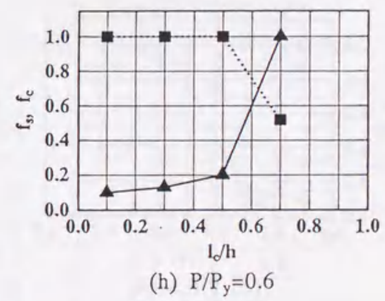

(h) $P/P_y$=0.6

Fig. 7.11 $f_s$ and $f_c$ Values of Analyzed Columns: $\overline{\lambda} = 0.6$ (to be continued)

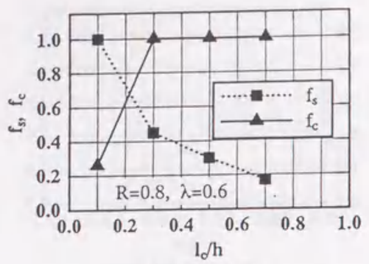

(i) $P/P_y$=0.0

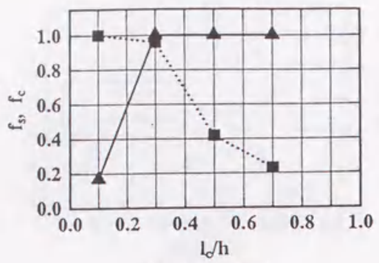

(j) $P/P_y$=0.2

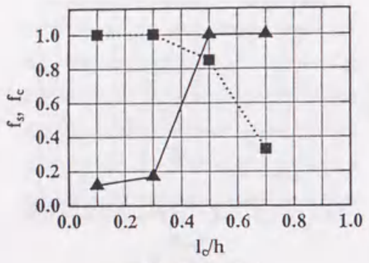

(k) $P/P_y$=0.4

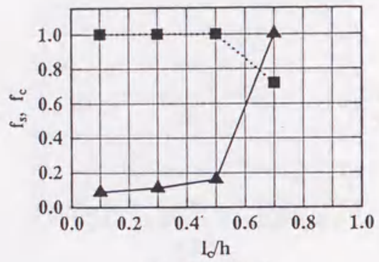

(l) $P/P_y$=0.6

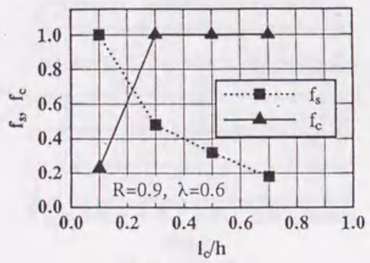

(m) $P/P_y$=0.0

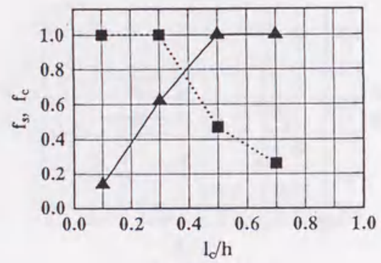

(n) $P/P_y$=0.2

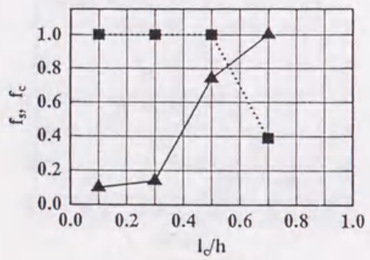

(o) $P/P_y$=0.4

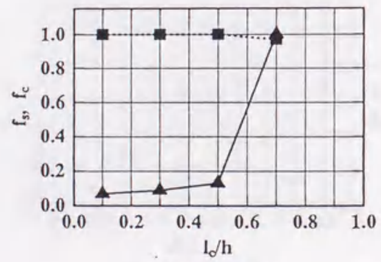

(p) $P/P_y$=0.6

**Fig. 7.11 $f_s$ and $f_c$ Values of Analyzed Columns: $\overline{\lambda} = 0.6$ (continued)**



**Table 7.2 Optimum Length of Filled-in Concrete**

| $R_f$ | $\overline{\lambda}$ | $\frac{P}{P_y}$ | $l_c/h$ | |
|---|---|---|---|---|
| | | | Calculated | Proposed |
| 0.6 | 0.2 | 0.0 | 0.3 | 0.3 |
| 0.6 | 0.2 | 0.2 | 0.3 | 0.3 |
| 0.6 | 0.2 | 0.4 | 0.5 | 0.5 |
| 0.7 | 0.2 | 0.0 | 0.3 | 0.3 |
| 0.7 | 0.2 | 0.2 | 0.3 | 0.3 |
| 0.7 | 0.2 | 0.4 | 0.5 | 0.5 |
| 0.8 | 0.2 | 0.0 | 0.3 | 0.3 |
| 0.8 | 0.2 | 0.2 | 0.5 | 0.5 |
| 0.8 | 0.2 | 0.4 | 0.5 | 0.5 |
| 0.9 | 0.2 | 0.0 | 0.3 | 0.3 |
| 0.9 | 0.2 | 0.2 | 0.5 | 0.5 |
| 0.9 | 0.2 | 0.4 | 0.5 | 0.5 |
| 0.6 | 0.4 | 0.0 | 0.3 | 0.3 |
| 0.6 | 0.4 | 0.2 | 0.3 | 0.3 |
| 0.6 | 0.4 | 0.4 | 0.5 | 0.5 |
| 0.7 | 0.4 | 0.0 | 0.3 | 0.3 |
| 0.7 | 0.4 | 0.2 | 0.3 | 0.3 |
| 0.7 | 0.4 | 0.4 | 0.5 | 0.5 |
| 0.8 | 0.4 | 0.0 | 0.3 | 0.3 |
| 0.8 | 0.4 | 0.2 | **0.3** | **0.5** |
| 0.8 | 0.4 | 0.4 | 0.5 | 0.5 |
| 0.9 | 0.4 | 0.0 | 0.3 | 0.3 |
| 0.9 | 0.4 | 0.2 | 0.5 | 0.5 |
| 0.9 | 0.4 | 0.4 | 0.5 | 0.5 |
| 0.6 | 0.6 | 0.0 | 0.3 | 0.3 |
| 0.6 | 0.6 | 0.2 | 0.3 | 0.3 |
| 0.6 | 0.6 | 0.4 | 0.5 | 0.5 |
| 0.7 | 0.6 | 0.0 | 0.3 | 0.3 |
| 0.7 | 0.6 | 0.2 | 0.3 | 0.3 |
| 0.7 | 0.6 | 0.4 | 0.5 | 0.5 |
| 0.8 | 0.6 | 0.0 | 0.3 | 0.3 |
| 0.8 | 0.6 | 0.2 | **0.3** | **0.5** |
| 0.8 | 0.6 | 0.4 | 0.5 | 0.5 |
| 0.9 | 0.6 | 0.0 | 0.3 | 0.3 |
| 0.9 | 0.6 | 0.2 | 0.5 | 0.5 |
| 0.9 | 0.6 | 0.4 | **0.7** | **0.5** |

## 7.6 Summary

A numerical analysis of the concrete-filled steel box column was presented. In the beginning, numerical method was discussed. In this simple analytical model, the moment-curvature relations given in Chapter 6 are integrated along the column axis, to obtain the load-deformation behavior of a column. In the analysis, a concept of effective failure length was introduced to define a failure criterion for the concrete-filled steel box column. The numerical results were then compared with the test results presented in Chapters 4 and 5. In order to be of practical use, design charts for determining the ultimate strengths and deformations were obtained by conducting a parametric study. Finally, a recommendation for the optimum length of the filled-in concrete was proposed for practical designs.



# 8 RECOMMENDATIONS FOR EARTHQUAKE-RESISTANT ULTIMATE-STRENGTH DESIGN METHOD FOR CONCRETE-FILLED STEEL BOX COLUMNS

## 8.1 General Remarks

In the previous chapters, the behavior of the concrete-filled steel box column modeling bridge pier has been experimentally and theoretically investigated. Based on the phenomena observed in the tests, it is feasible to define the maximum load point of the load-deformation curve as the failure point in the ultimate design of the concrete-filled steel box columns. It has been shown that the ductility and energy-absorption capacity of steel box column can be significantly improved by filling concrete inside. Hence, the concrete-filled steel box column is an excellent alternative structural member when the steel box column is not sufficient to withstand a strong earthquake. However, no code is available for ultimate seismic designs of such columns. In Chapter 7, a simple calculation method for the ultimate strengths and deformations was presented, and some design charts were given. Moreover, the optimum length of the filled-in concrete was described. In this chapter, a design recommendation for concrete-filled steel box columns is proposed on the basis of the previous experimental and theoretical studies.

## 8.2 Design Recommendations

It is recommended that only the hollow steel box column be designed as per the allowable stress design. Next, the optimum length of the filled-in concrete shall be decided. Finally, the equivalent seismic coefficient for the designed section shall be calculated for checking purpose.

Item 1. Material

Item 1.1 Steel

Structural steel shall be of the quality specified in the code (1990) of Japanese Road Association (JRA).

Item 1.2 Concrete

Standard design strength of concrete should be greater than 240 kgf/mm$^2$.

Table 8.1 Earthquake-Resistant Design

| Earthquake | Maximum Acceleration | Design Method | $k_e$ |
|---|---|---|---|
| medium and smaller | $\approx$ 200 gal | allowable-stress design | 0.2 |
| stronger | 300 $\sim$ 400 gal | ultimate-strength design | 1.0 |

Note: $k_e$ = Standard seismic design coefficient.

Item 2. Design of Steel Box Column

The structural calculations of steel box columns shall be based on the method of allowable stress design. Detailed procedures for design of hollow steel box columns shall follow the JRA code. Loads, and external forces and their combination for the structural calculation shall conform to the same code. It should be noted that the seismic load considered here is calculated with respect to the medium and smaller earthquakes (see **Table 8.1**). For the seismic load, $P_e$, it is assumed to act on the top of the bridge pier and given by

$$P_e = k_h \cdot W_U \tag{8.1}$$

where $k_h$ = the seismic design coefficient;

$W_U$ = the total weight of the superstructures.

In the JRA code, the seismic design coefficient $k_h$ is defined as the product of several factors such as the locality, natural period, important degree and ground zone.

$$k_h = C_Z \cdot C_G \cdot C_I \cdot C_T \cdot k_e \tag{8.2}$$

where $k_e$ = Standard seismic design coefficient = 0.2;

$C_Z$ = Locality correction factor;

$C_G$ = Ground zone correction factor;

$C_I$ = Important degree correction factor;

$C_T$ = Natural period correction factor.

Item 3. Determination of Length of Filled-in Concrete

Once the design of the steel box column is finished, the length of the filled-in concrete shall be determined according to the optimum length equations given in **Eqs. (7.41)** through **(7.46)**.



Item 4. Calculation of Reduction Factor ($RF_m$) for Equivalent Seismic Coefficient

Item 4.1 Ultimate Load and Deformation of Members

Ultimate Strength of a concrete-filled member shall be found by interpolation from design charts given in **Fig. 7.7**. The quantity $H_{yo}$ shall be as given by **Eq. (4.3)**.

Ultimate Deformation of a concrete-filled member shall be found by interpolation from design charts given in **Fig. 7.8**. The quantity $\delta_{yo}$ shall be as given by **Eq. (4.4)**.

If a more accurate value is necessary, it shall be calculated with the help of the proposed simple analytical method.

Item 4.2 Calculation of Reduction Factor $RF_m$ for Equivalent Seismic Coefficient

Calculation of reduction factor $RF_m$ for the equivalent seismic coefficient shall be as given in **Eq. (5.6)**. In this equation, the coefficient $\alpha$ is defined as the ratio of the maximum load $H_{max}$ and the yield load $H_y$. The yield load $H_y$ is to be computed ignoring the effect of the filled-in concrete and shall be calculated according to the following interaction equations (Usami, 1990).

$$\frac{P}{P_u} + \frac{0.85M}{Q_B \cdot M_y(1 - P/P_E)} = 1.0 \tag{8.3}$$

$$\frac{P}{Q \cdot P_y} + \frac{M}{Q_B \cdot M_y} = 1.0 \tag{8.4}$$

where $M = H \cdot h$. Thus, the smaller value of $H$ obtained from **Eqs. (8.3)** and **(8.4)** gives the yield load $H_y$. In the above equation, $P_E$ is the Euler buckling load ($=\pi^2 EI/4h^2$), while $Q$ and $Q_B$ are given by

$$Q = \frac{\sum A_e}{\sum A} = \frac{0.7}{R_f} \leq 1.0 \tag{8.5}$$

$$Q_B = [\frac{A_e}{A}]_{Flange} = \frac{0.7}{R_f} \leq 1.0 \tag{8.6}$$

for unstiffened box steel columns. And $P_u$ is given by

$$\begin{aligned} \frac{P_u}{QP_y} &= 1.0, \quad \text{for } \overline{\lambda}' \leq 0.2 \\ &= 1.109 - 0.545\overline{\lambda}', \quad \text{for } 0.2 \leq \overline{\lambda}' \leq 1.0 \\ &= \frac{1}{0.773 + \overline{\lambda}'^2}, \quad \text{for } \overline{\lambda}' \geq 1.0 \end{aligned} \tag{8.7}$$

$$\overline{\lambda}' = \sqrt{Q}\overline{\lambda} \tag{8.8}$$

in which $A$ = area of component plate; $A_e$ = effective area of component plate; $\sum$ = summation for all the component plates; and $R_f$ = width-thickness ratio parameter of component plate.

In **Eq. (5.6)**, the ductility, $\mu_m$, was defined as the ratio of $\delta_{max}$ (displacement corresponding to $H_{max}$) and $\delta_y$ (displacement corresponding to $H_y$). It is assumed that $\delta_y$ is calculated by the relation: $\delta_y/\delta_{yo}$=$H_y/H_{yo}$.

Item 5. Calculation of Lateral Load Resisting Capacity

Design calculation of steel bridge piers in Item 2 was conducted with respect to medium and smaller earthquakes. However, for a strong earthquake, the seismicity of the bridge pier filled with concrete has to be checked. For the purpose, the ultimate-strength design method should be employed. This design methodology requires a calculation of lateral load resisting capacity instead of re-design by allowable stress design method. That is, the lateral load resisting capacity should satisfy the following equation:

$$k_h \cdot W \leq H_a \tag{8.9}$$

where $k_h$ = Equivalent seismic coefficient;
$W$ = Equivalent weight;
$H_a$ = Allowable lateral strength.

Item 5.1 Calculation of $k_h$

For the equivalent seismic coefficient, $k_h$, it is calculated by

$$k_h = RF_m \cdot k_c \tag{8.10}$$

where $k_h$ = seismic design coefficient;
$RF_m$ = Reduction factor for equivalent seismic coefficient which has been found in Item 4.

According to the JRA code, the seismic design coefficient can be obtained by considering some correction factors as

$$k_c = C_Z \cdot C_I \cdot C_R \cdot k_e \tag{8.11}$$



where $k_e$ = Standard seismic design coefficient = 1.0;
$C_Z$ = Locality correction factor;
$C_I$ = Important degree correction factor;
$C_R$ = Vibration property correction factor.

Item 5.2 Calculation of $W$

The equivalent weight $W$ shall be calculated by

$$W = W_U + 0.5W_L \tag{8.12}$$

where $W_U$ = total weight of the superstructure;
$W_L$ = total weight of the pier.

Item 5.3 Calculation of $H_a$

The allowable lateral strength $H_a$ shall be calculated by

$$H_a = H_y + \frac{H_{max} - H_y}{\alpha_f} \tag{8.13}$$

where $H_y$ = Lateral yield load of the pier;
$H_{max}$ = Ultimate load of the pier;
$\alpha_f$ = Safety factor = 1.5.

## 8.3 Design Examples

In order to examine the capability of the proposed design recommendation, calculations of equivalent seismic coefficients for the columns designed according to the previous procedures are presented.

In the beginning, the dimensionless parameters $R_f$ and $\overline{\lambda}$ as well as axial force $P/P_y$ are determined using the allowable stress design method. The length of the filled-in concrete is then decided for each case. Since all the values of the parameters $R_f$, $\overline{\lambda}$, $P/P_y$ and $l_c/h$ are known, as given in **Table 8.2**, the ultimate strength and deformation of each designed column can be found from the design charts given in Chapter 7. The values of $H_{max}/H_{yo}$ and $\delta_{max}/\delta_{yo}$ for all the columns are also listed in **Table 8.2**, together with the calculated values of the yield load $H_y$ from the interaction **Eqs. (8.3)** and **(8.4)**. Finally, the values of reduction factor $RF_m$ for the equivalent

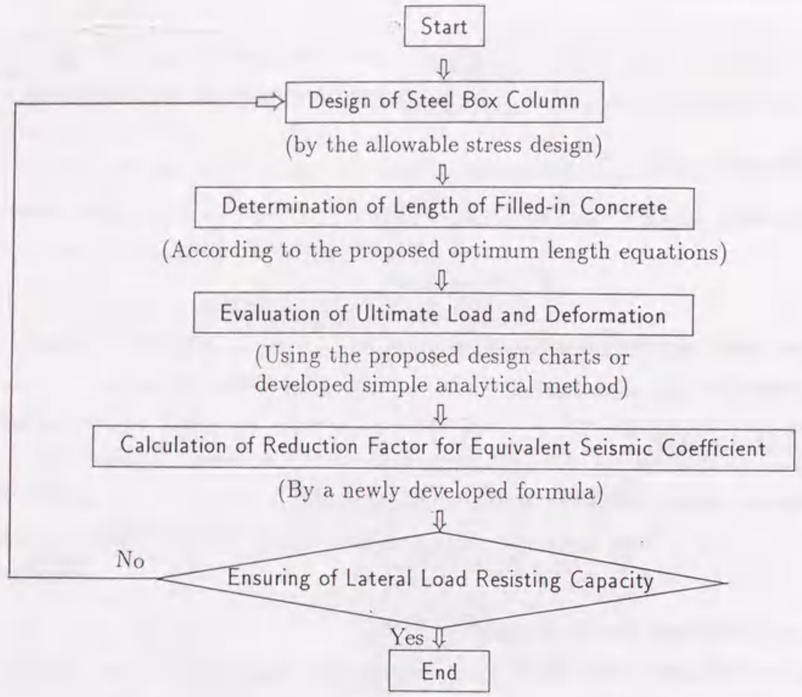


**Fig. 8.1 Design Flowchart**

seismic coefficient are obtained using **Eq. (5.6)** as displayed in the last column of the table. It is found that the values of $RF_m$ are less than 0.30 in most cases, while the maximum value is 0.386 for a column having $R_f$=0.6 and $\overline{\lambda}$=0.6 in the case of axial force $P/P_y$=0.0. **Fig. 8.2** shows the the calculated values of $RF$ of some designed columns.

## 8.4 Summary

Recommendations were proposed for practical design of concrete-filled steel box columns. These recommendations are based on both theoretical and experimental investigations. It is hoped that they will be of great use for obtaining a rational design.



**Table 8.2 Calculated Values of Reduction Factor (RF) for Equivalent Seismic Coefficients of Designed Columns**

| $R_f$ | $\overline{\lambda}$ | $\frac{P}{P_y}$ | $\frac{l_c}{h}$ | $\frac{H_{max}}{H_{yo}}$ | $\frac{\delta_{max}}{\delta_{yo}}$ | $\frac{H_{yo}}{H_y}$ | $RF_m$ |
|---|---|---|---|---|---|---|---|
| 0.6 | 0.2 | 0.0 | 0.3 | 1.479 | 6.911 | 1.000 | 0.252 |
| 0.6 | 0.2 | 0.2 | 0.3 | 1.463 | 5.375 | 1.250 | 0.241 |
| 0.6 | 0.2 | 0.4 | 0.5 | 1.407 | 4.189 | 1.666 | 0.218 |
| 0.7 | 0.2 | 0.0 | 0.3 | 1.486 | 7.033 | 1.000 | 0.250 |
| 0.7 | 0.2 | 0.2 | 0.3 | 1.507 | 5.619 | 1.250 | 0.233 |
| 0.7 | 0.2 | 0.4 | 0.5 | 1.480 | 4.354 | 1.666 | 0.210 |
| 0.8 | 0.2 | 0.0 | 0.3 | 1.495 | 7.136 | 1.142 | 0.221 |
| 0.8 | 0.2 | 0.2 | 0.5 | 1.546 | 5.579 | 1.481 | 0.200 |
| 0.8 | 0.2 | 0.4 | 0.5 | 1.548 | 4.541 | 2.105 | 0.163 |
| 0.9 | 0.2 | 0.0 | 0.3 | 1.494 | 6.841 | 1.285 | 0.205 |
| 0.9 | 0.2 | 0.2 | 0.5 | 1.562 | 5.346 | 1.733 | 0.177 |
| 0.9 | 0.2 | 0.4 | 0.5 | 1.600 | 4.427 | 2.652 | 0.132 |
| 0.6 | 0.4 | 0.0 | 0.3 | 1.364 | 3.970 | 1.000 | 0.353 |
| 0.6 | 0.4 | 0.2 | 0.3 | 1.306 | 3.141 | 1.250 | 0.338 |
| 0.6 | 0.4 | 0.4 | 0.5 | 1.233 | 2.487 | 1.666 | 0.307 |
| 0.7 | 0.4 | 0.0 | 0.3 | 1.366 | 3.870 | 1.000 | 0.358 |
| 0.7 | 0.4 | 0.2 | 0.3 | 1.343 | 3.088 | 1.250 | 0.339 |
| 0.7 | 0.4 | 0.4 | 0.5 | 1.301 | 2.456 | 1.666 | 0.304 |
| 0.8 | 0.4 | 0.0 | 0.3 | 1.386 | 4.135 | 1.142 | 0.306 |
| 0.8 | 0.4 | 0.2 | 0.5 | 1.383 | 3.405 | 1.481 | 0.273 |
| 0.8 | 0.4 | 0.4 | 0.5 | 1.359 | 2.676 | 2.105 | 0.230 |
| 0.9 | 0.4 | 0.0 | 0.3 | 1.405 | 4.527 | 1.285 | 0.262 |
| 0.9 | 0.4 | 0.2 | 0.5 | 1.424 | 3.621 | 1.733 | 0.227 |
| 0.9 | 0.4 | 0.4 | 0.5 | 1.415 | 3.018 | 2.664 | 0.170 |
| 0.6 | 0.6 | 0.0 | 0.3 | 1.336 | 3.442 | 1.000 | 0.386 |
| 0.6 | 0.6 | 0.2 | 0.3 | 1.195 | 2.812 | 1.250 | 0.370 |
| 0.6 | 0.6 | 0.4 | 0.5 | 1.071 | 2.278 | 2.032 | 0.282 |
| 0.7 | 0.6 | 0.0 | 0.3 | 1.350 | 3.572 | 1.000 | 0.376 |
| 0.7 | 0.6 | 0.2 | 0.3 | 1.231 | 3.026 | 1.250 | 0.352 |
| 0.7 | 0.6 | 0.4 | 0.5 | 1.129 | 2.431 | 2.032 | 0.267 |
| 0.8 | 0.6 | 0.0 | 0.3 | 1.366 | 3.784 | 1.142 | 0.324 |
| 0.8 | 0.6 | 0.2 | 0.5 | 1.262 | 3.229 | 1.481 | 0.290 |
| 0.8 | 0.6 | 0.4 | 0.5 | 1.178 | 2.623 | 2.634 | 0.199 |
| 0.9 | 0.6 | 0.0 | 0.3 | 1.369 | 3.730 | 1.285 | 0.295 |
| 0.9 | 0.6 | 0.2 | 0.5 | 1.301 | 3.066 | 1.733 | 0.257 |
| 0.9 | 0.6 | 0.4 | 0.5 | 1.254 | 2.197 | 3.426 | 0.167 |

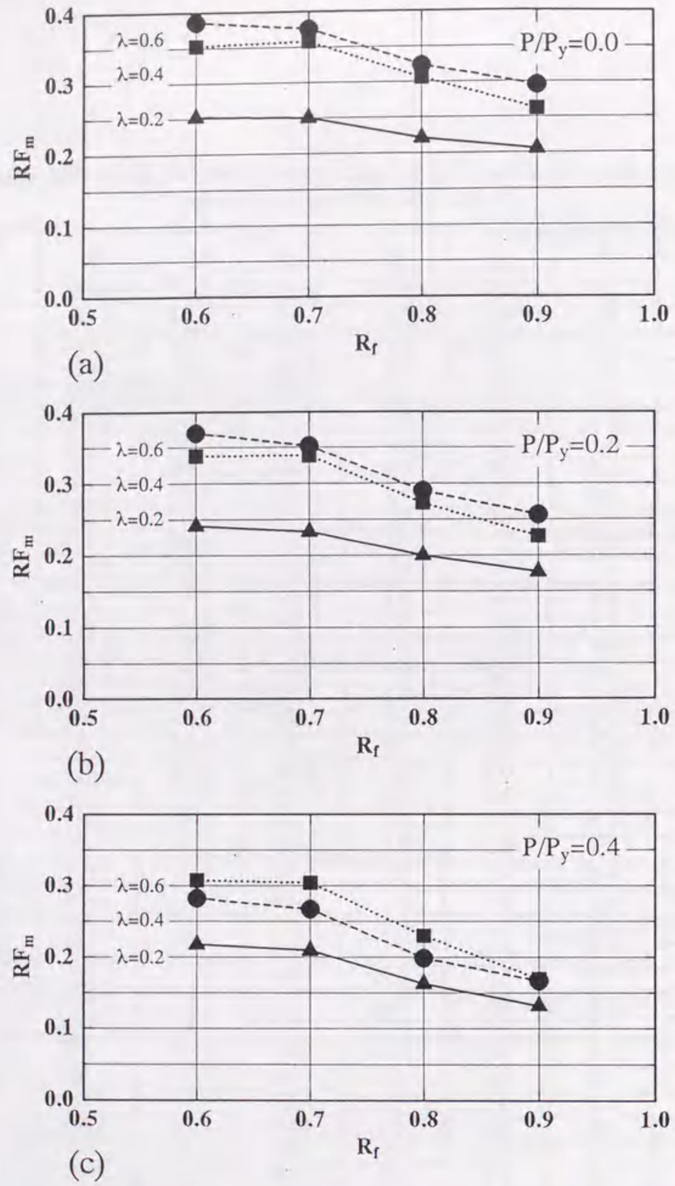


Fig. 8.2 Calculated Values of $RF_m$ for Equivalent Seismic Coefficients



# 9 SUMMARY AND CONCLUSIONS

With the rapid development of highway and bridge constructions, the use of steel bridge piers will be more and more popular. It has been recognized that seismic design of such structures becomes very important. That is, strength, ductility and energy-absorption capacity provided by a designed structure should be larger than the corresponding demand during an earthquake. The demand will be very high in the event of a severe earthquake. To assure the integrity of steel bridge piers, particularly those with large section or/and large height, filling of concrete inside the steel section is an effective method for improving their strength, ductility and energy-absorption capacity so that the structure will be able to withstand a severe earthquake without collapsing.

This research work was aimed at developing a reliable earthquake-resistant design method for concrete-filled steel bridge piers. For this purpose, extensive experimental investigations were made to understand how this type of structures behave under cyclic loading, and get important information for developing a simple analytical method. The study started with the experimental investigation on the strength and deformation behavior of concrete-filled steel box stub-columns subjected a pure compression as presented in Chapter 2. The following important conclusions were reached:

(1) Local buckling of plate panels toward the interior direction was prevented due to the presence of the filled-in concrete, and concrete-filled columns failed by buckling outward;

(2) Maximum strengths of concrete-filled columns were much larger than those of steel box columns, and average strains corresponding to the maximum strengths were about 0.2% in steel columns and about 0.4% in concrete-filled columns;

(3) Local buckling strengths of plate panels in concrete-filled columns were compared with available empirical design formulas. It was found that the characteristic compressive strength of the filled-in concrete should be evaluated by introducing a reduction factor $\beta$ on the cylinder compressive strength, e.g., $\beta = 0.7$ in the case of ordinary concrete;

(4) Failure of the concrete-filled column depends to a great extent on the fracture of

the filled-in concrete, and thus special care must be given to the casting of the concrete.

In order to develop a design method for determining strengths of concrete-filled steel box stub-columns in compression, elasto-plastic finite element analyses were conducted. In the beginning, the capability of an elasto-plastic hardening/softening model of concrete proposed by Wu and Tanabe was examined by comparisons with uniaxial, biaxial and triaxial test data. Computed load-deformation behavior of concrete-filled steel box columns was then compared with the experimental results presented in Chapter 2, and followed by a parametric study in which the effects of plate aspect ratio, width-thickness ratio, initial out-of-flatness and concrete compressive strength were investigated. Finally, a design recommendation was proposed for concrete-filled steel box stub-columns in compression. The main conclusions were as follows:

(1) An elasto-plastic model of concrete is observed to satisfactorily predict the stress-strain characteristic of concrete;

(2) The ultimate strengths of concrete-filled columns obtained from the analysis generally agreed well with the experimental results;

(3) An empirical reduction factor proposed in Chapter 2, $\beta = 0.7$, for the cylindrical compressive strength of concrete, was found to be adequate for the ordinary filled-in concrete, while $\beta = 0.85$ may be more rational for the high-performance filled-in concrete;

(4) The lowest ultimate strength of concrete-filled columns was obtained when the plate aspect ratio, $\alpha$, was about 2.0;

(5) Local plate buckling occurred when the width-thickness ratio parameter, $R$, was larger than about 0.9;

(6) The effects of initial geometrical imperfections of plate panels on the ultimate strength were relatively small;

(7) The nondimensionalized ultimate loads, $P_u/P_y$, are not sensitive to the concrete strength, though the ultimate strengths, $P_u$, of concrete-filled columns were increased when the concrete strength was increased;



(8) Design formulas [**Eqs. (3.31) and (3.32)**] were proposed to account for the effects of local plate buckling on the strength of concrete-filled columns.

In actual practice, thin-walled steel bridge piers were partially filled with the concrete in many cases, since it was important to reduce the dead weight of the structure for designing the foundations. Chapters 4 and 5 were devoted to the discussions of experimental results of partially concrete-filled steel box columns modeling steel bridge piers under cyclic loading. In Chapter 4, four steel box column specimens and seven partially concrete-filled steel box column specimens with relatively large slenderness ratio were discussed; and Chapter 5 focused on the discussions of twelve partially concrete-filled steel box column specimens with relatively small slenderness ratio. The test results were discussed in the light of improvement of ductility and energy-absorption capacity of steel bridge piers, and the main conclusions can be summarized as follows.

(1) Tests on 19 steel box columns, partially filled with concrete up to 0.3 or 0.5 times of the column height, showed a very effective earthquake-resistant capacity. The concrete-filled columns exhibited significant increase in both ductility and energy-absorption capacity, e.g., comparing with specimen SS1 (without concrete infill), ductility and energy-absorption capacity of specimen SS8 ($l_c/h = 0.3$) increased two times and four times, respectively. This is because the inward local plate buckling displacements were prevented by filled-in concrete. Local buckling deformations were delayed in their initiation and also moderated considerably, which lead to a remarkable increase in ductility and in energy-absorption capacity;

(2) A diaphragm over the filled-in concrete was found to be very effective in improving the strength, ductility and energy absorption capacity of the column. In the seismic design of partially concrete-filled steel bridge piers of box sections, it appears beneficial to provide a diaphragm over the filled-in concrete;

(3) Concrete-filled steel box columns tested had flexural cracks, which were perpendicular to the column axis, rather than diagonal. As a result, it can be said that these columns failed in flexure;

(4) In the specimens with small slenderness ratios, crack occurred vertical to the weld at approximately $H = H_{yo}$ with the exception of specimen SC45-25-5[3],

which had a crack near the column base early at 88% of the maximum load. It might have resulted from low cycle fatigue. Accordingly, special attention is necessary to be paid to the welding surrounding the triangular ribs in practical constructions;

(5) When "collapse" was defined as occurring at the maximum load point ($H_{max}$), or at a point where the load-carrying capacity is reduced to 95% of the maximum load (i.e., $H_{95}$) or reduced to the yield load ($H_y$), the ductility and energy absorption capacity were much different. However, due to the fact explained in (4), it is adequate for the concrete-filled steel box columns to define "collapse" as occurring at the point of $H_{max}$ or $H_{95}$. However, it will be more convenient to assume failure of such columns to take place at the maximum load point, since it is a safe yet simple definition.

Based on the experimental investigations, it was found that concrete-filled steel box columns generally exhibit flexural failure. This means that, the load-deflection relationships of concrete-filled steel box columns may rationally be determined from flexural failure theory. One of the approximate methods is to integrate the moment-curvature relations along the member length. For this purpose, the moment-curvature relations of hollow steel box section and concrete-filled steel box section were computed and presented in Chapter 6. Based on this part of the work, it can be concluded that

(1) An analytical model for computing the $M-P-\Phi$ curves was proposed for locally buckled steel box column segments. As a result, an interaction strength formula [**Eq. (6.18)**] was proposed for ultimate bending strengths of steel columns, and the moment-thrust-curvature relationship can be accurately predicted by a set of proposed formulas [**Eqs. (6.22) - (6.24)**];

(2) The analytical model was modified to take into account the effect of moment gradient, and a modification factor f(G, R) was introduced to predict the moment-thrust-curvature relationship;

(3) A set of approxomate expressions [**Eqs. (6.36) - (6.38)**] were also proposed without considering local buckling for predicting the $M-P-\Phi$ relations of steel box column segments;



(4) The moment-curvature relations for concrete-filled steel box column segments were computed by a simple numerical method in which local buckling was not taken into account. When the strain-hardening effect is not considered, the ultimate bending strength can be predicted using a proposed interaction formula [**Eq. (6.66)**]. The $M-P-\Phi$ curves can be closely approximated by two continuous functions [**Eqs. (6.68)** and **(6.69)**]. Moreover, in order to take into account the effect of strain-hardening, a modification was made in the approximation expressions of the $M-P-\Phi$ relationships.

In many instances, the determination of the maximum loads and displacements is of great practical importance. Therefore, the development of efficient methods for computing the load-carrying and deformation capacities in a simple way is of interest to engineers.

Chapter 7 was concerned with the development of such a method. To obtain the load-deformation behavior of the columns, the appriximate $M-P-\Phi$ relations given in Chapter 6, wherein local buckling was not considered, were integrated along the member axis by using the finite integral technique. The following main conclusions were drawn:

(1) An effective failure length concept was introduced to define a failure criterion for partially concrete-filled steel box columns;

(2) The present simple analytical model was found to give satisfactory predictions of the maximum loads and corresponding deformations and it will be of great importance in practical seismic design;

(3) Design charts for determining the ultimate strengths and corresponding deformations of the concrete-filled steel box columns under constant axial force and lateral load were presented;

(4) A design recommendation for determining the optimum length of the filled-in concrete was proposed. It was found that in design the length of filled-in concrete can be taken as 0.3 or 0.5 times of the column height in most cases.

In Chapter 8, recommendations were proposed for practical design of concrete-filled steel box columns on the basis of both theoretical and experimental investigations. It

was found that the equivalent horizontal seismic coefficient, which will be used to check the bearing capacity of bridge piers for lateral force, can be reduced to be a value smaller than 0.4 using the proposed recommendations. It is hoped that they will be of great use in obtaining a rational design.

For future studies, the analytical method for determining the ultimate strength and deformation might be extended to the case of concrete-filled stiffened steel box columns. For this purpose, the moment-curvature relations for the stiffened column segments should be studied in order to obtain approximate expressions for predicting the $M - P - \Phi$ behavior. In addition, it is necessary to investigate the behavior of concrete-filled steel box columns under simulated strong earthquake ground motions through the hybrid tests. This work is now underway in Nagoya University.



## References


[1] *AIJ Standards for Structural Calculation of Steel Reinforced Concrete Structures.* (1987). Architectural Institute of Japan.

[2] Bazant, Z. P., and Bhat, P. D. (1976). "Endochronic Theory of Inelasticity and Failure of Concrete." *J. Mech. Div., ASCE*, **102(4)**, pp.331-344.

[3] Bergmann, R. (1990). "Composite Columns." Eurocode 4, pp.39-68.

[4] Bouwkamp, Ir. Jack G. (1991). "Composite Construction in Earthquake Resistant Design." *Prof. of the 4th International on Structural Stability*, Mediterranean Session, pp.390-409, Istanbul.

[5] Bradfield, C. D. (1982). "An Evaluation of the Elastic-Plastic Analysis of Steel Plates Loaded by Uniaxial In-Plane Compression." *Int. J. Mech. Sci.*, **24(3)**, pp.127-146.

[6] *BS5400, Steel, Concrete and Composite Bridges, Part 5, Code of Practice for Design of Composite Bridges.* (1979). British Standards Institution, London.

[7] *Building Code Requirements for Reinforced Concrete.* (1983). ACI 318-83, American Concrete Institute, Detroit, Michigan.

[8] Chen, W. F. (1982). *Plasticity in Reinforced Concrete.* McGraw-hill, New York.

[9] Chen, W. F., and Atsuta, T. (1976). *Theory of Beam-Columns, vol. 1: In-Plane Behavior and Design.* McGraw-hill, New York.

[10] *Concrete Strength and Strains.* (1981). Development in Civil Engineering, Vol. 3, C. Avram, I. Facaoaru, O. Mirsu, I. Filimon, and I. Tertea, ed., Elsevier.

[11] DIN 18806 Teil 1. (1981) *Trägfähigkeit von Verbundstützen, Berechnung und Bemessung.*

[12] DIN 4114, Blatt2. (1953). Stahlbau, Stabilitätsfälle (Knickung, Kippung, Beulung), Berechnungsgrundlagen, Richtlinien.

[13] Dwight, J. B. (1969). "Welded Steel Plates in Compression." *The Structural Engineer,* **47(2)**, pp.49-66.

[14] Elnasfi, A. S., El-ghazouli, A. Y., and Dowling, P. J. (1990). "International Assessment of Design Guidance for Composite Columns." *J. of Construct. Steel Research,* **15**, pp.191-213.

[15] Eurocode 4. (1990). *Design of Composite Structures, Composite Columns.*

[16] Fukumoto, Y., and Kusama, H. (1985). "Cyclic Bending Tests of Thin Walled Box Beams." *Proc. of Japan Society of Civil Engineers (JSCE), Struct. Engrg./Earthquake Engrg.*, **2(1)**, pp.141-151.

[17] Furlong, R. W. (1977). "Composite Columns — A Bridge Between AISC and ACI Regulations." *Proc. of International Colloquium on Stability and Dynamic Loads*, 700-717, SSRC/ASCE/Washington, D. C.

[18] Furlong, R. W. (1967). "Strength of Steel-encased Concrete Beam Columns." *J. Struct. Div., ASCE*, **93(5)**, pp.113-124.

[19] Furlong, R. W. (1968). "Design of Steel-Encased Concrete Beam-Columns." *J. Struct. Div., ASCE*, **94(1)**, pp.267-281.

[20] Gardner, N. J., and Jacobson, E. R. (1967). "Structural Behavior of Concrete Filled Steel Tubes." *J. ACI*, **64(7)**, pp.404-413.

[21] Ge, H. B., and Usami, T. (1992). "Strength of Concrete-Filled Steel Thin-Walled Box Columns: Experiment." *J. Struct. Engrg., ASCE,* **118(11)**, pp.3036-3054.

[22] Ge, H. B., Usami, T., and Terada, M. (1992). "Experimental and Theoretical Study on the Ultimate Strength of Concrete-Filled Steel Box Stub-Column." *J. of Struct. Engrg., JSCE,* **38A**, pp.119-132.

[23] Ge, H. B., and Usami, T. (1992). "A Numerical Study on Ultimate Strength of Concrete-Filled Thin-Walled Steel Box Columns." *Proc. of the 3rd Pacific Structural Steel Conference*, pp.577-584.



[24] Ge, H. B., and Usami, T. (1994). "Strength Analysis of Concrete-Filled Thin-Walled Steel Box Columns." Accepted for Publication in *J. Construct. Steel Research.*

[25] Ge, H. B., Usami, T., and Toya, K. (1994). "A Study on Strength and Deformation Capacity of Concrete-Filled Steel Box Columns under Cyclic Loading." Accepted for Publication in *J. of Struct. Engrg., JSCE,* **40A**.

[26] Ge, H. B., Usami, T. (1994). "Behavior of Partially Concrete-Filled Steel Box Columns under Cyclic Lateral Loading." Accepted by *the Fourth Int. Conf. on Steel-Concrete Composite Structures,* Slovakia.

[27] *Guide to Stability Design Criteria for Metal Structures.* (1988). T. V. Galambos, ed., 4th Ed., John Wiley & Sons, New York.

[28] *Guidelines for Design of Steel-Concrete Composite Constructions.* (1989). Ikeda, S., ed., Task Committee of Steel-Concrete Composite Constructions, Committee of Structural Engineering, JSCE(in Japanese).

[29] *Guidelines for Stability Design of Steel Structures.* (1987). Fukumoto, Y., ed., Subcommittee on Stability Design, Committee on Steel Structures, JSCE(in Japanese).

[30] Janss, J (1991). "Eurocode 4 and Some Stability Problems". *Prof. the 4th International on Structural Stability,* Mediterranean Session, pp.286-305, Istanbul.

[31] "JRA 90" (1990). *Specification for Highway Bridges,* Japan Road Association.

[32] Kansai International Airport Inc. & Public Works Research Institute of Ministry of Construction. (1987). *Experiment on Partial-Composite Columns (Research Report).*

[33] Kawashima, K., Hasegawa, K., Yoshida, T., and Ikeuchi, T. (1989). "Effects of Stiffener Rigidities on the Dynamic Strength of Steel Bridge Piers." *Proc. of the 20th Annual Meeting of Earthquake Engrg., JSCE*, pp.433-436, Tokyo, Japan.

[34] Kitada, T., and Nakai, H. (1991). "Experimental Study on Ultimate Strength of Concrete-Filled Square Steel Short Members Subjected to Compression or Torsion". *Proc. of the Third International Conference on Steel-concrete Composite Structures*, pp.137-142, Fukuoka, Japan.

[35] Kitada, T., Nakai, H., and Yoshida, Y. (1989). "Experimental Study on Ultimate Strength of Composite Square Short Columns Using Rolled Steel Plate with Small Ribs." *Proc. of the 2nd Symposium on Research and Application of Composite Constructions.* Committee of Struct. Engrg., JSCE, pp.189-194(in Japanese).

[36] Knowles, R. B., and Park, R. (1969). "Strength of Concrete Filled Steel Tubular Columns." *J. Struct. Div., ASCE*, **95(12)**, pp.2565-2587.

[37] Knowles, R. B., and Park, R. (1970). "Axial Load Design for Concrete Filled Steel Tubes". *J. Struct. Div., ASCE*, **96(10)**, pp.2125-2153.

[38] Krawinkler, H., and Mohasseb, S. (1987). "Effects of Panel Zone Deformations on Seismic Response". *J. of Construct. Steel Research*, **8**, pp.233-250.

[39] Kupfer, H. B., Hilsdorf, H. K. & Rüsch, H. (1969). "Behavior of Concrete under Biaxial Stresses." *American Concrete Institute Journal*, **66(8)**, pp.656-666.

[40] Little, G. H. (1979). "The Strength of Square Steel Box Columns—Design Curves and Their Theoretical Basis." *The Structural Engineer*, **57A(2)**, pp.49-61.

[41] Maeda, Y. (1984). "History and Trend of Progress of Studies on Hybrid Construction." *Proc. of JSCE,* **344**, I-1, pp.13-25(in Japanese).

[42] *MARC background information.* (1988). MARC Analysis Research Corporation.

[43] *MARC user information manual.* (1988). MARC Analysis Research Corporation.

[44] Mirza, S. A. (1989). "Parametric Study of Composite Column Strength Variability." *J. of Construct. Steel Research*, **14**, pp.121-137.

[45] Miwa, K., Sakimoto, T., and Yamao, T. (1993). "Ultimate Strength Analysis of Steel Frames of Box-Sections Including Local Buckling Effects." *Proc. of the 48th annual conference of JSCE.*



[46] Murata, Y. (1984). *Seismic Design of Steel Structures.* Omu, Tokyo.

[47] Nakai, H., Kawai, A., Yoshikawa, O., Kitada, T., and Miki, T. (1982). "A Survey on Steel Piers." *Bridge and Foundation Engineering*, **16(6)**, pp.35-40, **16(7)**, pp.43-49.

[48] Nakai, H., Kitada, T., and Miki, T. (1985). "An Experimental Study on Ultimate Strength of Thin-Walled Box Stub-columns with Stiffeners Subjected to Compression and Bending." *Proc. of JSCE, Struct. Eng./ Earthquake Eng.*, **2(2)**, pp.87-97.

[49] Nakai, H., Kitada, T., and Yoshikawa, O. (1985). "A Design Method of Steel Plate Element in Concrete-Filled Square Steel Tubular Columns." *Proc. of JSCE,* **356**, I-3, pp.405-413(in Japanese).

[50] Nakai, H., and Yoshikawa, O. (1984). "Experimental Study on Strength of Concrete-Filled Steel Piers." *Proc. of JSCE*, **344**, I-1, pp.195-204.

[51] Nakai, H., Yoshikawa, O., Nakamura, I., Hakamada, F., and Terada, H. (1985). "Fundamental Experimental Study on Compression/Bending Ultimate Strength and Bonding of Composite Columns." *Bridge and Foundation Engineering*, **19(6)**, pp.19-27.

[52] Nakai, H., Yoshikawa, O., and Terada, H. (1986). "An Experimental Study on Ultimate Strength of Composite Columns for Compression or Bending." *Proc. of JSCE, Struct. Engrg./Earthquake Engrg.*, **3(2)**, pp.235s-245s.

[53] Ohno, T., and Nishioka, T. (1984). "An Experimental Study on Energy Absorption Capacity of Columns in Reinforced Concrete Structures." *Proc. of JSCE, Struct. Engrg./Earthquake Engrg., JSCE*, **1(2)**, pp.23-33.

[54] Ozawa, K., Maekawa, K., Kunishima, M., and Okamura, H. (1989). "High Performance Concrete Based on the Durability Design of Concrete Structures." *Proc. of the 2nd East Asia-Pacific Conference on Structural Engineering and Construction*, Chiang-Mai.

[55] Park, R., Nigel Priestley, M. J., and Gill, W. D. (1982). "Ductility of Square-Confined Concrete Columns". *J. of Struct. Div., ASCE*, **108(4)**, pp.929-950.

[56] *Plastic Design in Steel.*(1971). A Guide and Commentary, ASCE Manuals and Reports on Engineering Practice, **No. 41**.

[57] *Recommendation of Design and Construction of Steel Bridges Piers with Composite Columns (Concrete Filled Structures),* Draft.(1986). Hanshin Expressway Highway Public Cooperation, Japan.

[58] Sakurai, T., Kato, K., Uno, Y., Chu, K., and Kusama, H. (1988). "Experimental Study on Strength of Concrete-Filled Steel Square Beams under Alternating Bending." *J. of Struct. Engrg., JSCE*, **34A**, pp.265-274.

[59] Salani, H. J., and Sims, J. R. (1964). "Behavior of Mortar Filled Steel Tubes in Compression." *J. of ACI*, **61(10)**, pp.1271-1282.

[60] Schickert, G., and Winkler, H. (1977). "Results of Tests Concerning Strength and Strain of Concrete Subjected to Multiaxial Compressive Stresses." *Bundesanstalt fur Materiaprufung (BAM)*, **46**, Berlin, Germany, Bericht.

[61] Shakir-khalil, H. (1991). "Bound Strength in Concrete-Filled Steel Hollow Sections." *Proc. of the International Conference on Steel & Aluminium Structures*, Composite Steel Structures, pp.157-168, Singapore.

[62] Sheikh, S. A. (1982). "A Comparative Study of Confinement Models." *J. of ACI*, pp.296-306(July-August).

[63] *Stability of Metal Structures (a world view).* (1991). Beedle Lynn S., editor-in-chief, 2nd Ed., Structural Stability Research Council, Pennsylvania, U.S.A.

[64] *Steel-Concrete Composite Structures: Stability and Strength.* (1988). Narayanan, R., ed., Elsevier Applied Science, London and New York.

[65] Takemoto, K. (1993). "An Experimental Study on the Restoring-Force Characteristics of Steel Compression Members under Cyclic Loading." Master's thesis, Department of Civil Engineering, Nagoya University, Japan.

[66] Tanabe, T., and Wu, Z. S. (1991). "Strain Softening under Bi-axial Tension and Compression. *IABSE Colloquium Report*, **62**, pp.623-636.



[67] Tomii, M. (1988). *Investigations on Transversely Super Reinforced Concrete Structures and Concrete Filled Steel Tube Structures.* Report to the Ministry of Education, Science and Culture. Department of Architecture, Faculty of Engineering, Kyushu University, Japan.

[68] Tomii, M., and Sakino, K. (1979). "Experimental Studies on the Ultimate Moment of Concrete Filled Square Steel Tubular Beam-columns". *Trans. of A.I.J.*, pp.55-65.

[69] Tomii, M., and Sakino, K. (1979). "Elasto-plastic Behavior of Concrete Filled Square Steel Tubular Beam-columns". *Trans. of A.I.J.*, pp.111-122.

[70] Tomii, M., and Sakino, K. (1979). "Experimental Studies on Concrete Filled Square Steel Tubular Beam-Columns Subjected to Monotonic Shearing Force and Constant Axial Force." *Trans. of A.I.J.*, pp.81-92.

[71] Tomii, M., Yoshimura, K., and Morishita, Y. (1977). "Experimental Studies on Concrete-Filled Steel Tubular Stub Columns under Concentric Loading." *International Colloquium on Stability of Structures under Static and Dynamic Loads*, pp.718-741, Washington, D.C.

[72] Usami, T. (1993). "Effective Width of Locally Buckled Plates in Compression and Bending." *J. Struct. Engrg., ASCE*, **119(5)**, pp.1358-1373.

[73] Usami, T. (1982). "Post-Buckling of Plates in Compression and Bending." *J. Struct. Engrg., ASCE*, **108(3)**, pp.591-609.

[74] Usami, T. (1990). "Experimental Verification of Ultimate Strength Formulas for Plane Rigid Frames." *J. of Struct. Engrg., JSCE*, **36A**, pp.79-88(in Japanese).

[75] Usami, T., and Fukumoto, Y. (1982). "Local and Overall Buckling of Welded Box Columns." *J. Struct. Engrg., ASCE*, **108(3)**, pp.525-542.

[76] Usami, T., and Fukumoto, Y. (1984). "Welded Box Compression Members." *J. Struct. Engrg., ASCE*, **110(10)**, pp.2457-2470.

[77] Usami, T., and Fukumoto, Y. (1989). "Deformation Analysis of Locally Buckled Steel Compression Members." *J. of Construct. Steel Research*, **13**, pp.111-135.

[78] Usami, T., Ge, H. B., and Mizutani, S. (1993). "Cyclic Elasto-Plastic Behavior of Partially Concrete-Filled Unstiffened Steel Box Columns." *J. of Struct. Engrg., JSCE,* **39A**, pp.249-262.

[79] Usami, T., Ge, H. B. (1993). "Ductility of Concrete-Filled Thin-Walled Steel Box Columns under Cyclic Loading, Accepted for Publication in *J. Struct. Engrg., ASCE.*

[80] Usami, T., Imai, Y., Aoki, T., and Itoh, Y. (1991). "An Experimental Study on the Strength and Ductility of Steel Compression Members under Cyclic Loading." *J. of Struct. Engrg., JSCE,* **37A**, pp.93-106(in Japanese).

[81] Usami, T., Mizutani, S., Aoki, T., Itoh, Y., and Yasunami, H. (1992). "An Experimental Study on the Elasto-Plastic Cyclic Behavior of Stiffened Box Members." *J. of Struct. Engrg., JSCE*, **38A**, pp.105-117.

[82] Usami, T., Mizutani, S., Aoki, T., and Itoh, Y. (1992). "Steel and Concrete-Filled Steel Compression Members under Cyclic Loading." *Stability and Ductility of Steel Structures under Cyclic Loading,* Y. Fukumoto and G. Lee, ed., pp.123-138, CRC Press, Florida.

[83] Usami, T., and Terada, K.(1988). "Strength of Locally Buckled Steel Framed Structures of Box Sections." *Prof. of JSCE*, **398**, I-10, pp.197-206.

[84] Usami, T., Wada, M., Kato, M., and Ge, H. B. (1991). "Ultimate Compressive Strength of Plate Assemblies." *Proc. of the International Conference on Steel & Aluminium Structures,* Steel Structures & Aluminium Structures, pp.471-480, Singapore.

[85] Washizu, K. (1982). *Variational Methods in Elasticity and Plasticity.* 3rd Ed., Pergamon Press, Oxford.

[86] Watanabe, E., Emi, S., Isami, H., and Yamanouchi, T. (1988). "An Experimental Study on Strength of Thin Walled Steel Box Beam-Columns under Repetitive Bending." *Proc. of JSCE, Struct. Engrg./Earthquake Engrg., JSCE*, **5(1)**, pp.43-57.



[87] Watanabe, E., Sugiura, K., Kanou, M., Kitahara, T., and Mori, T. (1989). "Cyclic Response of Thin Tubular Beam Columns." *Recent Developments in Buckling of Structures, ASME*, **183**, pp.73-78.

[88] Watanabe, E., Sugiura, K., Kanou, M., Takao, M., and Emi, S. (1990). "Hysteretic Behavior of Thin Tubular Beam-Columns with Round Corners." *J. of Struct. Engrg.*, Tokyo, Japan, **36A**, pp.33-40.

[89] Wu, Z. S., and Tanabe, T. (1990). "A Hardening-Softening Model of Concrete Subjected to Compressive Loading." *J. of Struct. Engrg., Architectural Institute of Japan*, **36B**, pp.153-162.

[90] Zienkiewicz, O. C., and Morgan, K. (1984). *Finite Elements and Application.* trans. by Iri, M. and Iri, Y., Wiley Japan, Tokyo.